TABLE OF CONTENTS - Appendix K

List of Figures ..... K–iii
List of Tables ..... K–vi

Appendix K
Interim Report on Subsystem Structural Analysis of the WTC Towers K–1

K.1 Purpose K–1
K.2 Scope of Work K–1
K.3 Description of Subsystem Structures K–2
K.3.1 Full Floor Subsystem Description K–2
K.3.2 Exterior Wall Subsystem Description K–3
K.4 Loads K–4
K.5 Materials K–4
K.5.1 Concrete K–5
K.5.2 Steel K–8
K.5.3 Welds K–15
K.5.4 Bolts K–15
K.5.5 Coefficient of Friction K–16
K.5.6 Symbols K–16
K.6 Model Conversion From SAP to ANSYS K–17
K.6.1 Translation Procedure K–18
K.6.2 Challenges K–19
K.6.3 Status K–19
K.7 Full Floor Subsystems K–24
K.7.1 Full Floor Model K–24
K.7.2 Knuckle Analysis K–26
K.7.3 Column Truss Seats K–31
K.7.4 Modeling Connection Failure by Break Elements K–40
K.7.5 Truss Model K–42
K.8 Exterior Wall Subsystem K–57
K.8.1 Description of Exterior Wall Subsystem Model K–61
K.8.2 Validation of the Exterior Wall Subsystem Model K–61
K.8.3 Model of One-Story High Exterior Column K–61

K.8.4 Model of Nine-Story High Exterior Model K–61
K.8.5 Models of the Column Splice K–61
K.8.6 Prefabricated Panel Model K–61
K.8.7 Ongoing Work on the Exterior Wall Subsystem Model K–61
K.9 Floor Truss Dynamic Response Due to Impact of Dropping Floor K–61
K.9.1 Impact of Dropping Floor K–61
K.9.2 Purpose and Scope K–61
K.9.3 Method of Analysis K–61
K.9.4 Results K–61
K.9.5 Conclusions K–61
K.10 References K–61

LIST OF FIGURES

Figure K–1. Temperature–dependent concrete properties. K–6

Figure K–2. Concrete stress-strain curves. K–7

Figure K–3. Temperature-dependent properties for all steels. K–9

Figure K–4. Stress-strain relationships for Material ID 1 steel. K–11

Figure K–5. Creep behavior at elevated temperatures for Material ID 1 steel. K–13

Figure K–6. Maximum plastic strain from the finite element analysis and limiting plastic strain. K–14

Figure K–7. 7/8 in. A325 bolt load–elongation curves at elevated temperatures. K–15

Figure K–8. Converted ANSYS model for floor 96 of WTC 1: overall view. K–20

Figure K–9. Converted ANSYS model for floor 96 of WTC 1: partial view near corner of building. K–20

Figure K–10. Converted ANSYS model for floor 96 of WTC 1: close-up view at corner of building. K–21

Figure K–11. Converted ANSYS model for floor 96 of WTC 1: view of floor beams and columns. K–21

Figure K–12. Deformed shape of gravity load case for SAP floor model. K–22

Figure K–13. Deformed shape of gravity load case for ANSYS floor model with BEAM44 (Euler beam) elements. K–22

Figure K–14. Dominant mode shape of floor structure for SAP floor model. K–23

Figure K–15. Dominant mode shape of floor structure sase for ANSYS floor model. K–23

Figure K–16. Transverse shear test of a knuckle. K–27

Figure K–17. Longitudinal shear test of a knuckle. K–27

Figure K–18. Finite element models of knuckle shear tests. K–29

Figure K–19. Compressive stresses in longitudinal shear finite element model. K–29

Figure K–20. Compressive stresses in transverse shear finite element model. K–30

Figure K–21. Shear force versus displacement from finite element model for longitudinal shear of two knuckles. K–30

Figure K–22. Shear force versus displacement from finite element model for transverse shear of two knuckles. K–30

Figure K–23. Interior seat. K–32

Figure K–24. Exterior seat. K–32

Figure K–25. Truss seat detail location on northeast quadrant of floor 96 of WTC 1. ..... K–33

Figure K–26. Finite element model of exterior seat. K–35

Figure K–27. Failure sequence of the exterior seats against tensile force. K–36

Figure K–28. Typical tensile force resistance from exterior seat. K–36
Figure K–29. Strength of combined vertical and horizontal force. K–38
Figure K–30. Basic mathematical model of connection failure. K–41
Figure K–31. Simplified model of interior seat. K–43
Figure K–32. Results of simplified seat model capturing failure from truss walking off interior seat. K–44
Figure K–33. Results of simplified seat model capturing failure from exceeding the interior seat vertical shear capacity. K–44
Figure K–34. Simplified model of exterior seat. K–45
Figure K–35. Simplified model of knuckle. K–46
Figure K–36. Truss model. K–48
Figure K–37. Boundary conditions. K–50
Figure K–38. Break elements at the interior end of slab. K–50
Figure K–39. Comparison of resistance weld strength and yield strength of web member at elevated temperatures. K–52
Figure K–40. Displacement versus temperature. K–53
Figure K–41. Axial force in truss members versus temperature. K–54
Figure K–42. Axial stress contour in the truss members at 663 ^{o}C. K–55
Figure K–43. Force in the knuckles versus temperature. K–55
Figure K–44. Reaction forces at seats. K–56
Figure K–45. Finite element analysis results from increasing gravity. K–56
Figure K–46. Exterior wall subsystem structure. K–58
Figure K–47. Column and floor number materials and splice types. K–59
Figure K–48. Spandrels and spandrel splices. K–60
Figure K–49. Exterior wall subsystem model, viewed from inside of WTC 1. K–61
Figure K–50. Portion of exterior wall subsystem model showing number of elements used. K–61
Figure K–51. Schematic representation of columns used in the exterior wall subsystem model. K–61
Figure K–52. One-story exterior column model. K–61
Figure K–53. Load-deflection of column at room temperature and 700 °C. K–61
Figure K–54. Local buckling of column at room temperature. K–61
Figure K–55. Plastic hinge in column at room temperature. K–61
Figure K–56. Deformed shape of column at maximum axial load at 700 °C. K–61
Figure K–57. Nine-story column model. K–61
Figure K–58. Variation of maximum temperature and corresponding yield stress with time, fire scenario G. K–61

Figure K–59. Maximum compressive and tensile axial stress and corresponding yield stress with time, fire scenario G. K–61
Figure K–60. Deformed shape of column at 400 s, 3,200 s, and 5,000 s (floors 95–97). K–61
Figure K–61. Plate model of column splice, floors 97-98. K–61
Figure K–62. Simplified model of column splice. K–61
Figure K–63. Column splice details, plate model and simplified model. K–61
Figure K–64. Variation of axial displacement with axial load. K–61
Figure K–65. Variation of lateral displacement with shear load. K–61
Figure K–66. Variation of rotation with moment, out of wall plane. K–61
Figure K–67. Variation of rotation with moment, in plane of wall. K–61
Figure K–68. Variation of twist angle with torque. K–61
Figure K–69. SAP2000 model of prefabricated panel. K–61
Figure K–70. ANSYS model of prefabricated panel showing geometry and number of elements used. K–61
Figure K–71. ANSYS model of prefabricated panel showing loading and boundary conditions. K–61
Figure K–72. Deflection of prefabricated panels under 100 kip lateral load. K–61
Figure K–73. Deflection of prefabricated panels under 100 kip transverse load. K–61
Figure K–74. Deflection of prefabricated panels under 10 kip vertical load. K–61
Figure K–75. Schematic of full truss or partial truss drop and diagonal crushing at impact. K–61
Figure K–76. Target truss resistance against increasing acceleration. K–61

LIST OF TABLES

Table K–1. Steel types used in WTC 1 and WTC 2. ..... K–9
Table K–2. Parameters for *k(T) and n(T)*. K–11
Table K–3. Uniaxial plastic strain at fracture K–14
Table K–4. Comparison of SAP and ANSYS results for gravity load case. K–19
Table K–5. Comparison of SAP and ANSYS Modal Analysis Results. K–23
Table K–6. Material properties used for truss seat calculations. K–34
Table K–7. Interior seat capacity against vertical force. K–37
Table K–8. Interior seat capacity against tensile force. K–38
Table K–9. Exterior seat capacity against vertical force. K–39
Table K–10. Exterior seat capacity against horizontal tensile force. K–39
Table K–11. Compression strength of gusset plate. K–40
Table K–12. Material assignments in truss model. K–51
Table K–13. Resistance weld strength. K–51
Table K–14. Column sectional properties. K–60
Table K–15. Spandrel splice details. K–60
Table K–16. Column splice details. K–60
Table K–17. Validation results. K–61
Table K–18. Demand-to-Capacity ratio of long-span truss for static gravity load. K–61
Table K–19. Demand-to-Capacity ratio of long-span truss for dynamic impact load from full truss drop. K–61
Table K–20. Peak deflection response due to static gravity and dynamic impact. K–61

Appendix K
INTERIM REPORT ON SUBSYSTEM STRUCTURAL ANALYSIS OF THE WTC TOWERS

K.1 PURPOSE

Project 6 addresses the first primary objective of the technical investigation led by the National Institute of Standards and Technology (NIST) of the World Trade Center (WTC) disaster: to determine why and how the WTC towers (WTC 1 and WTC 2) collapsed following the initial impacts of the aircraft. Specifically, the objectives of this project are to determine the response of the structural components and systems to the fire environment in WTC 1 and WTC 2 and to identify probable structural collapse mechanisms. This appendix documents the progress achieved to date on Project 6 in thermal/structural modeling of WTC 1 and WTC 2.

Project 6 seeks to determine the response of structural components and systems to the fire environment in the WTC 1 and WTC 2 and to identify probable structural collapse mechanisms by (1) evaluating the response of floor and column systems under fire conditions, (2) evaluating the response of the WTC towers without and with aircraft impact damage under fire conditions, (3) conducting tests of structural components and systems under fire conditions, and (4) evaluating competing failure hypotheses for the WTC towers.

K.2 SCOPE OF WORK

The scope of the work consists of the following three tasks:

- **Task 1, Subsystem Structural Analysis.** The objective of Task 1 includes structural analysis of components and two subsystems, a full-floor subsystem, and an exterior wall subsystem. Task 1 is intended to provide guidance for the development of the global finite element models (FEMs) with respect to element types and sizes, appropriate constitutive models, and failure criteria for any given structural component. The subsystem analyses also will help to validate the accuracy of the global analyses, and correlate the results of the fine mesh component analyses with the coarser mesh global analyses of Task 2 and Task 3.

- **Task 2, Global Analysis of the WTC Towers' Response to Fire without Impact Damage.** The objectives of this task are to determine the general vulnerability of the towers to fire-initiated collapse and the role of fire in the towers with respect to structural stability, sequential failures of components and subsystems, and collapse initiation for the towers without impact damage.

- **Task 3, Global Analysis of the WTC Towers' Response to Fire with Impact Damage.** The objectives of this Task are to determine the relative roles of the impact damage and fires in the towers with respect to structural stability and sequential failures of the components and subsystems and to determine probable structural collapse initiation sequences.

Work under Task 1 includes the following:

- Develop and validate ANSYS models of the full floor and exterior wall subsystems.
- Evaluate structural responses for the following loading conditions.
  - Service loads due to gravity (dead and live loads).
  - Elevated structural temperatures.
- Identify the possible, likely and most likely failure modes and failure sequences, and the associated temperatures at failure and times-to-failure.
- Identify the changes in mechanical properties or geometry at initiation of component and subsystems collapse.
- Identify simplifications for the global structural models and/or analyses of subsystem models to use in Task 2 and Task 3.

The scope of this report is to present the progress made in Task 1 work.

K.3 DESCRIPTION OF SUBSYSTEM STRUCTURES

The full floor subsystem modeled is floor 96 of WTC 1. The model is believed to be typical in the upper floors of both towers. The exterior wall subsystem is a nine-column (three-panel) wide by nine-story (three-panel) high section of the WTC 1 between floor 91 and floor 100 and column 150 and column 158. This area is typical of the exterior walls of the towers and connects to a part of the floor system near the corner with different types of trusses.

K.3.1 Full Floor Subsystem Description

Floor 96 of WTC 1 was identified as an office floor with typical floor construction and loading and, therefore, was selected as the basis for this model. Components of the floor subsystem are examined for performance under loads and elevated temperatures in different possible failure modes. Understanding of these component behaviors is used to define the floor models for global analyses of WTC 1 and WTC 2.

The full floor subsystem of floor 96 of WTC 1 includes both office area and core area horizontal framing, as well as columns immediately above and below this floor.

The floor support in the office area consisted of pairs of steel floor trusses (nominally 60 ft in north-south and 36 ft in east-west directions) that span between exterior walls and the central core at 6 ft 8 in. on center. Each of these primary trusses consisted of top and bottom chords fabricated from steel angles and diagonals fabricated from round bars that extended 3 in. above the top chord at the panel points into the concrete slab in the form of a knuckle. The top chords of the primary trusses were supported at the central core by truss seats connected to a steel channel that ran continuously between the core columns. Each pair of trusses was connected to this channel with a seat that included two 1 3/4 in. long slotted holes and two 5/8 in. bolts (one bolt in each truss) as shown in Fig. K–25. Note that the floor truss was not welded to the seat support.

At the exterior wall, the truss pair was supported by a seat angle and fastened with two 5/8 in. diameter bolts in 2 in. long slotted holes. In addition, a gusset plate welded to the spandrel and to the truss top chord tied the supporting column to the truss, and a pair of straps welded to the top chord and to adjacent columns tied those columns into the primary trusses. Primary trusses were interconnected by a transverse bridging system consisting of bridging trusses and bridging angles. These bridging trusses were of similar construction to the primary trusses, although the knuckles for the diagonals did not project above the top chords. The top chord of the bridging trusses sat 1 1/2 in. below the top chord of the primary trusses and provided support for the 1 1/2 in., 22 gauge steel deck and the 4 in. thick lightweight concrete slab. At each corner of the building core, a 36 ft long transfer truss extended out from the corner core column to the exterior wall and supported the 60 ft long primary trusses. The core area floor consisted of a 5 in. thick normal-weight concrete slab on 1 1/2 in., 22 gauge steel deck, supported by wide flange girders and beams connected to the core columns.

Task 1 analyses use the nominal dimensions and design details shown on the drawings, without modifications resulting from any construction deviations or tenant modifications. Those modifications are considered in subsequent Task 3 analyses, which are based on the reference model developed by Leslie E. Robertson Associates (LERA) under a contract for Project 2. Material properties are based on information provided by Project 3.

K.3.2 Exterior Wall Subsystem Description

Each side of the towers' exterior wall consisted of fifty-nine 14 in. square box columns spaced at 3 ft 4 in. on center, with 52 in. deep spandrel plates at each floor level. The exterior wall was constructed from shop-welded prefabricated panels, each consisting, in general, of three columns and three spandrel beams, 13 ft 4 in. wide by 36 ft high. Except at mechanical floors, the base and top of the structure, vertical splices in prefabricated panels were staggered such that within any story, every third prefabricated panel had a vertical splice. Exterior column splices at the upper stories typically consisted of four 7/8 in. diameter ASTM A325 bolts fastened through the welded butt plates at the tops and bottoms of adjoining columns. Special prefabricated panels existed for the mechanical floors where no stagger existed at floors 7, 41, 75, and 108. At these mechanical floors, the column splice detail included supplemental field welding in addition to the bolted connection. Horizontal (spandrel-to-spandrel) connections between prefabricated panels were all field-bolted using splice plates. Corner panels that connected the orthogonal walls at corners were two-stories tall (24 ft) and consisted of two columns, two spandrel plates, and a third column midway between the two columns on alternate floors.

Various grades of steel, having yield strengths ranging between 42 ksi and 100 ksi, were specified to fabricate the perimeter column and spandrel plates. However, fewer grades were actually used with somewhat coarser gradation in yield strength than specified. Plate thicknesses also varied, both vertically and around the building perimeter. Plate thicknesses in the exterior wall were as thin as 1/4 in. at the upper stories, and increased toward the base of the building. The specified plate thicknesses and material yield strengths differed between the two towers, among NS and EW directions and through the height of the tower.

An exterior wall subsystem model, nine columns wide and nine floors high, was selected to study the structural behavior and failure modes of the exterior wall system. This subsystem model represents the exterior wall of WTC 1 between floors 91 and 100 and includes column lines 150 through 158. This area

is located near the corner of the tower (column 159 is at the corner of the north face of WTC 1. See Fig. K–27.) The wall subsystem allows evaluations of the interaction of the wall subsystem with thermal expansion of the floor near the corners. It also connects to various types of trusses with different behaviors.

K.4 LOADS

The subsystems and components are analyzed for Dead (D), Live (L), and thermal (T_a) loads. The dead load consists of structural weights and superimposed dead loads. The superimposed dead loads for floors outside the core consist of the weights of ceiling, mechanical and electrical, fireproofing, and floor finish, estimated at 8 psf. The superimposed dead load and design live load are defined in the World Trade Center Design Criteria (LERA 2001). Twenty five (25) percent of the design live load is selected as a reasonable approximation of the load that likely existed at the time of the collapse. (For example, 25 percent of the design live load results in a load of 13.75 psf for the long-span trusses in the two way zone of floor 96 with 55 psf design live load.) The service dead and live loads are applied first, followed by the thermal loads.

The dead and live loads are defined as weights, so that during the collapse process, the gravity loads remain acting on the structure. The weight of debris from the plane will be considered where provided by Project 2.

The thermal loads, T_a, are temperature time histories for all structural members provided by Project 5 for the standard test fire ASTM E119 and between three and five representative building fire scenarios of different intensities and three fire protection conditions.

For analysis of some of the components, discrete values of temperature or temperature distributions in the form of a ramp from 0 °C to 700 °C (or to a temperature below 700 °C that results in the failure of the component) over 0.5 h followed by a constant temperature of 700 °C for another 0.5 h are used. Failure modes of the components are evaluated at room temperature and at different elevated temperatures, as failure modes and failure loads may change with increasing temperature.

Although wind may have had a minor role in the collapse of the towers, Task 1 analyses do not include wind load effects.

K.5 MATERIALS

The mechanical properties of both steel and concrete are affected significantly by temperature. In the following sections, the material properties used in this project are specified as a function of temperature. A material properties catalog is prepared and made accessible to all analysis models. For use in ANSYS, each material is identified with a number; steels are Material ID 1 through Material ID 29, and concretes are Material ID 51 through Material ID 83.

K.5.1 Concrete

Aggregate Types

Two types of concrete were generally used for the flooring inside the towers; lightweight concrete was used in the office areas, and normal-weight concrete in the core area. Thermal properties of normal-weight concrete depend on the type of aggregate. Petrographic inspection by SGH of several samples of lightweight concrete taken from the debris at NIST showed siliceous sand in the lightweight concrete. Because source of coarse and fine aggregates is usually the same, the available data for normal-weight concrete with siliceous aggregates are used.

Actual Compressive Strength

Specified concrete strength for lightweight concrete is 3,000 psi and for normal-weight concrete either 3,000 psi or 4,000 psi, as shown on Drawing Book 8, Sheet AB1–2.1 (SHCR 1973). The actual strength, f_a, of in-place concrete at room temperature is calculated from the specified strength, f'_c, as follows:

$$f_a = f'_c \cdot F_1 \cdot F_2 \cdot F_3 \tag{1}$$

where the factor F_1 is the ratio of the average strength of cylinders to specified strength, F_2 is the ratio of in-situ 28-day strength to 28-day cylinder strength, and F_3 accounts for the change in concrete strength with age.

By using F_1 = 1.25 and F_2 = 0.95 (Bartlett and MacGregor 1996) and F_3 = 1.16 based on the formula specified in Section 2.2.1 of American Concrete Institute (ACI) 209 for change of concrete strength with age of concrete, the mean of the ratio of actual strength of in-place concrete to the specified concrete strength f_a / f'_c = 1.38. Based on this mean value, the actual strength of in-place concretes are f_a = 5,500 psi for the specified 4,000 psi normal-weight concrete, 4,100 psi for the specified 3,000 psi normal-weight concrete, and 4,100 psi for the specified 3,000 psi lightweight concrete.

Concrete Properties

The unit weight of the lightweight concrete is 100 pcf according to the WTC Design Criteria (LERA 2003); however, 110 pcf is used based on the two concrete samples described above. The unit weight of the normal-weight concrete is 150 pcf, according to LERA.

Poisson's ratio, ν_c, of 0.17 is used for both normal-weight and lightweight concrete at all temperatures.

Temperature dependent properties of concrete are modulus of elasticity, instantaneous coefficient of thermal expansion, compressive strength, and tensile strength:

Modulus of elasticity at room temperature is evaluated by the following formula:

$$E_c(RT) = 33\gamma_c^{1.5}\sqrt{f_a} \tag{2}$$

The actual strength, f_a, is used as room temperature compressive strength, and $5\sqrt{f_a}$ is used as room temperature tensile strength. Effects of elevated temperature on the listed properties are based on NIST research (Phan 1996, 2003), and plotted in Fig. K–1.

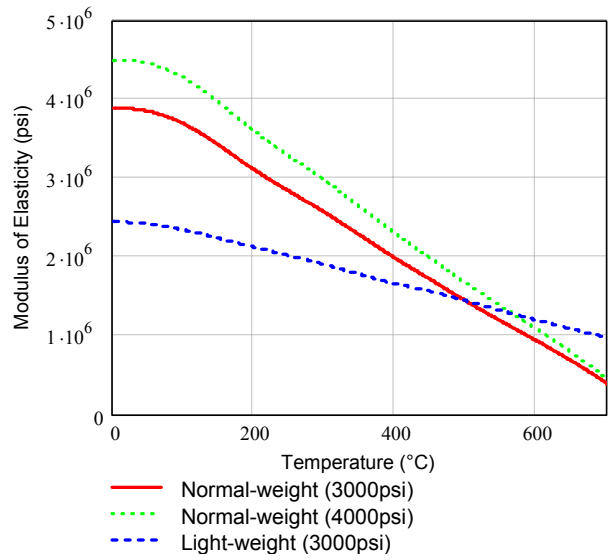

(a) Modulus of elasticity

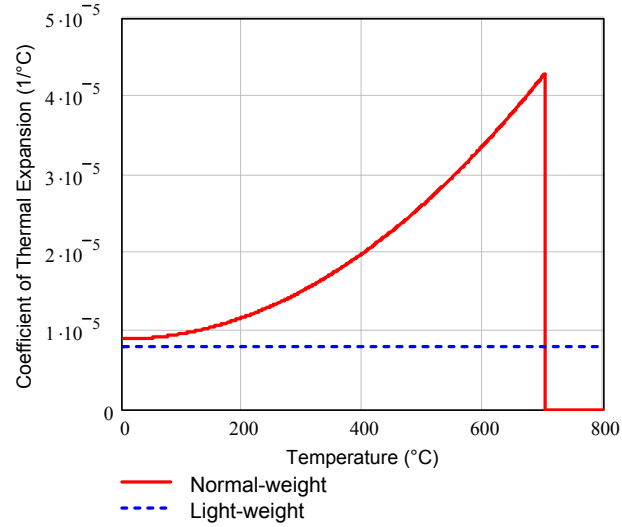

(b) Instantaneous coefficient of thermal expansion

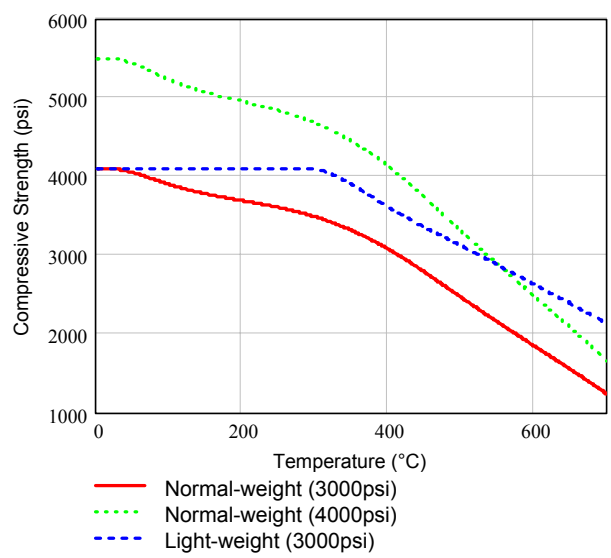

(c) Compressive strength

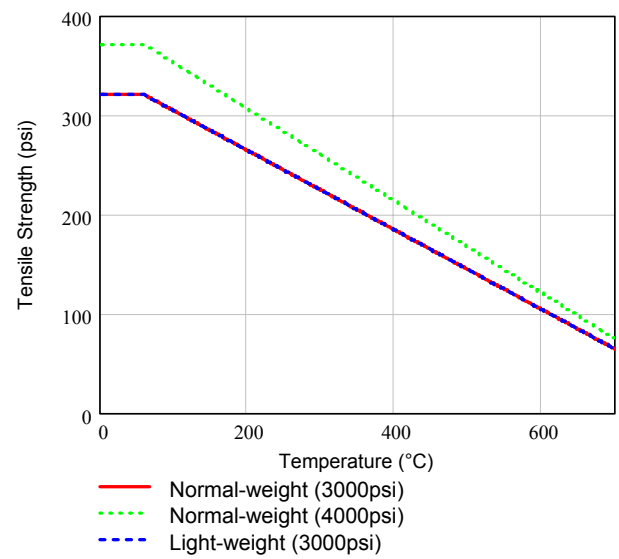

(d) Tensile strength

Figure K–1. Temperature–dependent concrete properties.

Concrete Stress-Strain Relationships

The compressive stress-strain curve, based on the formula by Seanz (1964), is given by:

$$\sigma = \frac{K_c f_c \left(\dfrac{\varepsilon}{\varepsilon_{c1}}\right)}{1 + a\left(\dfrac{\varepsilon}{\varepsilon_{c1}}\right) + b\left(\dfrac{\varepsilon}{\varepsilon_{c1}}\right)^2 + c\left(\dfrac{\varepsilon}{\varepsilon_{c1}}\right)^3} \tag{3}$$

where:

$$c = \frac{K_s - 1}{(K_e - 1)^2} K_c - \frac{1}{K_e} \ , \quad b = 1 - 2c \ , \quad a = c + K_c - 2 \, ,$$

$$K_c = 2 \ , \quad K_s = \frac{1}{0.85} \ , \quad K_e = 1.41 \ , \quad \varepsilon_{c1} = K_c \frac{f_c}{E_c}$$

In tension, stress increases linearly up to the tensile strength. When strained in tension beyond its strength will soften and the stress will drop. However, the descending branch of stress-strain relationship causes significant numerical instability problems which can be avoided by assuming that concrete becomes plastic in tension. Figure K–2 shows a few examples of concrete stress-strain curves at room and elevated temperatures.

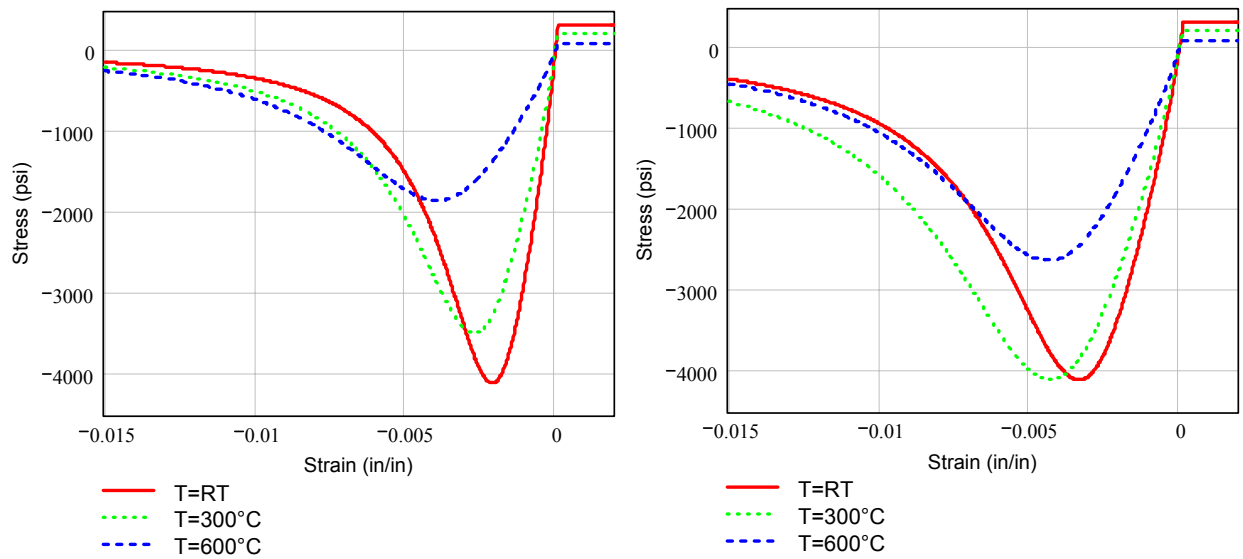

(a) Normal-weight concrete (3000psi) (b) Light-weight concrete

Figure K–2. Concrete stress-strain curves.

For the knuckle model in LS-DYNA, solid concrete elements are modeled with Pseudo Tensor material model, where the cap model is used. Since this material model is not temperature dependent, different material types are specified for the lightweight concrete at RT, 150 °C, 300 °C, 450 °C, 600 °C, and 750 °C (Material IDs 51 through 56) with their different stress-strain relationships.

The concrete slab in the truss is modeled with SHELL181 elements with a concrete material model that accounts for different behaviors in tension and compression. One such material model in ANSYS is the cast iron plasticity model which uses the Rankine maximum stress criterion in tension, and the expression for von Mises yield criterion in compression (ANSYS, Inc. 2004). Cast iron plasticity material models for specified 3,000 psi normal-weight concrete, specified 4,000 psi normal-weight concrete, and specified 3,000 psi lightweight concrete are assigned to Material ID 81, 82, and 83, respectively.

K.5.2 Steel

Steels used in WTC 1 and WTC 2 are listed in Table K–1 along with the yield and tensile strengths used in our analysis.

Steel Properties

Figure K–3 shows mechanical properties of steel at high temperatures: (a) modulus of elasticity; (b) Poisson's ratio; (c) yield strength reduction factor; (d) tensile strength reduction factor; and (e) instantaneous coefficient of thermal expansion. All properties, except yield and tensile strength reduction factors for bolt steels, are the same for all steels shown in Table K–1.

Stress–Strain Relationship

Plasticity: Stress-strain relationships at room temperature were provided by Project 3. They were constructed from mill report data, actual test data, and literature information using the Voce hardening law.

Stress–strain relationships at elevated temperatures, without consideration of creep, are obtained by the power law:

$$\sigma = R_{TS} R_C K(T) \varepsilon_{ep}^{n(T)} \tag{4}$$

where:

$$K(T) = (k4 - k0)\exp\left\{-0.5\left[\left(\frac{T}{tk1}\right)^{k1} + \left(\frac{T}{tk2}\right)^{k2}\right]\right\} + k0 \tag{5}$$

$$n(T) = (n4 - n0)\exp\left\{-0.5\left[\left(\frac{T}{tn1}\right)^{n1} + \left(\frac{T}{tn2}\right)^{n2}\right]\right\} + n0 \tag{6}$$

The steel stress-strain relationships at different temperatures vary depending on the type of steel used in the construction of the towers. Values for R_{TS}, R_C, given in Table K–1, and parameters of $K(T)$ and n(T) given in Table K–2, were provided by Project 3. The stress-strain curve is linear with Young's modulus up to the "linearity limit": At the linearity limit, the linear stress-strain curve intersects the power law stress strain curve. (Stress at the linearity limit is not necessarily equal to the yield stress. The linearity limit is required for ANSYS input.)

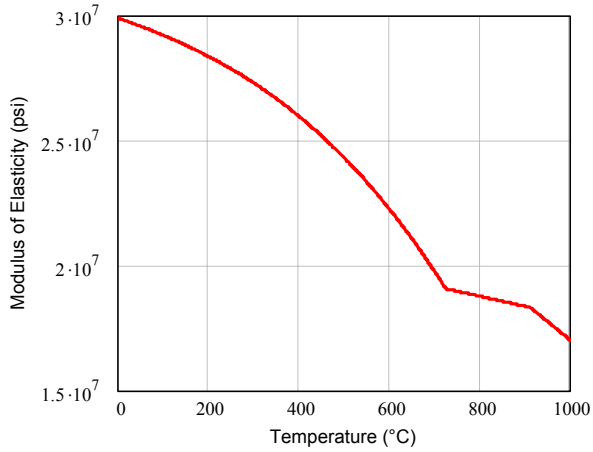

(a) Modulus of elasticity

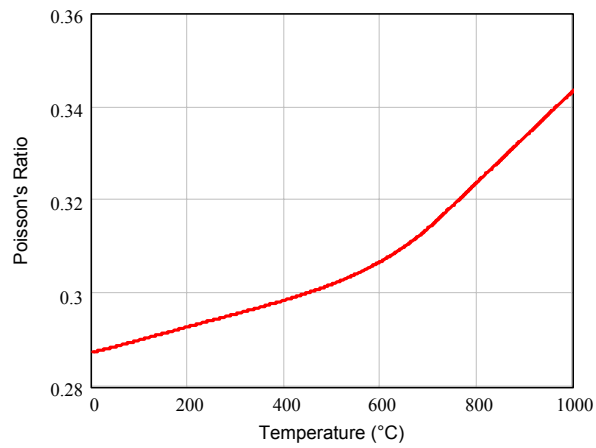

(b) Poisson's ratio

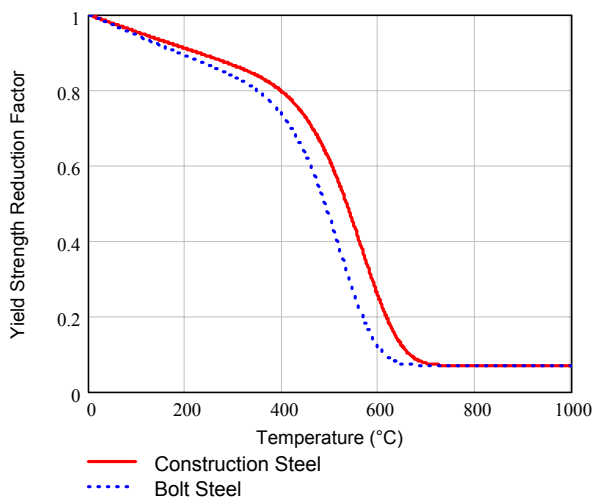

(c) Yield strength reduction factor

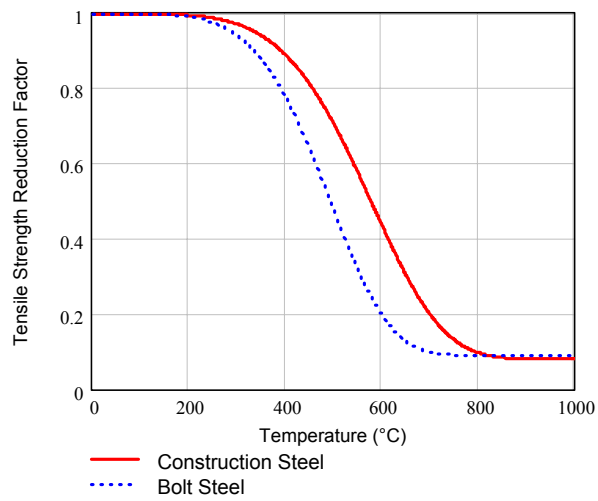

(d) Tensile strength reduction factor

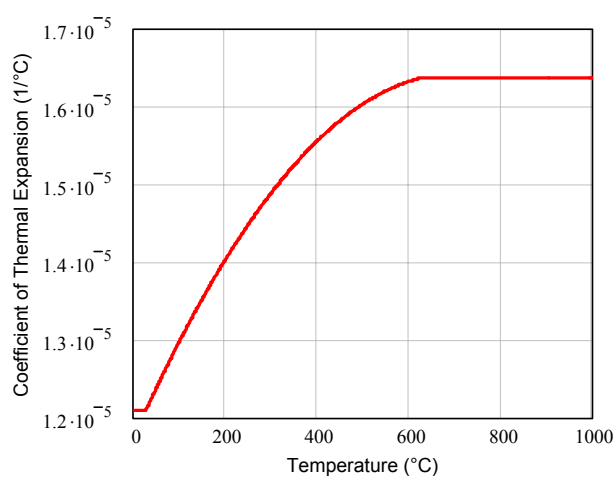

(e) Instantaneous coefficient of thermal expansion

Figure K–3. Temperature-dependent properties for all steels.

Table K–1. Steel types used in WTC 1 and WTC 2.

Material ID	Description	σ_{yRT} (psi)	σ_{uRT} (psi)	RTS	RC
1	All 36 ksi core box columns, plates, straps[a]	36,720	64,470	1.086	0.857
2	All 36 ksi core WF, channels, and tubes 36 ksi large area and large inertia "rigid" beams in SAP2000 model[a]	37,000	63,450	1.069	0.954
3	All 42 ksi box columns (1<=0.75 in.)	51,400	79,200	1.070	0.884
4	All 42 ksi box columns (0.75 in. < t <= 1.5 in.)	47,000	74,800	1.010	0.884
5	All 42 ksi box columns (t > 1.5 in.)	42,600	70,400	0.951	0.880
6	42 ksi or 45 ksi Group 3 WF core columns	53,800	74,400	1.005	0.977
7	42 ksi or 45 ksi Group 3 WF core columns	49,000	71,040	0.960	0.954
8	42 ksi Group 4&5 WF core columns	44,200	66,640	0.900	0.948
9	45 ksi Group 4&5 WF core columns	47,800	71,074	0.960	0.939
10	All 36 ksi Plates 1, 2, and 4 in perimeter columns	35,630	61,170	1.031	0.875
11	All (42, 45, or 46) ksi Plates 1, 2, and 4 in. perimeter columns	53,051	74,864	1.011	0.948
12	All 50 ksi Plates 1, 2, and 4 in. perimeter columns. All 50 ksi channels and plates[a]	53,991	75,618	1.021	0.978
13	All 55 ksi Plates 1, 2, and 4 with t<=1.5 in. in perimeter columns	60,817	82,558	1.115	0.903
14	All 60 ksi Plates 1, 2, and 4 with t<=1.25 in. in perimeter columns	62,027	87,250	1.178	0.894
15	All 65 ksi Plates 1, 2, and 4 with t<=0.5 in. in perimeter columns[b]	69,642	90,442	1.221	0.979
16	All 70 ksi Plates 1, 2, and 4 in. perimeter columns	76,735	91,951	1.242	0.955
17	All 75 ksi Plates 1, 2, and 4 in perimeter columns	82,469	96,821	1.308	0.936
18	All 80 ksi perimeter columns steels, regardless of plate	91,517	99,442	1.343	0.987
19	All (85, 90, 100) ksi perimeter column steels, regardless of plate	104,783	115,983	1.566	0.976
20	Laclede truss web bar rounds specified as A36	38,067	59,567	1.004	0.935
21	Laclede truss chord angels (regardless of ASTM Spec) and all rounds specified as A242	55,332	74,050	1.000	0.959
22	A325 bolts[c]	104,783	115,983	1.566	0.976
23	All 42 ksi Plate 3 in perimeter columns	42,600	67,216	0.900	0.912
24	All 45 ksi Plate 3 in perimeter columns	45,900	69,831	0.940	0.921
25	All 50 ksi Plate 3 in perimeter columns	51,400	74,188	1.000	0.935
26	All 55 ksi Plate 3 in perimeter columns	56,900	78,546	1.070	0.906
27	All 60 ksi Plate 3 in perimeter columns	62,400	83,903	1.130	0.949
28	All 65 ksi Plate 3 in perimeter columns	67,900	87,261	1.190	0.975
29	All 70 ksi and 75 ksi Plate 3 in perimeter columns	78,900	95,976	1.310	0.997

a. Steels in the following members are assumed to have the properties shown in the table:
36 ksi plates and straps (Material 1).
36 ksi channels, tubes, and "rigid" beams (Material 2).
50 ksi channels and plates (Material 12).
b. 65 ksi steels in perimeter columns with t>0.5 in. are assumed to have the same properties as those in Material 15.
c. In the column model, stress-strain relationships of bolts are used.
Note: Bolt properties are assumed to be the same as those in Material 19.

Table K–2. Parameters for *k(T) and n(T).*

	σ_{yRT} = 36,000 psi	σ_{yRT} > 36,000 psi
tk1, °C	524.1812	511.8266
tk2, °C	523.6799	511.8938
k0, psi	29049.2	26472.1
k1	9.4346	6.5764
k2	9.3532	6.5971
k4, psi	121605.6	122516.7
tn1, °C	524.4304	519.634
tn2, °C	521.241	499.6031
n0, psi	0.1235	0.0342
n1	19.0000	10.0000
n2	19.0000	10.0000
n4, psi	0.2168	0.1511

Figure K–4 shows stress-strain curves of Material ID 1 (see Table K–1 for the material description) at room and elevated temperatures. Figure K–4 (a) is a close-up view of a low strain range, while Fig. K–4 (b) shows strain levels up to 0.3.

The elastic-plastic behavior of steels is modeled with ANSYS material model "Multi–linear isotropic hardening von Mises plasticity."

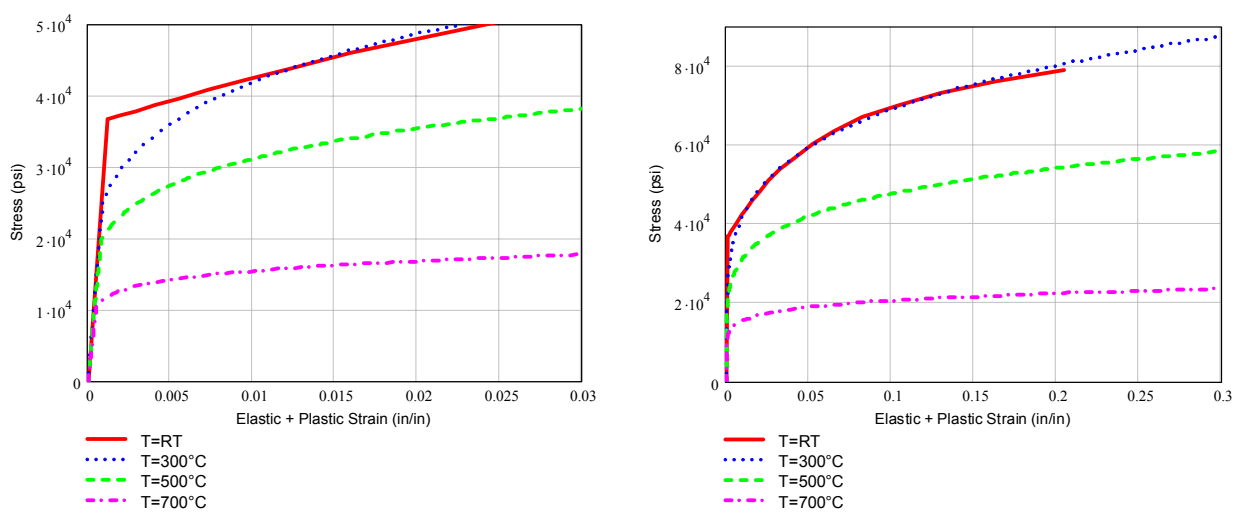

(a) Strain < 0.03 (b) Strain < 0.30

Figure K–4. Stress-strain relationships for Material ID 1 steel.

Creep: Steel creeps at elevated temperatures ($T \geq 350^{\circ}C$), and the creep behavior for steels is based on the creep model by Fields and Fields (1991), expressed as:

$$\varepsilon_{cr}(t,T,\sigma) = \frac{1}{100} a(T) \left(\frac{t}{60} \right)^{b(T)} \left(35.5 \frac{\sigma}{\sigma_{yRT}} \right)^{c(T)} \tag{7}$$

where:

$$a(T) = \begin{cases} 0 & \text{for} \quad T < 350^{\circ}C \\ 10^{-(6.1+0.00573T)} & \text{for} \quad 350^{\circ}C \leq T < 500^{\circ}C \\ 10^{-(13.25-0.00851T)} & \text{for} \quad 500^{\circ}C \leq T < 725^{\circ}C \end{cases}$$

$$b(T) = -1.1 + 0.0035T \quad \text{for} \quad T < 725^{\circ}C$$

$$c(T) = 2.1 + 0.0064T \quad \text{for} \quad T < 725^{\circ}C$$

This model is valid for the temperature range of $350^{\circ}C \leq T \leq 725^{\circ}C$. ANSYS uses the "time hardening creep" model, where creep strain rate is given by:

$$\frac{d\varepsilon_{cr}}{dt} = C_1(T)\sigma^{C_2(T)} t^{C_3(T)} \tag{8}$$

and $C_1(T)$, $C_2(T)$, and $C_3(T)$ are temperature-dependent parameters determined by Fields' (1991) creep model given as:

$$C_1(T) = \frac{1}{100} a(T) b(T) \left(\frac{1}{60} \right)^{b(T)} \left(\frac{35.5}{\sigma_{yRT}} \right)^{c(T)}$$

$$C_2(T) = c(T)$$

$$C_3(T) = b(T) - 1$$

Figure K–5 illustrates creep behavior of steel at elevated temperatures for Material ID 1. Figure K–5 (a) shows creep strain rate at different stress levels and different temperatures, and Fig. K–5 (b) compares elastic, plastic, creep, elastic plus plastic, and total strains at $T = 400^{\circ}C$ and after constant loading for 1,800 s.

Failure Criteria

The failure criteria for steel are defined in terms of plastic strains. The multiaxial fracture strain criterion for different steels and temperatures (Fields 2004) is as follows:

$$\bar{\varepsilon}_f = \alpha(T) \exp\left[-\frac{3}{2} \frac{\sigma_m}{\bar{\sigma}} \right] \tag{9}$$

where stress and strain are true stress and true strain.

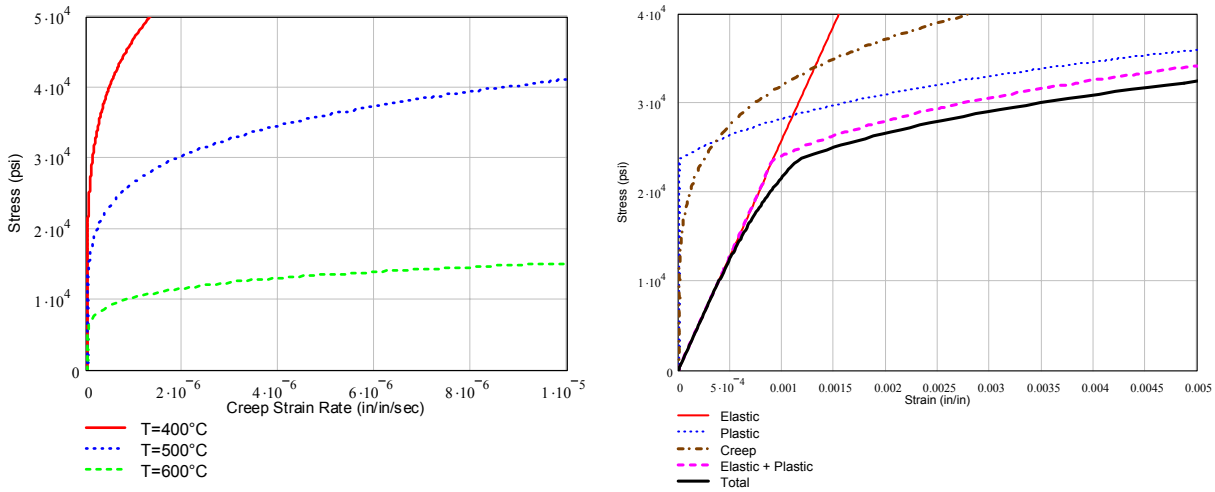

(a) Creep strain rate

(b) Comparison of different strains at T=400 °C and t=1,800 s

Figure K–5. Creep behavior at elevated temperatures for Material ID 1 steel.

For the uniaxial stress condition, the plastic strain at fracture reduces to:

$$\bar{\varepsilon}_{f_uni} = \exp(-0.5)\alpha(T) \tag{10}$$

Table K–3 shows the uniaxial plastic strain at fracture, $\bar{\varepsilon}_{f_uni}$, at different temperatures calculated by the equation above. This criterion is valid for the finite element analysis (FEA) with very fine mesh. For coarse mesh, the equivalent steel fracture criterion was determined numerically as follows. A standard tension test specimen was modeled in ANSYS. The gauge length, width, and thickness of the specimen were 8 in, 1.5 in, and 1 in., respectively, and Material ID 1 steel properties were used. Six different models (Model 0 to 5) were created, each having a different mesh size. Element sizes of Models 0 to 5 were 0.025 in., 0.050 in., 0.0125 in., 0.250 in., 0.375 in., and 0.75 in. It was assumed that Model 0 was able to capture tensile fracture in a uniaxial tension.

Model 0 was subjected to tension until the maximum plastic strain in the direction of applied displacement reached the uniaxial fracture strain determined by Eq. (10) for uniaxial stress condition, and the corresponding elongation of the specimen, Δ_0, was obtained. Models 1 to 5 were then subjected to the same elongation, Δ_0, and the maximum plastic strain in the direction of applied displacement was measured for each model. The maximum plastic strain due to the elongation of Δ_0 is defined as the limiting plastic strain (equivalent fracture plastic strain) for the corresponding element size.

From these six cases, a relationship between element size and equivalent uniaxial fracture plastic strain was established. This process was repeated for temperatures 20 °C, 100 °C, 300 °C, 500 °C, and 700 °C. Figure K–6 (a) shows the ratio of the maximum plastic strain in the direction of applied displacement due to displacement Δ_0 to uniaxial plastic strain by Eq. (10) vs. element size at different temperatures. The FEA results were extrapolated up to the element size of 50 in. Plastic strain shown in Fig. K–6 (b) is used as fracture criterion for the corresponding element size in the FEA.

Table K–3. Uniaxial plastic strain at fracture by Eq. (10).

Material ID	Plastic Strain at Fracture in the Uniaxial Test					
	20	100	300	500	700	1000
1	0.8411	0.6989	0.6610	1.0446	1.8100	3.5862
2	0.8411	0.6989	0.6610	1.0446	1.8100	3.5862
3	0.4908	0.4078	0.3857	0.6095	1.0561	2.0924
4	0.4908	0.4078	0.3857	0.6095	1.0561	2.0924
5	0.4908	0.4078	0.3857	0.6095	1.0561	2.0924
6	0.4908	0.4078	0.3857	0.6095	1.0561	2.0924
7	0.4908	0.4078	0.3857	0.6095	1.0561	2.0924
8	0.4908	0.4078	0.3857	0.6095	1.0561	2.0924
9	0.4908	0.4078	0.3857	0.6095	1.0561	2.0924
10	0.8891	0.7388	0.6987	1.1042	1.9142	3.7907
11	0.4908	0.4078	0.3857	0.6095	1.0561	2.0924
12	0.4908	0.4078	0.3857	0.6095	1.0561	2.0924
13	0.2846	0.2364	0.2236	0.3534	0.6123	1.2132
14	0.3774	0.3136	0.2965	0.4686	0.8120	1.6088
15	0.5338	0.4436	0.4195	0.6629	1.1486	2.2758
16	0.5623	0.4672	0.4418	0.6983	1.2099	2.3972
17	0.7752	0.6442	0.6092	0.9628	1.6681	3.3051
18	0.6545	0.5439	0.5143	0.8129	1.4084	2.7906
19	0.4254	0.3535	0.3343	0.5283	0.9154	1.8137
20	0.8411	0.6989	0.6610	1.0446	1.8100	3.5862
21	0.4908	0.4078	0.3857	0.6095	1.0561	2.0924

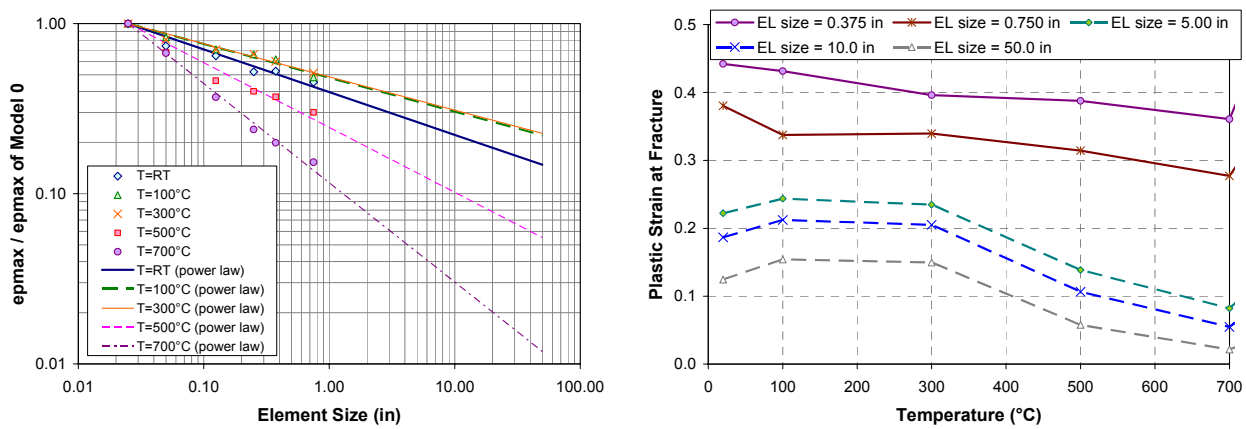

(a) FEA Results and Extrapolation (b) Recommended Limiting Plastic Strain

Figure K–6. Maximum plastic strain from the finite element analysis and limiting plastic strain.

K.5.3 Welds

The weld properties at all temperatures are assumed to be the same as those of the base metal of the same ultimate tensile strength. This assumption is validated by the following observations: the exterior column welds are strong enough to fail the base metal; the observed fractures in the exterior columns are mostly through the base metal; and the welds in trusses are resistance welds with no filler added. For the core columns, the area of the welds is significantly less than that of the base metal, and several fractures through the welds have been observed. Fractures in the truss seats and truss connections have also been observed. High temperature properties of the welding metals have not been found in the literature. Susceptibility of existing cracks in the welds to growth (fracture toughness) does not increase with temperature (Stevick 1994).

K.5.4 Bolts

A load-elongation relationship for 7/8 in. A325 bolt with 4 in. length at room temperature was provided by Project 3. Load-elongation relationships at elevated temperatures are constructed by scaling the loads by the yield and ultimate tensile strength reduction factors for bolt steels shown in Fig. K–3 (c) and (d). Figure K–7 shows the load-elongation relationships of a 7/8 in. bolt at different temperatures. Load-elongation relationships of A325 bolts of different size are scaled by proportioning the load by the ratio of the bolt thread area to the bolt body area for a 7/8 in. bolt.

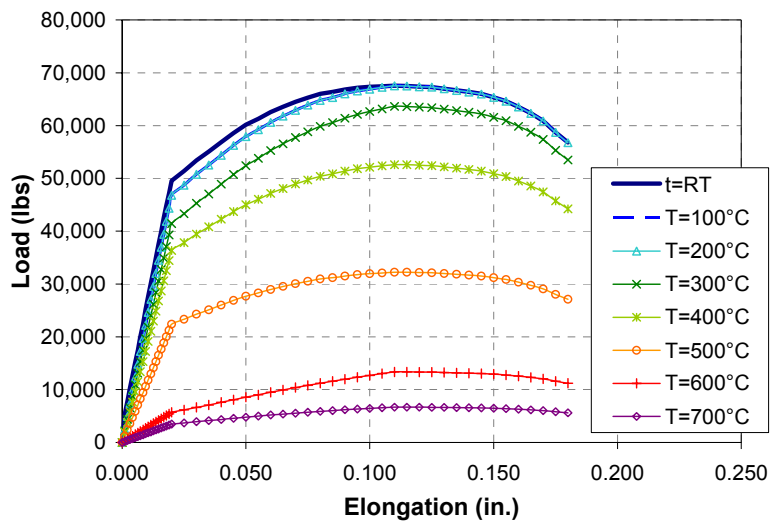

Figure K–7. 7/8 in. A325 bolt load-elongation curves at elevated temperatures.

The load-elongation relationship for bolts with a different length than 4.0 in. is expected to be very similar to the load-elongation relationship of 4.0 in. length as deformations are localized.

Based on the AISC formulas, C-J3–2 to C-J3–4, (AISC 2003), the shear strength for a single shear plane is calculated as 0.67 of the tensile strength given in Fig. K–7 when threads are excluded from the shear plane. When threads are not excluded from the shear plane, the nominal shear strength for a single shear plane is 0.53 of the tensile strength given in Fig. K–7. No shear ductility is assumed at failure.

K.5.5 Coefficient of Friction

The coefficient of friction of 0.33 for calculation of shear in friction-type connections is the AISC LRFD (2003) friction coefficient for uncoated clean mill scale steel surfaces, or surfaces with Class A coatings on blast-cleaned steel surfaces.

K.5.6 Symbols

$\alpha(T)$ = temperature-dependent material property that defines fracture criterion

$\alpha_c(T)$ = instantaneous coefficient of thermal expansion of concrete

$\alpha_s(T)$ = instantaneous coefficient of thermal expansion of steel

$\beta_y(T)$ = steel yield strength reduction factor due to elevated temperature

$\beta_u(T)$ = steel ultimate strength reduction factor due to elevated temperature

γ_c = unit weight of concrete (110 pcf and 150 pcf for lightweight and normal-weight concrete, respectively)

γ_s = Unit weight (490 pcf = 0.284 pci for all steel types at any temperature)

ε_{c1} = concrete strain at maximum compressive stress

ε_{cr} = creep strain of steel

ε_e = elastic strain

ε_{ep} = elastic plus plastic strain

$\bar{\varepsilon}_f$ = effective plastic strain at fracture

$\bar{\varepsilon}_{f_uni}$ = uniaxial plastic strain at fracture

ε_p = plastic strain

ε_{t1} = concrete strain at maximum tensile strength

ε_{tu} = concrete strain at full crack formation (separation) in tension

ν_c = Poisson's ratio of concrete

ν_s = Poisson's ratio of steel

$\bar{\sigma}$ = effective stress

σ_m = mean stress

σ_{yRT} = room temperature yield strength of steel

σ_{uRT} = room temperature tensile strength of steel

$E_s(T)$ = modulus of elasticity of steel

$E_c(T)$ = modulus of elasticity of concrete

F_1 = mix design factor = ratio of the actual 28 day cylinder strength to f_c'

F_2 = in-situ factor = ratio of in-situ 28 day strength to the 28 day cylinder strength

F_3 = aging factor = ratio of mature concrete strength to 28 day concrete strength

f_a = actual strength of in-place concrete

f_c' = specified 28 day strength

$f_c(T)$ = compressive strength of concrete

$f_t(T)$ = tensile strength of concrete

$K(T)$ = sigmoidal function of temperature with six parameters

$n(T)$ = sigmoidal function of temperature with six parameters

R_C = correction factor that has the following two functions: (1) to correct the strain rate effect introduced in the material testing and create the stress-strain curve for zero strain rate, and (2) to match the room temperature stress-strain curve at strain of 0.05

R_{TS} = ratio of the room temperature tensile strength of the steel of interest to the room temperature tensile strength of the steel used to develop the power law model

K.6 MODEL CONVERSION FROM SAP TO ANSYS

The SAP2000 (SAP) floor 96 Model of WTC 1 and the SAP Global Model of WTC 1 are converted into ANSYS. The goal of the conversion is to develop ANSYS models that match the SAP baseline models developed by Project 2 and can be used as a basis of the detailed thermal-structural evaluation. The converted ANSYS models will be modified to incorporate the nonlinear behaviors of the components and simplified for the thermal/structural evaluation of collapse initiation study.

K.6.1 Translation Procedure

Automatic translation software was developed to partially convert the floor model and global model from SAP2000 to ANSYS 8.0:

- The Joints, Frames, and Shells in the SAP model were translated into ANSYS Keypoints, Lines, and Areas. Using geometry definition instead of nodes and elements directly allows for ease in local mesh refinement.

- Lines were meshed with both section and real constants so that a translation between BEAM44 and BEAM188 elements can be achieved by simply changing element types. Areas were meshed with SHELL63 elements in ANSYS to match the Shell elements in SAP. Eventually, Lines and Areas will be changed to nonlinear BEAM188 and SHELL181 elements with a type change.

- Material properties were assigned according to the Criteria Document based on the material definitions and Frame section properties in SAP.

- Frame section properties in SAP were converted into Real Constants for BEAM 44 in ANSYS. Cross section properties in SAP were retained for future conversion into cross section data for BEAM188 elements. Shell thicknesses in SAP were converted into Real Constants for SHELL63 in ANSYS.

- Joint restraints in SAP were translated into DOF constraints in ANSYS.

- Frame distributed loads and area uniform loads were translated into surface loads on Lines and Areas in ANSYS.

- The ANSYS BEAM44 elements support element moment releases, but the ANSYS nonlinear BEAM188 elements do not. Therefore, Frame releases in SAP were modeled by coincident nodes with coupled (CP) degrees of freedom in ANSYS.

- The ANSYS BEAM44 elements allow beam end offsets in three directions, but the ANSYS nonlinear BEAM188 elements only allow beam end offsets perpendicular to the element axis through section offset (SECOFFSET) command. Frame insertion points in SAP were converted in two ways. For offsets along the element axis, additional nodes and rigid MPC184 elements with the proper lengths were used in ANSYS. For offsets perpendicular to the element axis, beam end offsets were defined using Real Constants for BEAM 44, and eventually will be defined using SECOFFSET command for nonlinear BEAM 188.

- Frame offsets and rigid panel factor in SAP were modeled by adding additional nodes and rigid MPC184 elements with the proper lengths in ANSYS.

Those parts of the model that were not converted by the translation software were converted manually.

K.6.2 Challenges

During the conversion of the SAP Floor Model, the following conditions were encountered and were resolved:

- The SAP Floor Model allows automatic division of the frames at joints. This causes problems in the translation software because the frame connectivities in the Graphical User Interface do not show the actual internal element connectivities used in the SAP analysis engine. In order to resolve this problem, the translation software was modified to use the internal element connectivities. The table of internal connectivities was exported from the SAP model after the execution of the analysis.

- Automatic offsets in the SAP model are not available in the ASCII SAP input file prior to the execution of the analysis. The table of element offsets was exported after the execution of the analysis.

- There are both intentional and unintentional duplicate elements in the SAP Floor Model. Each leads to problems in the translator since ANSYS cannot have duplicate lines sharing the same key points. Some duplicate elements are used to model additional steel plates at the ends of the trusses. The duplicate elements were manually deleted and the section properties of the remaining elements were modified to account for the additional steel. Some duplicate elements are from frame elements which have different lengths and are overlapping each other. These were manually corrected.

K.6.3 Status

The automatic translation software developed to convert models from SAP2000 to ANSYS was applied to the floor model and will be applied to the global model shortly. Figures K–8 through K–11 show the converted floor model.

The following analyses were performed to validate the converted ANSYS floor model against the original SAP model.

- One static analysis with gravity loads as defined in SAP as Load Case "DEAD" which include self-weight plus 3.5 psf uniform load in the office area.
- One modal analysis, using structural mass only.

Table K–4 summarizes the comparison of the SAP and ANSYS results for the gravity load case. The total reactions for the SAP and ANSYS models are within 0.1 percent of each other. The maximum slab displacement predicted by the ANSYS model is 3.2 percent smaller than that obtained from the SAP model. This discrepancy is currently under study and is being resolved. The deformed shapes of the gravity load case for the SAP and ANSYS models are shown in Figs. K–12 and K–13.

Table K–4. Comparison of SAP and ANSYS results for gravity load case.

	SAP	ANSYS (BEAM 188)
Total reaction, kip	2,212.81	2,210.85 (-0.09 %)
Maximum slab displacement, in.	0.718	0.695 (-3.2 %)

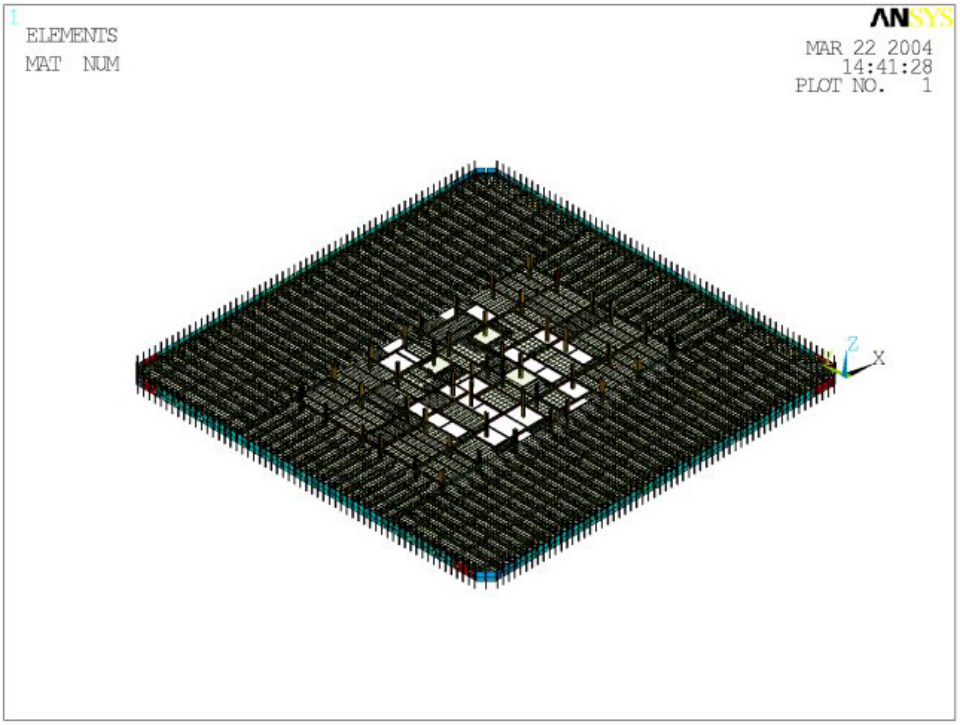

Figure K–8. Converted ANSYS model for floor 96 of WTC 1: overall view.

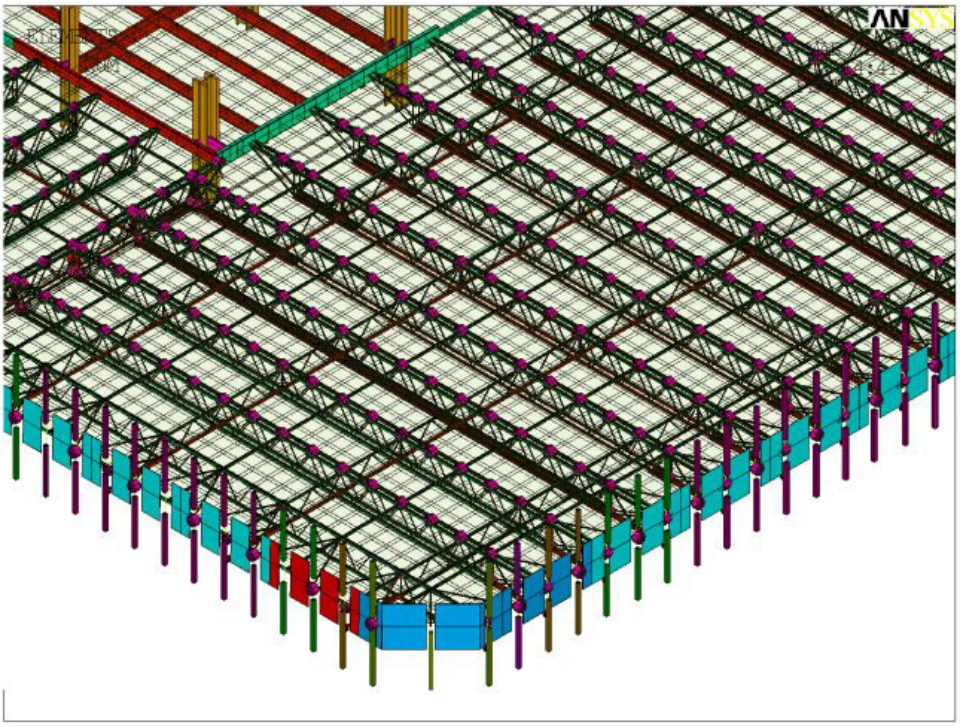

Figure K–9. Converted ANSYS model for floor 96 of WTC 1: partial view near corner of building.

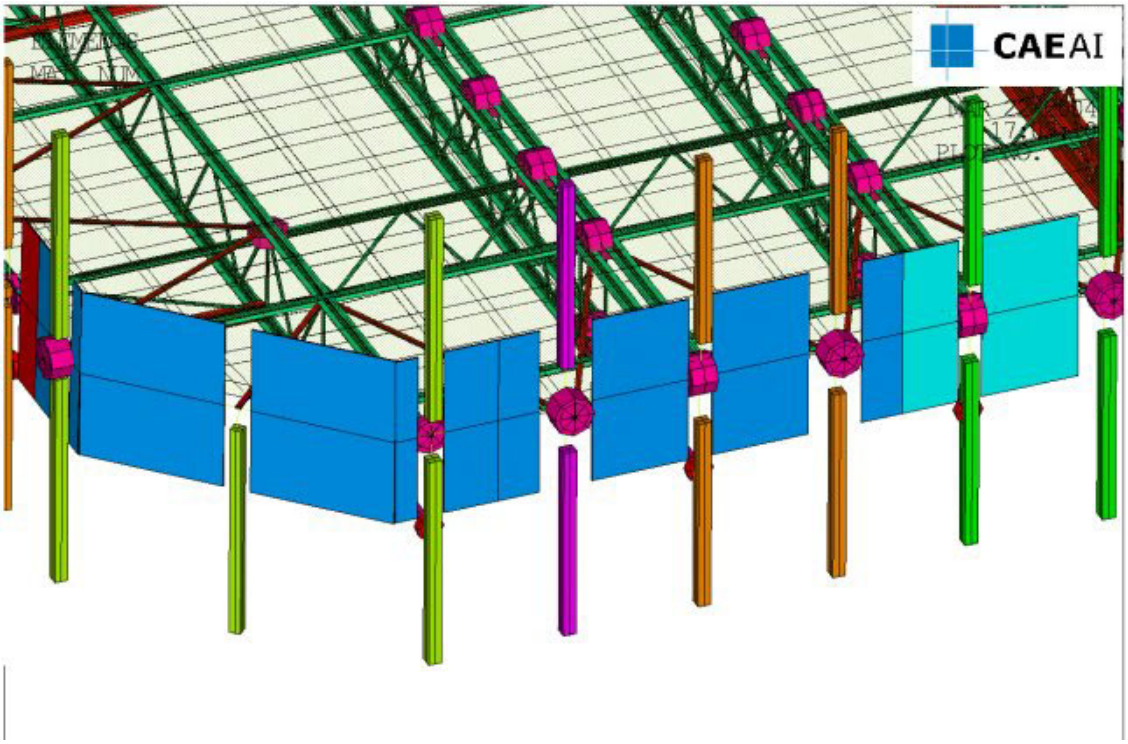

Figure K–10. Converted ANSYS model for floor 96 of WTC 1: close-up view at corner of building.

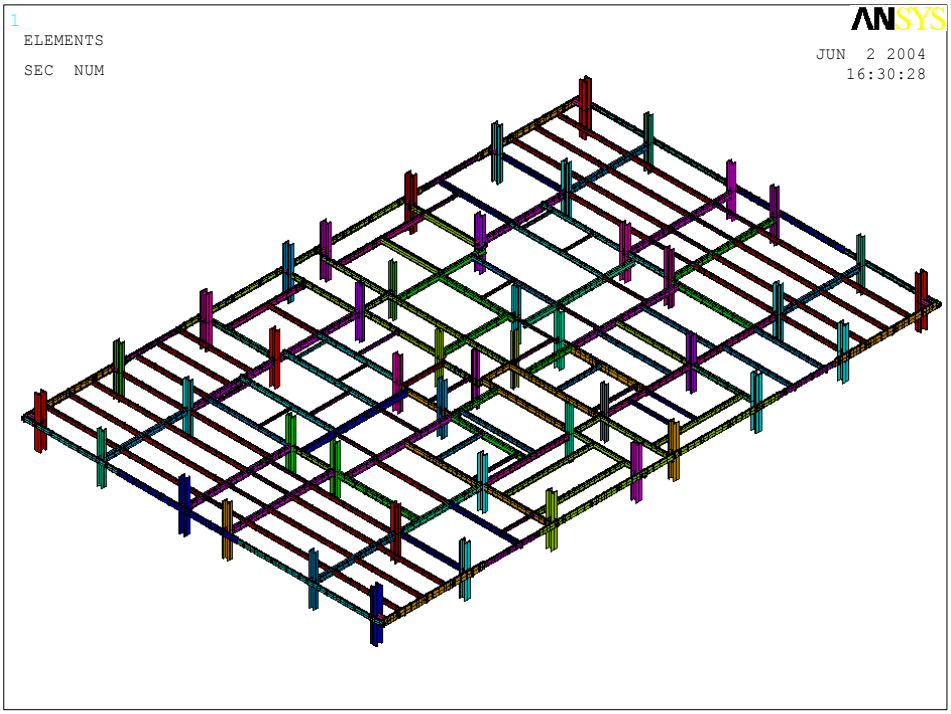

Figure K–11. Converted ANSYS model for floor 96 of WTC 1: view of floor beams and columns.

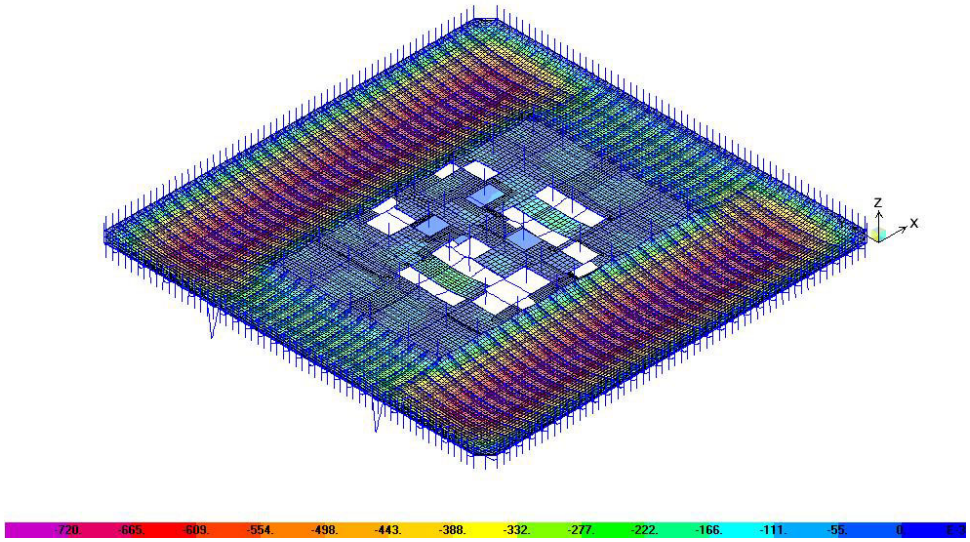

Figure K–12. Deformed shape (x100) of gravity load case for SAP floor model.

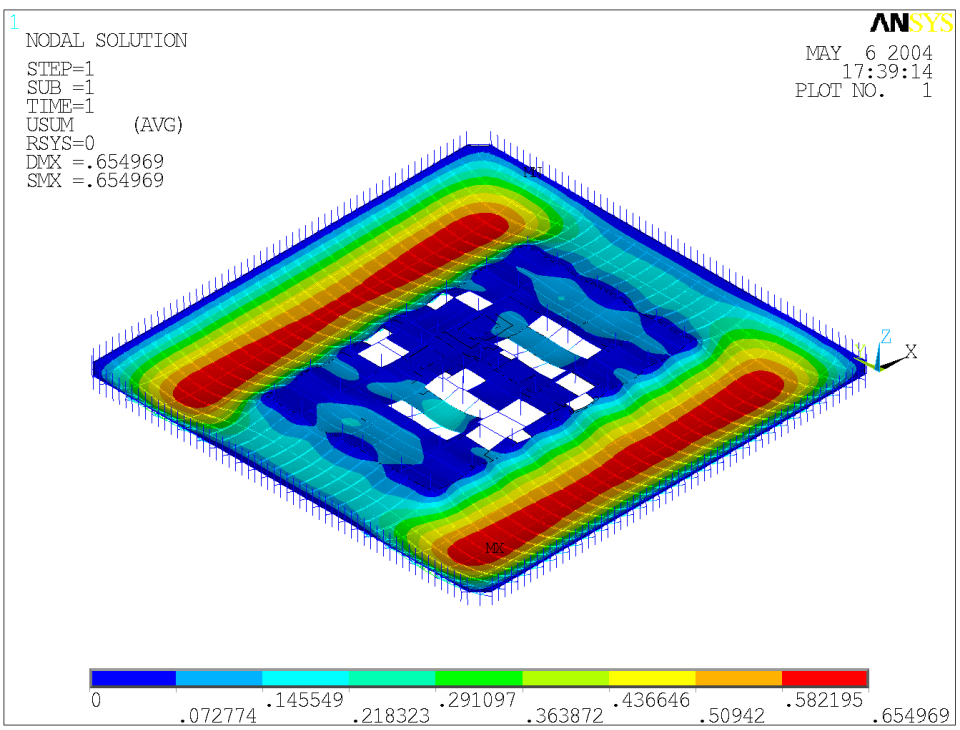

Figure K–13. Deformed shape (x100) of gravity load case for ANSYS floor model with BEAM44 (Euler beam) elements.

Table K–5 summarizes the comparison of the SAP and ANSYS results for the modal analysis. The total masses of the SAP and ANSYS models are within 0.02 percent of each other. The dominant natural frequency of the floor predicted by the ANSYS model is 2.5 percent higher than that obtained from the

SAP model. This discrepancy is consistent with the discrepancy observed for gravity displacement, and is currently under study and is being resolved. The dominant mode shapes of the floor for SAP and ANSYS models are shown in Figs. K–14 and K–15.

Table K–5. Comparison of SAP and ANSYS Modal Analysis Results.

	SAP	ANSYS (BEAM 188)
Total mass, lb·sec^2/in.	5448.7	5447.7 (-0.018 %)
Dominant natural frequency of floor, Hz	4.32	4.43 (+2.5 %)

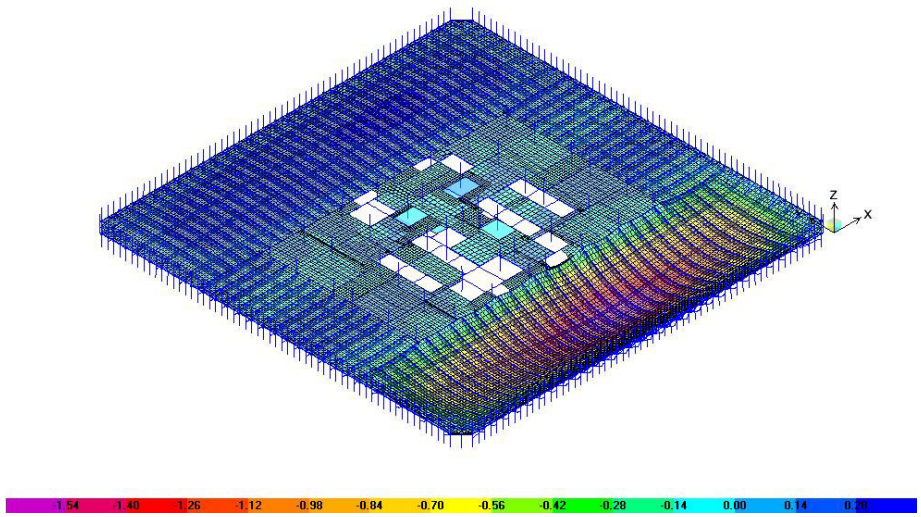

Figure K–14. Dominant mode shape (frequency = 4.32 Hz) of floor structure for SAP floor model.

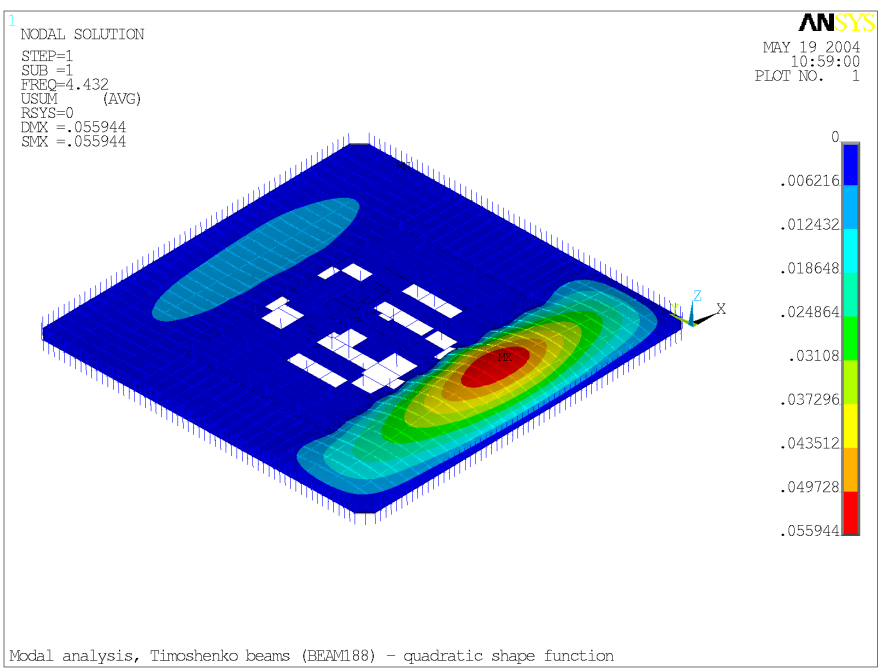

Figure K–15. Dominant mode shape (frequency = 4.43 Hz) of floor structure for ANSYS floor model.

K.7 FULL FLOOR SUBSYSTEMS

The full floor model is analyzed using the ANSYS general purpose finite element program Version 8.0. The objectives of the analysis are:

- To identify the most likely failure modes,
- To evaluate
  - Failure loads,
  - Temperatures at failure,
  - Time-to-failure, and
  - Changes in mechanical properties and geometry at failure.
- To simplify the model and to reduce the computational efforts for incorporation into the global model.

The failure modes and the failure loads of different components of the full floor subsystem are evaluated through analysis of detailed models of those components, using either hand calculations or FEAs. Simplified models that capture the failure loads and failure modes are then developed for each component. These simplified models of components are incorporated in the full floor subsystem model.

In this chapter, after a general description of the full floor model, the analyses of important components are presented and discussed.

K.7.1 Full Floor Model

Model Description

The floor model is developed using the converted SAP2000 model for floor 96, with the following modifications:

1. Combine two adjacent trusses into a single truss. The elements in the truss model have double the areas of elements in each real truss.

2. Change rigid beams at knuckle locations to user-defined elements with the properties of the knuckle determined by the component knuckle model.

3. For compression diagonals, add user-defined elements to account for buckling of diagonals.

4. For truss ends and connections, add user-defined elements to account for truss seat failure.

5. Pin concrete slab for out-of-plane rotation at both its interior and exterior edges.

6. Use user-defined elements along the edge nodes of the concrete slab to model the tensile strength of the concrete slab and the in-plane shear capacity at the connection to the spandrel plate.

7. Remove the spandrels defined as beam sections in SAP2000 model and replace them with SHELL181 elements in ANSYS. (This modification eliminates the need for defining panel zone stiffness.) The new spandrels will wrap continuously around the floor. Each spandrel plate between columns will be represented by 16 elements, 4 in. height and 4 in. width. Material and geometry assignments are carried through to ANSYS.

8. Change the elastic column elements as translated into ANSYS to user-defined sections with BEAM189 elements with plasticity and creep.

9. Make new column sections within the limits of the spandrels with reduced Plate 3 thickness, say 0.005 in. in thickness, to insure correct modeling of torsional stiffness. Spandrel thicknesses should be reduced within the limits of the column by the same thickness. Connect the centerline of column to spandrel with rigid elements.

Material Properties

ANSYS's multilinear isotropic hardening von Mises plasticity with time hardening for temperatures below 350 ^{o}C is used for the beam elements representing the truss system, girders, beams, and columns in areas where plasticity is either anticipated or expected to occur by analysis. This material model with creep is used for temperatures above 350 °C. This material model is used for shell elements representing the spandrel plates, when appropriate.

Loading

The full floor model is analyzed for dead and live loads first, and then thermal loads are applied to model the path dependent nonlinear response. The thermal loads are provided by Project 5 and include temperatures and temperature gradient time-histories for all structural members in the full floor model for (1) standard fire, (2) representative building fire scenarios, and (3) different fire protection scenarios.

Boundary Conditions

The beam elements representing the columns are restrained vertically at floor 95. The outward and tangential displacements and all rotations of the column ends at floors 95 and 97 are fixed to restrain thermal expansion. Mass elements defined by the tributary dead and live loads are added to the top of the columns and at connections to floor 96.

Failure Modes

The possible failure modes of the floor subsystem are as follows:

1. Sagging: Floor sagging along the axis of the main trusses may be caused by (1) loss of stiffness and softening of truss at high temperature, (2) catenary action of the truss due to plastic bending or buckling of critical members required for truss action, or (3) loss of composite action of floor-to-knuckle failure. These are discussed in some detail under truss failure modes. Floor sagging may result in component failure due to tension in the truss seats, tension in the floor subsystem, tension on the connections to the exterior walls, lateral

loads on columns, and increased demand on other components of the floor subsystem, for example, bridging trusses and transfer trusses and their connections.

2. Edge Sagging: Edge sagging results from failure of truss seat connections at either the interior or exterior supports and is evidenced in videos. Edge sagging, similar to sagging, increases demand on other components of the floor subsystem, reduces buckling strength of columns, and can lead to failure of a floor.

3. Loss of Support: Abrupt failure of the floor subsystem can result from loss of truss support for a large number of adjacent parallel trusses. Loss of a truss support can occur due to (1) vertical shear load due to debris and/or impact load of the dropping floor above, (2) vertical and horizontal shear loads resulting from slab expansion acting on column truss seats (3) tension acting on column truss seats, and (4) cooling of a truss shortened by plastic deformation and loss of composite action. Failure of truss support will increase the demand on the adjacent trusses and can result in sequence of truss seat failure, edge sagging, and ultimately failure of the floor subsystem.

4. Expansion of Floor System: Expansion of floor results in deformation of columns and forces at corners of the exterior wall subsystem. Such corner forces can initiate a failure sequence of columns near the corners. Such a failure includes development of horizontal shear in the gusset plates and the exterior column truss seats, large forces in the straps, and large lateral x and y forces in columns, especially near the corners.

K.7.2 Knuckle Analysis

The “knuckle” is formed by the extension of the truss diagonals into the concrete slab and provides for composite action of the steel truss and concrete slab. The composite action is due to the shear transfer between the knuckle and the concrete slab both in the truss transverse and longitudinal directions.

The objective of this analysis is to predict the knuckle capacity when the truss and concrete deck act as a composite member and to develop a simplified model of the knuckle behavior to be included in the full floor subsystem model.

Knuckle Shear Tests

Two sets of experiments were performed in 1967 at Laclede Steel Company in Saint Louis, Missouri, to determine the transverse and longitudinal shear capacities of the knuckle.

The transverse shear test consists of double knuckles placed into two reinforced concrete blocks that were confined on the corners by angles as shown in Fig. K–16. The concrete density of 110 pcf corresponds to the lightweight concrete in the office areas. The concrete compressive strengths reported for 7 day and 27 day cylinder tests were 1,330 psi, and 2,600 psi, respectively. The inner ends of the two knuckles were connected through channels to a #11 rebar and the rebar was loaded until the concrete failed. The tests were conducted at concrete age of 6 and 27 days. The primary failure mode observed was concrete shear failure. The pictures from the tests show formation of the shear crack in one of the concrete blocks and edging of the channel into the concrete. The transverse shear capacity of the knuckle as the average of the

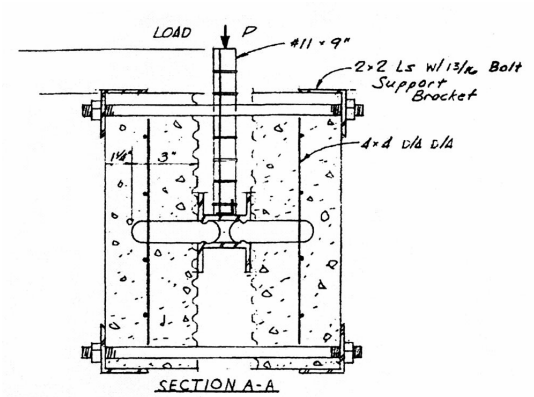

Drawing provided by Laclede Steel.

Figure K–16. Transverse shear test of a knuckle.

two reported tests is 16.9 kip per knuckle. After adjusting it for the strength of in-place, mature, lightweight concrete in the slab of 4,100 psi relative to the average strength of the lightweight concrete used in the test of 1,965 psi, by multiplying by the ratio of 4,100 to 1,965 psi, the transverse shear capacity of the knuckle is approximately 35 kip per knuckle.

The longitudinal shear test consists of double knuckles placed into two concrete blocks as shown in Fig. K–17. The test specification shows corner angles confining concrete blocks and no reinforcement for the concrete. However, the test pictures show reinforcement in both directions for each concrete block, with the corner angles dismantled. The test specification calls for concrete density of 152 pcf, which corresponds to a normal-weight concrete. The slab in office areas is of lightweight concrete. The average strength of two 28 day cylinders tested is 4,290 psi. A third sample, tested after 96 days, showed a strength of 2,850 psi. The test specification does not identify the weld size connecting the inner ends of the two knuckles to two channels. However, the primary failure mode observed for three tests is weld failure. Weld failure is not identified as the failure mode of the knuckle for the other two tests. The results of the shear tests of the knuckle in the longitudinal direction based only on these two tests are approximately 28.3 kip per knuckle. After adjusting for the strength of in-place, mature, lightweight concrete in the slab of 4,100 psi relative to the 28 day corrected average strength of the normal-weight concrete used in the test of 3,707 psi, by multiplying by the ratio of 4,100 psi to 3,707 psi, the longitudinal shear capacity of the knuckle is approximately 31 kip per knuckle.

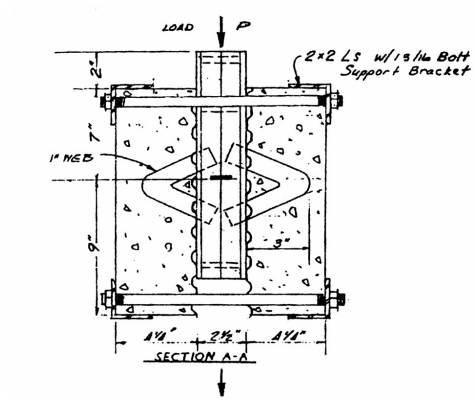

Drawing provided by Laclede Steel.

Figure K–17. Longitudinal shear test of a knuckle.

The effect of temperature on the knuckle is as follows:

- The steel knuckle conducts the temperature of the diagonal without much loss into the cool concrete. Concrete has a low coefficient of conductivity and does not respond rapidly to the rise of temperature.

- Concrete in the intermediate proximity of the metal knuckle will heat to a temperature close to that of the steel.

- Shear failure of the knuckle is initiated by the failure of concrete in close proximity to the knuckle. Final failure will engage not only the hot concrete in close proximity of knuckle, but the cooler concrete farther away.

- It is reasonable to assume that for gas temperatures in the range of RT to 450 °C, 650 °C, 850 ^{o}C, and 1050 ^{o}C , the knuckle metal temperature is below 375 ^{o}C, 550 ^{o}C, 725 ^{o}C, and 900 ^{o}C, and the average concrete temperature is below 300 ^{o}C, 450 ^{o}C, 600 ^{o}C, and 750 ^{o}C, respectively.

Neglecting the difference in thermal expansion of concrete and steel, for gas temperatures of RT, 450 ^{o}C, 650 ^{o}C, 850 ^{o}C , and 1050 ^{o}C, the expected concrete strength is in the range of 4,100 psi, 3,300 psi, 2,600 psi, and 2,000 psi, and the knuckle capacity in either direction is 30 kip, 24 kip, 19 kip, and 15 kip, respectively.

Knuckle Test Finite Element Model

Finite element models, shown in Fig. K–18, represent one quarter of the knuckle test specimens. The knuckle and channel members in the test set up are modeled by solid steel elements. Concrete Pseudo Tensor model and the LS-DYNA computer program were used for the analysis. An imposed ramped displacement was applied to the angle member.

The concrete strength used in the finite element model for the longitudinal shear of the knuckle was 4,100 psi and for the transverse shear of the knuckle was 2,500 psi. In addition 0.47 percent steel reinforcement representing welded wire fabric reinforcement of the slab was added in a distributed way to the concrete. Also, two different assumptions were made about the interface condition between the concrete and the steel: fully bonded and frictionless.

The results of the analysis are shown in Figs. K–19 through K–22. They show significant dependence on the characteristic of the interface between the steel and concrete. The longitudinal shear test FEA results, shown in Fig. K–21, show that each knuckle has strength in the range of 15 kip to 35 kip, depending on interface. The test results show that the interface is closer to fully bonded case. For the transverse shear, the FEM results, Fig. K–22, show that transverse knuckle strength is about 24 kip for 2,500 psi concrete, corresponding to 39 kip for 4,100 psi concrete. Figure K–20 shows that for transverse shear concrete crushes in a small region next to the knuckle and extending in front of the shear load. Figure K–20 also shows large regions of crushing at the lower boundary of the model. These regions are the result of imposing the boundary condition UY=0. This boundary condition, and the crushing at the boundary, although realistic for the test, would not obtain in a pair of transversely loaded knuckles of the double

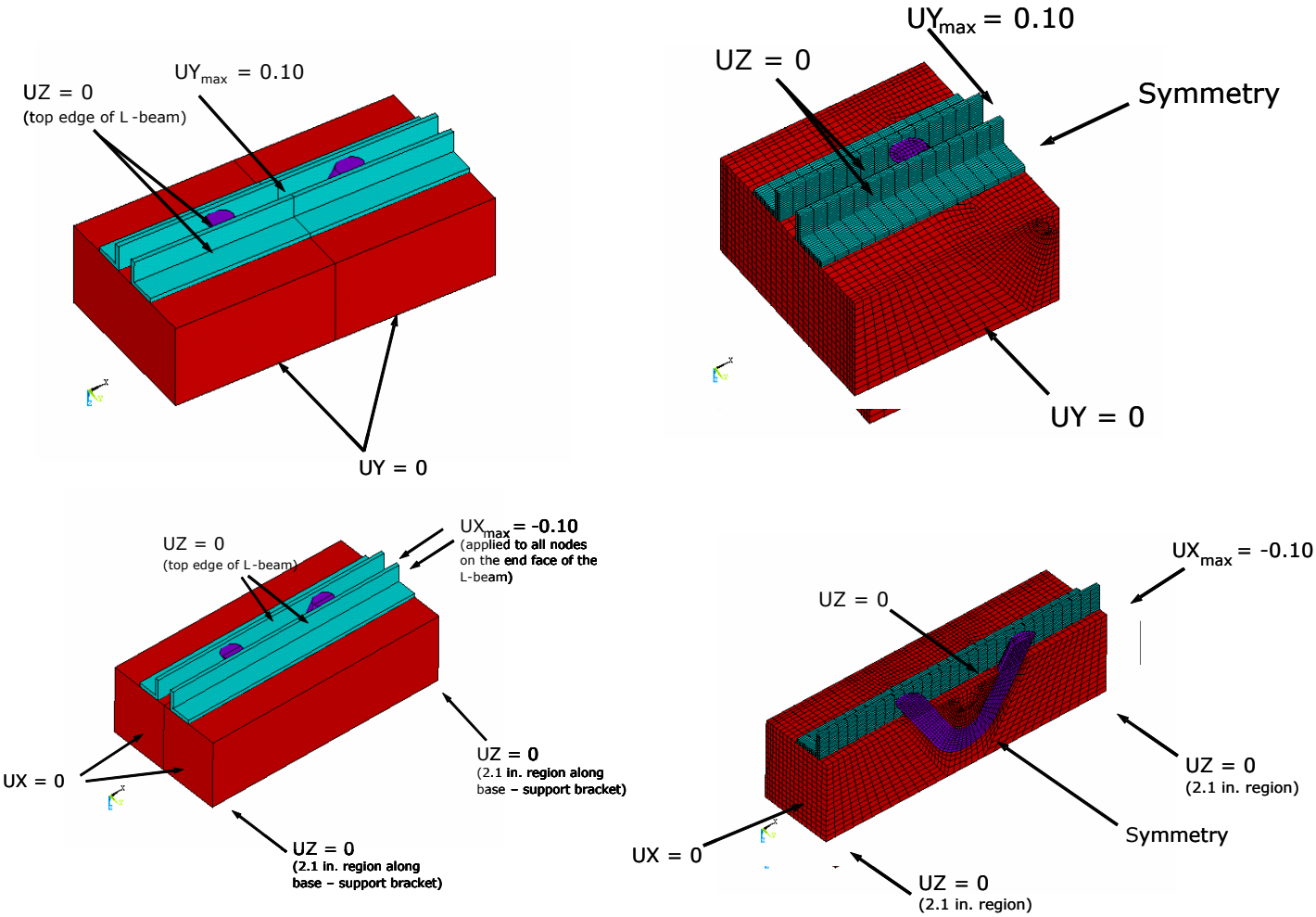

Figure K–18. Finite element models of knuckle shear tests.

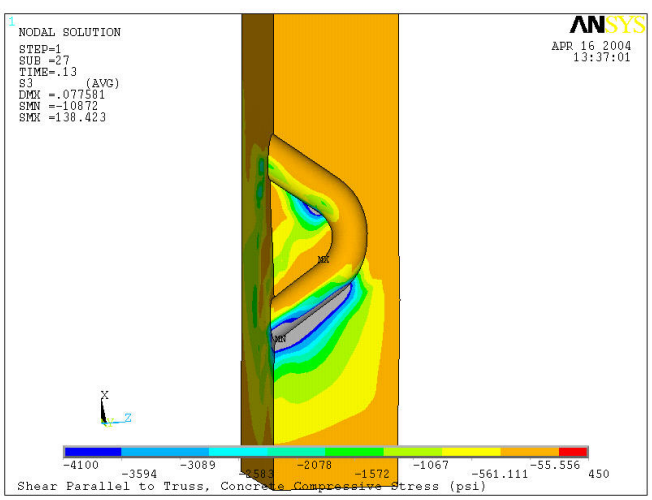

Figure K–19. Compressive stresses in longitudinal shear finite element model.

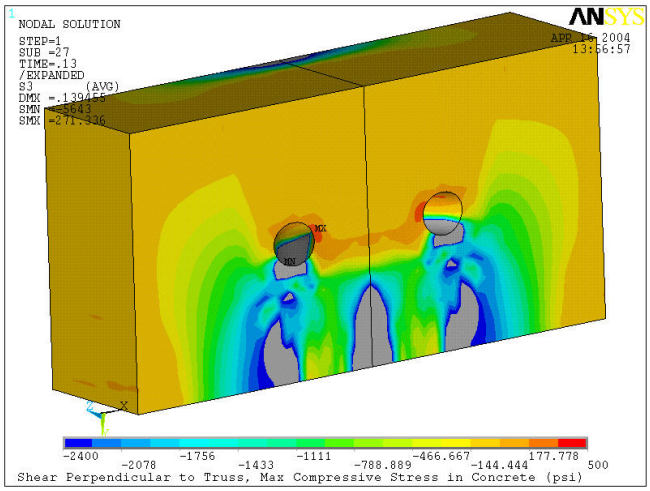

Figure K–20. Compressive stresses in transverse shear finite element model.

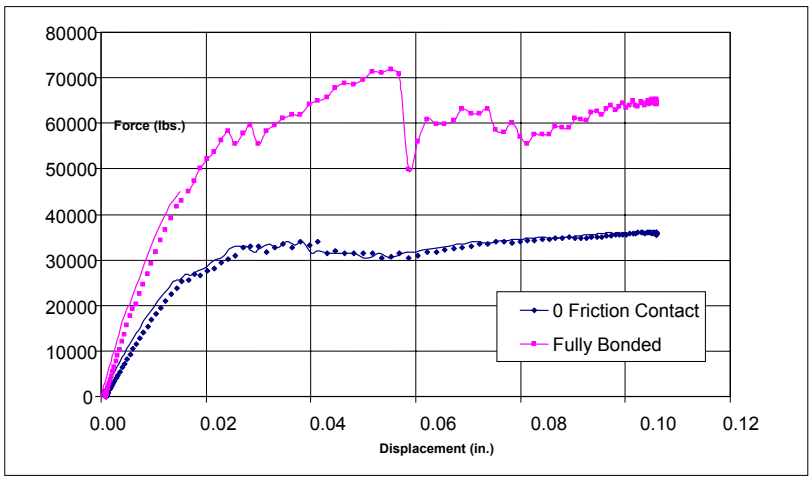

Figure K–21. Shear force versus displacement from finite element model for longitudinal shear of two knuckles.

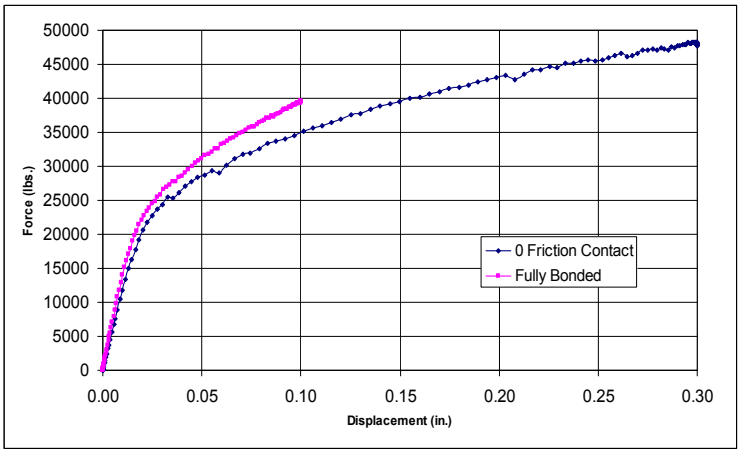

Figure K–22. Shear force versus displacement from finite element model for transverse shear of two knuckles.

truss. The small crushing regions at the knuckle indicate that a pair of knuckles in a double truss can be expected to behave nearly independently of each other, and, therefore, have nearly double the capacity of a single knuckle. Unfortunately, test results are not available that would confirm this conclusion.

Although the analysis shows the sensitivity of the results to the interface assumptions, it justifies the shear capacities computed from the test results.

Knuckle Model

The purpose of the detailed finite element analysis of the knuckle is to provide a basis for deriving a simple model for use in analyses of the full floor. The knuckle model includes segments of concrete floor and truss diagonal that protrudes into the 4 in. thick concrete. The dimensions of the concrete included in the model are one half of the double truss spacing of 40 in. The diameter of the truss diagonal included in the model is 1.09 in., and the center line of the knuckle is 3 9/16 in. from the center line of the double truss. The concrete slab wire mesh reinforcement is modeled by distributed reinforcement properties.

The model is bounded by four planes. Two of these planes are parallel to the chord of the truss, and the other two planes are perpendicular to the chord. Symmetry conditions are applied to these planes consistent with the loads. For the tension loading, in addition to the symmetry conditions, the model is supported vertically at both symmetry planes that are perpendicular to the truss chord. For the shear load parallel to the chord, the model is supported ahead of the shear load in the direction parallel to the chord.

The knuckle has the properties of ASTM A36 (Material ID 20) round bar steels and the concrete has lightweight concrete properties specified for LS-DYNA with concrete-cap model.

K.7.3 Column Truss Seats

In this section, likely failure modes of truss seats are identified, and the corresponding failure loads are determined. The following loading conditions were considered: vertical force, horizontal tensile force, horizontal compressive force, and combined vertical and horizontal force.

Description of Column Truss Seats

The floor truss is supported at the exterior wall and at the core by seats. The truss seat at the exterior wall and at the core will be referred to as *exterior seat* and *interior seat*, respectively.

The interior seat consists of a horizontal plate with two vertical plate stiffeners as shown in Fig. K–23. These plates are fillet welded together and fillet welded to the core channel beam. Two 5/8 A325 bolts (one bolt in each truss) connect the truss to the seat. The bolt connection is a friction type connection with 1 3/4 in. long slotted holes in the seat and 7/8 in. oversize holes in the bearing angles.

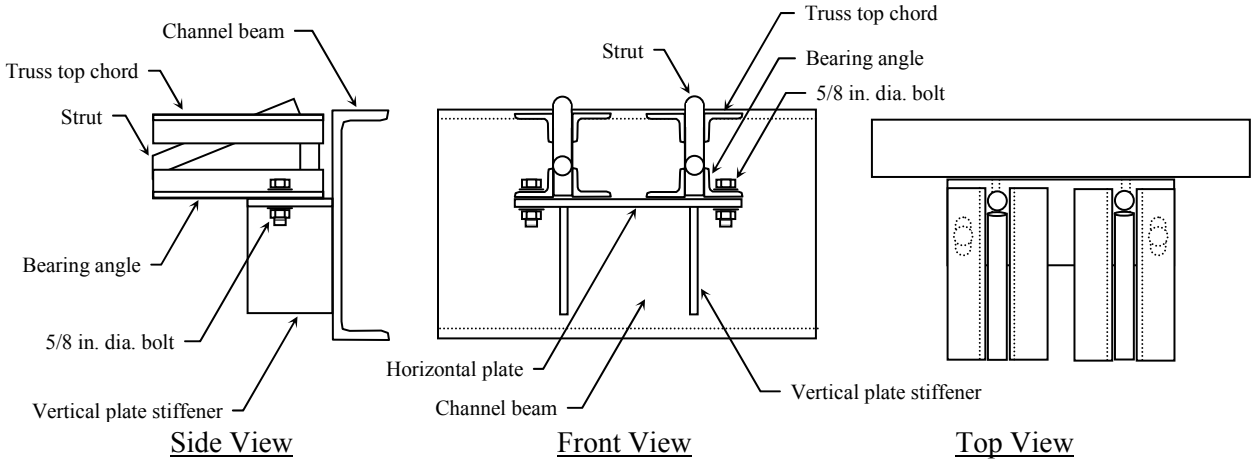

Figure K–23. Interior seat.

The exterior seat consists of a seat angle attached to the spandrel with two vertical plates (stand-off plates), and a gusset plate as shown in Fig. K–24. Fillet welds connect the seat angle to the stand-off, the stand-off to the column/spandrel, and the gusset plate to truss top chord. A complete-joint-penetration groove weld connects the gusset plate to the column/spandrel. Similar to the interior seat, each pair of trusses is attached to the exterior seat by two 5/8 in. A325 bolts. The bolt connection is a friction type connection with 2 in. long slotted holes in the seat angle and 7/8 in. oversize holes in the truss-bearing angle.

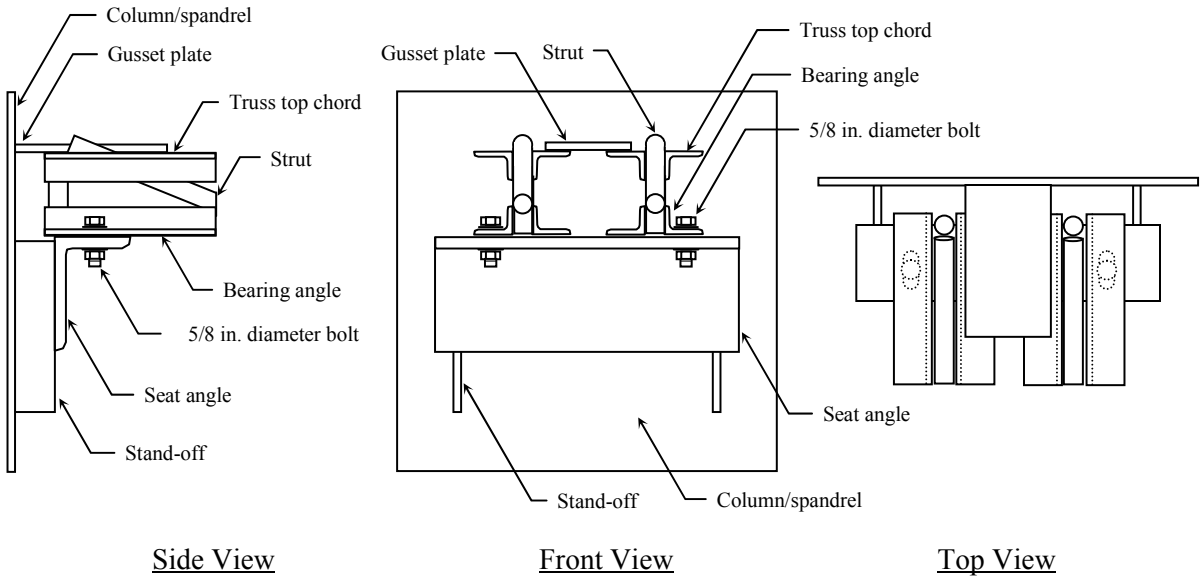

Figure K–24. Exterior seat.

In floor 96 of WTC 1, there are seven types of interior seats and eight types of exterior seats. The different types of interior seats are identified with Detail Numbers 15, 17, 20, 21, 22, 23, and 226A; and the exterior seats with Detail Numbers 1013, 1111, 1212, 1311, 1313, 1411, 1511, and 1611, as shown in Fig. K–25.

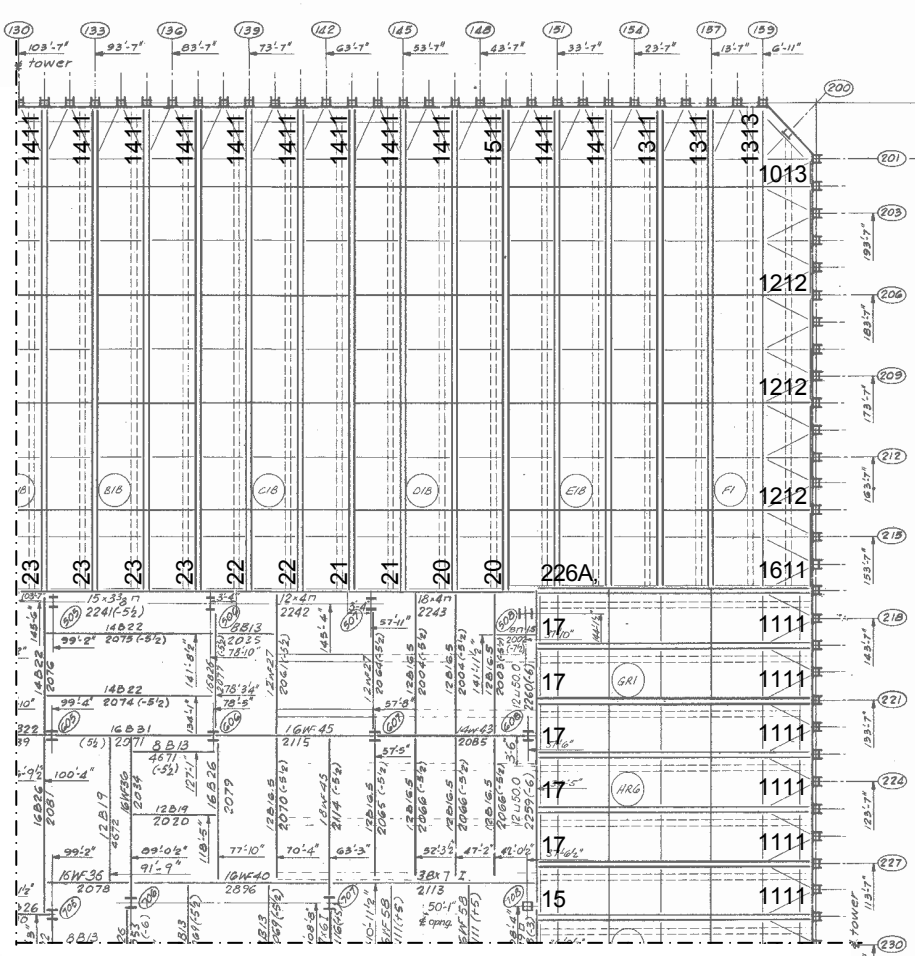

Original drawing provided with permission from PANYNJ.

Figure K–25. Truss seat detail location on northeast quadrant of floor 96 of WTC 1.

All types of interior seats are similar in their design, but are all unique because of the variation in the size of the vertical and horizontal plates, the location of the bolt holes, and the size of the fillet welds. The thickness of the plates ranges from 0.375 in. to 0.75 in.; the distance between bolt holes ranges from 8.5 in. to 10.5 in.; and the size of the fillet welds ranges from 0.25 in. to 0.375 in. All types of exterior seats are also similar in their design, but are all unique because of the variation in the size of the stand-off, and size of the seat angle, the size and shape of the gusset plate, the location of the bolt holes, and the size of fillet welds. The vertical height of the stand-off ranges from 8 in. to 11 in. The smallest seat angle size is L4 × 4 × 1/2, and the largest is L6 × 4 × 3/4. The shapes of the gusset plate are rectangular and trapezoid, and the plate ranges in width from 4.5 in. to 6 in. The distance between bolt holes ranges from 3.25 in. to 10.5 in., where it is 3.25 in. when the seat is supporting a single truss. The size of the fillet welds ranges from 0.2125 in. to 0.375 in.

Truss Seat Material Properties

The material properties used in the calculations were selected from Table K–1 to best match the material properties indicated in the design drawings. Figure K–3 was used to determine the material mechanical

properties at high temperature. The material properties used for truss seat calculations are summarized in Table K– 6.

Table K–6. Material properties used for truss seat calculations.

Description		Selected Material ID
Exterior and interior seat	A325 bolts	Material 22
	Fillet welds	Material 7
	Truss bearing angles	Material 21
Exterior seat	Seat angle	Material 1
	Gusset plate	Material 12
	Stand-off	Material 23
	Truss top chord angles	Material 21
	Cover plate for bridging truss top chord	Material 1
Interior seat	Vertical plate stiffener	Material 12
	Horizontal plate	Material 12

Truss Seat Failure Modes and Sequence

The failure modes of different truss seats are identified for vertical force, horizontal tensile force, horizontal compressive force, and combined vertical and horizontal force.

Failure Modes of Interior Seat against Vertical Force: The location of the vertical load on the truss seat is eccentric to the plane of fillet weld connection between the truss seat and the channel beam. Hand calculations have shown that the fillet welds at this connection, which must resist shear and bending, control the truss seat capacity. The failure mode is fracture of the fillet welds at this connection, which results in loss of the truss vertical support.

Failure Modes of Interior Seat against Horizontal Tensile Force: The failure modes considered are (1) bolt shearing, (2) bolt bearing, (3) bolt tear-out, and (4) block shear failure. Hand calculations have shown that the bolt shear strength controls the truss seat capacity. Bolt shear by itself, however, does not cause the truss to lose its vertical support, but it is the prerequisite to the truss walking off the seat. The travel distance required for the truss to walk off of the seat is 4 in.

Failure Modes of Interior Seat against Horizontal Compressive Force: The concrete slab above the truss seat connection provides the compressive force resistance. If the concrete slab fails, the truss seat has resistance against compressive force from bolt friction and surface friction between the seat and bearing angles. Additional resistance is developed when the truss comes into contact with the channel beam. Travel distance for the truss to come into contact with the channel beam is 1/2 in. Under compressive force, the truss will not lose its vertical support.

Failure Modes of Interior Seat against Combined Vertical and Horizontal Forces: Under combined vertical and horizontal forces, the failure modes are a combination of the individual failure modes for vertical and horizontal forces.

Failure Modes of Exterior Seat against Vertical Force: The location of the vertical load on the seat is eccentric to the plane of connection between the seat and the spandrel. Because of this eccentricity, the

truss seat must resist both shear and bending. Finite element analysis of the truss seat was used to determine load paths and evaluate the behavior of the seat connection.

Figure K–26 shows the finite element model of the seat connection, where half of the seat was modeled and symmetry boundary conditions were applied. The results of the finite element analysis show that shear force is carried primarily by the stand-off plates shown in Fig. K–24, while the bending moment is resisted by tensile force in the gusset plate and compressive force in the stand-off plate. The seat restrains the moment until horizontal force in the connection causes slippage between the seat angle and bearing angle. Fillet welds at the stand-off to spandrel connection, which must resist shear, bending, and compression, control the seat capacity. The failure mode is fracture of the fillet welds as this connection, which results in loss of truss vertical support.

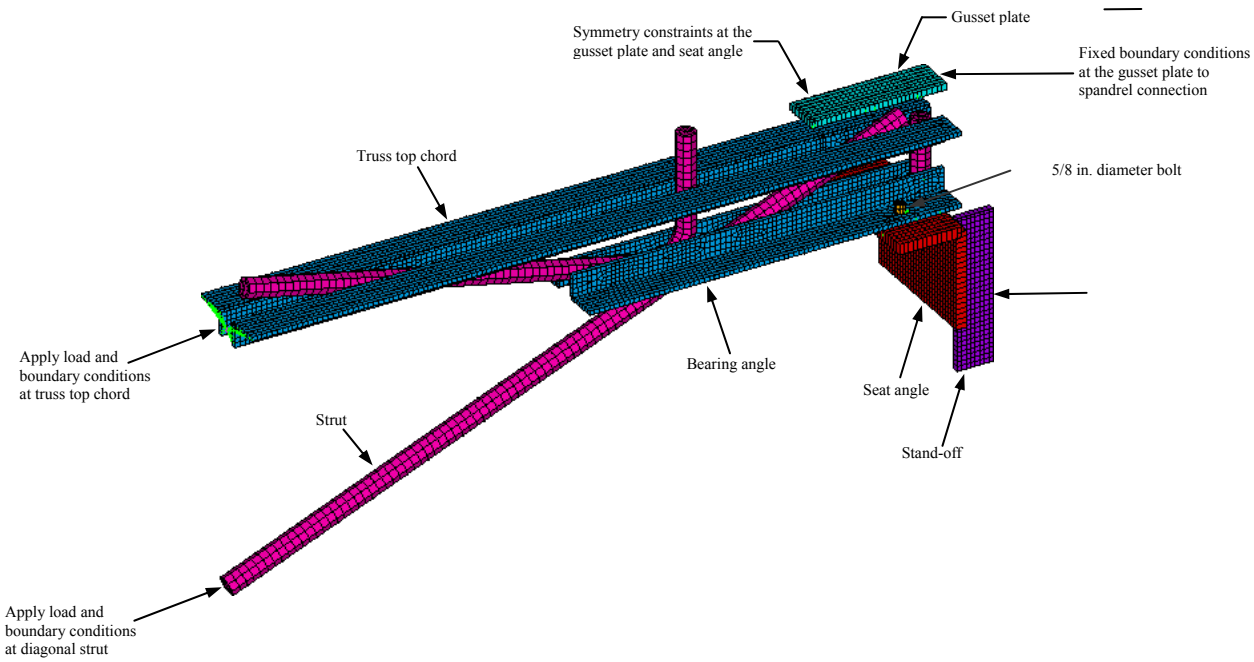

Figure K–26. Finite element model of exterior seat.

Failure Modes of Exterior Seat against Horizontal Tensile Force: The failure modes considered are: (1) failure of the groove weld between gusset plate and spandrel, (2) failure of the fillet weld between the gusset plate and the truss top chord, (3) tensile failure of the gusset plate, (4) bolt shearing off, (5) bolt bearing, (6) bolt tear-out, and (7) block shear failure. For calculation purposes, the bolts are assumed to be centered in the slotted holes. The typical failure sequence of the truss seat is as follows: first the gusset plate yields, then it fractures, followed by truss deformation and bolt bearing against the slotted hole, the bolt shears off, and then finally the truss walks off the seat. The travel distance for the truss to walk off of the seat is 4 5/8 in. This failure sequence is illustrated in Fig. K–27 as path (A) and shown in Fig. K–28, where the relationship between the tensile force resistance from the seat connection and the truss travel distance is plotted. In this plot, frictional resistance between the seat angle and bearing angle was not included.

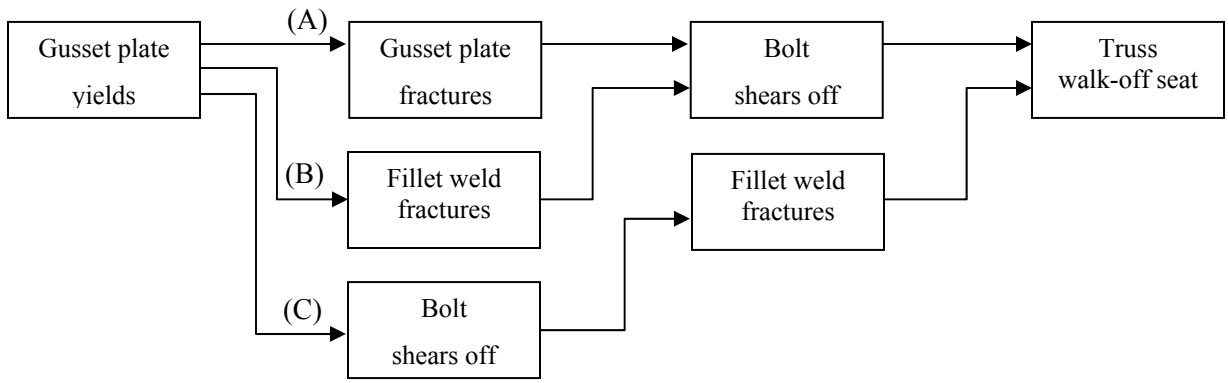

(A) Seat details 1111, 1311, 1411, 1511, and 1611 at all temperatures.
(B) Seat detail 1013 at temperatures below 100 °C.
(C) Seat details 1212 and 1313 at all temperatures, and detail 1013 at temperatures more than or equal to 100 °C.

Figure K–27. Failure sequence of the exterior seats against tensile force.

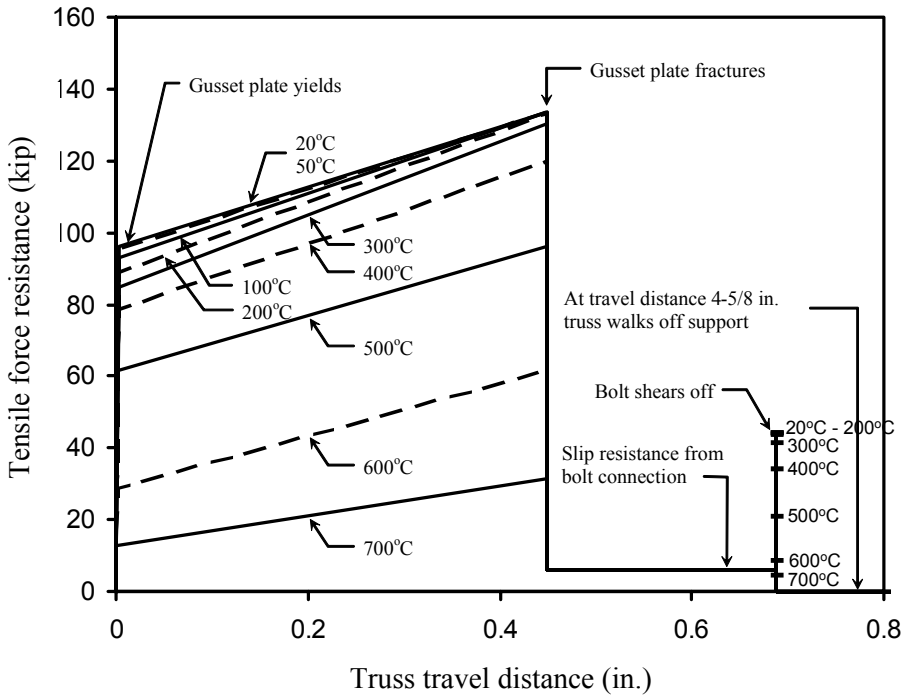

Figure K–28. Typical tensile force resistance from exterior seat (Detail 1411).

Seat details 1212 and 1313 have a wider gusset plate and follow path (C) which differs from the typical sequence where the bolts will bear against the slotted hole then shear off before the gusset plate connection fails. The failure sequence of seat detail 1013 is temperature-dependent. At temperatures below 100 °C, the fillet weld connection between the gusset plate and the truss top chord fractures before bolts shear off. At temperatures greater than or equal to 100 °C the failure sequence is the same as for Details 1212 and 1313.

Failure Modes of Exterior Seat against Horizontal Compressive Force: The concrete slab above the truss seat connection provides the compressive force resistance. If the concrete slab fails, the truss seat

has resistance against compressive force provided by the gusset plate until it buckles, and from bolt friction and bolt shear until the bolt bears against the slotted hole and then shears off. Surface friction between the seat angle and bearing angles will also provide some resistance. Additional resistance is developed when the truss comes into contact with the spandrel. Travel distance for the truss to come into contact with the column spandrel is 1 1/2 in. Under compressive force, the truss will not lose its vertical support.

Failure Modes of Exterior Seat against Combined Vertical and Horizontal Force: Under combined vertical and horizontal forces, the failure modes are a combination of the individual failure modes for vertical and horizontal forces.

Truss Seat Capacity Calculations

In this section, truss seat capacities corresponding to the failure modes described in the previous section are given. The capacity is computed for the different types of the truss seat at different temperatures. Calculation of the connection capacity was performed using the methods in the *Manual of Steel Construction: Load and Resistance Factor Design* (AISC 2001) with the resistance factor, ϕ, assumed to be equal to one.

Capacity of Interior Seat against Vertical Force: Failure mode of the truss seat against vertical force is fracture of the fillet welds at the seat-to-channel beam connection. Strengths of the fillet welds at this connection are summarized in Table K–7. The symbol # in this table refers to seat detail number.

Table K–7. Interior seat capacity against vertical force.

Temp. (°C)	Connection Capacity Against Vertical Force (kip)						
	#15	#17	#20	#21	#22	#23	#226A
20	226	226	265	221	187	187	385
50	226	226	265	221	187	187	385
100	226	226	265	221	187	187	384
200	225	225	264	220	187	187	383
300	220	220	258	215	182	182	374
400	201	201	236	197	167	167	343
500	160	160	188	156	132	132	272
600	98	98	116	96	82	82	167
700	45	45	53	44	37	37	76

Capacity of Interior Seat against Horizontal Tensile Force: Failure loads were computed for the failure modes described above. Table K–8 summarizes the results for Seat Detail 22. This table shows that the shear strength of the two bolts controls the horizontal tensile strength of the truss seat connection. As can be seen from this table at temperature 500 °C, bolt shear capacity is reduced by half, and at 600 °C it is reduced to less than a quarter of the original capacity at room temperature. Other seat details also have the same failure mode, and, therefore, the same failure load.

Table K–8. Interior seat capacity against tensile force.

Temp. (°C)	Resistance against Tensile Force (kip)							
	Bolt Slip Critical	Bolt Shearing Off	Bolt Bearing		Bolt Tear-out		Block Shear	
			On Seat	On Truss	From Seat	From Truss	Of Seat	Of Truss
20	6	44	124	69	87	101	60	59
50	6	44	124	69	87	101	60	59
100	6	44	124	69	87	101	60	59
200	6	44	124	69	87	100	59	59
300	6	42	121	68	85	98	58	57
400	6	34	111	62	77	90	53	52
500	6	21	88	49	61	71	42	42
600	6	9	54	30	38	44	24	24
700	6	4	25	14	17	20	10	10

Capacity of Interior Seat against Horizontal Compressive Force: Under compressive force, the truss will come into contact with the channel beam before the bolt bears against the slotted hole. The truss seat connection does not fail under compressive force.

Capacity of Interior Seat against Combined Vertical and Horizontal Force: A typical interaction relationship for combined vertical and horizontal tensile force is shown in Fig. K–29. As can be seen from this figure, the vertical shear strength of the seat reduces because of the additional horizontal tensile force that the fillet weld connection between the truss seat and the channel beam must resist.

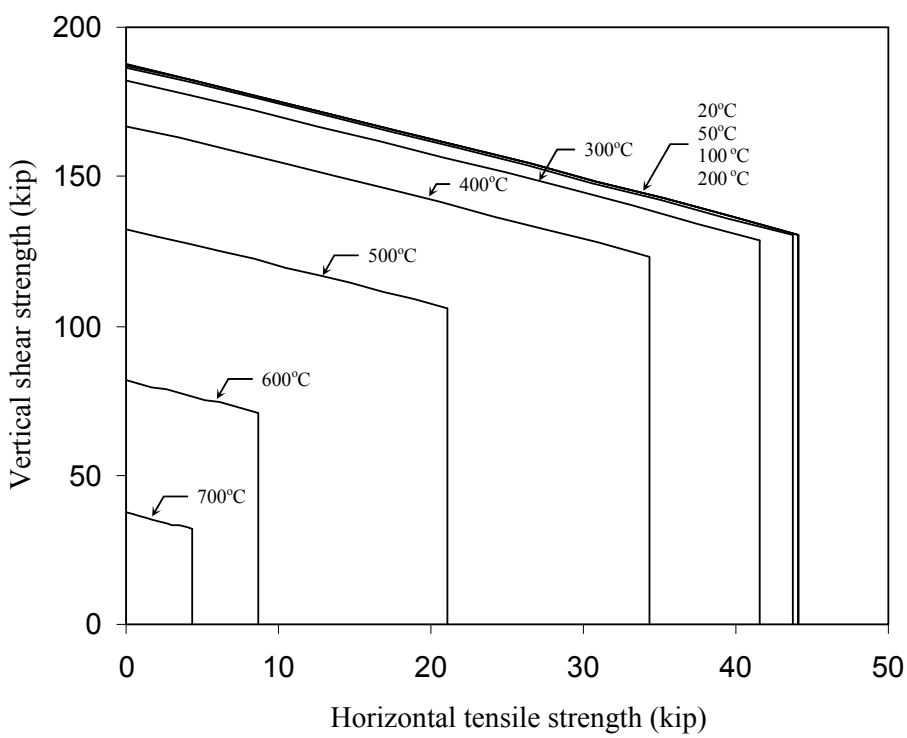

Figure K–29. Strength of combined vertical and horizontal force (Detail 22).

Capacity of Exterior Seat against Vertical Force: The failure mode of the truss seat against vertical force is fracture of the fillet welds at the stand-off-to-spandrel connection. Strength of the fillet welds at this connection is summarized in Table K–9.

Table K–9. Exterior seat capacity against vertical force.

Temp. (°C)	Connection Capacity against Vertical Force (kip)							
	#1013	#1111	#1212	#1311	#1313	#1411	#1511	#1611
20	94	94	111	94	94	140	193	207
50	94	94	111	94	94	140	193	207
100	94	94	111	94	94	140	193	207
200	93	93	110	93	93	139	192	206
300	91	91	108	91	91	136	187	201
400	84	84	100	84	84	126	172	184
500	69	69	81	69	69	102	136	146
600	45	58	53	60	45	78	84	90
700	29	26	34	27	29	35	38	41

Capacity of Exterior Seat against Horizontal Tensile Force: The connection capacity of truss seats that follow failure sequence (A), as shown in Fig. K–27, equals the failure load for mode (3) defined previously. The connection capacity of truss seats that follow failure sequence (B) equals the failure load for mode (2). The connection capacity of truss seats that follow failure sequence (C) equals the failure load for mode (4) plus the developed resistance from the gusset plate. The results of the exterior seat capacity calculations are summarized in Table K–10. Note that the strength of the truss seat #1013 increases by about 38 percent at a temperature of about 100 °C. For temperatures less than 100 °C, the capacity is controlled by the gusset seat fillet weld strength, and for temperatures in excess of 100 °C, the bolt reaches the end of its travel in the elongated bolt hole and increases the capacity of the connection.

Table K–10. Exterior seat capacity against horizontal tensile force.

Temp. (°C)	Connection Capacity against Tensile Force (kip)							
	#1013	#1111	#1212	#1311	#1313	#1411	#1511	#1611
20	100	104	182	134	182	134	134	134
50	100	104	182	134	182	134	134	134
100	138	104	181	134	181	134	134	134
200	135	103	180	133	180	133	133	133
300	130	101	174	130	174	130	130	130
400	115	93	156	120	156	120	120	120
500	84	75	117	96	117	96	96	96
600	42	49	67	62	67	62	62	62
700	20	25	32	31	32	31	31	31

Capacity of Exterior Seat against Horizontal Compressive Force: Under compressive force, the gusset plate will buckle before the bolts shear off. Compression strength of the gusset plate governs the truss seat capacity. The compressive strength of the gusset plate is summarized in Table K–11.

Table K–11. Compression strength of gusset plate.

Temp. (C)	Compression Strength of Gusset Plate (kip)							
	#1013	#1111	#1212	#1311	#1313	#1411	#1511	#1611
20	77	69	99	90	99	90	90	90
50	76	68	98	89	98	89	89	89
100	74	66	96	87	96	87	87	87
200	71	63	91	83	91	83	83	83
300	67	60	87	79	87	79	79	79
400	62	55	80	72	80	72	72	72
500	48	42	61	55	61	55	55	55
600	20	17	25	22	25	22	22	22
700	6	5	8	7	8	7	7	7

Capacity against Combined Vertical and Horizontal Force: Interaction relationships for combined vertical and horizontal forces are under development.

K.7.4 Modeling Connection Failure by Break Elements

In this section, simplified finite element models of the exterior and interior seat, knuckle, stud on strap anchor, and stud on spandrel are described. These connection models were developed for incorporation in the floor truss analysis to capture the connection failure modes and determine the sequence of the failure modes that may lead to the failure of the floor truss.

The developed simplified model of these connections simulates the loss of connection resistance after failure either by exceeding the connection force capacity or by exceeding the allowable deformation (truss walking off the seat). The connection capacity can also be temperature-dependent. The finite element modeling assumptions are as follows:

Break element, a unidirectional linear spring element with the capability of turning on and off during an analysis, is used for modeling connection failure. The element is a part of the structure that connects two "active" nodes in the "on" mode and disconnects them in the "off" mode, depending on the relative displacement of two "control" nodes. The break element is defined as follows:

$$B_m[iI,j,dof_{ij});(k,l,dof_{kl});(K,\Delta_0)] \tag{11}$$

where m is the break element number, i and j are the active nodes, dof_{ij} is the degree of freedom for the active nodes, k and l are the control nodes, dof_{kl} is the degree of freedom for the control nodes, K is the elastic stiffness of the break element, and Δ_0 is the differential displacement limit of the control nodes.

A beam element with temperature-dependent thermal expansion material properties is used to make the connection capacity temperature-dependent. This is done by using the deformation of the beam element from thermal expansion to control the status (on/off) of the break element. Figure K–30 illustrates the basic mathematical model of the connection. The connection capacity is made temperature-dependent by defining the thermal expansion of the beam element to be temperature dependent.

Basic mathematical model:

– Let node *l* and *i* have same displacement.

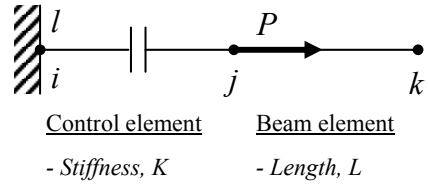

– In this example, control node *k* and *l* relative displacement has the form:

$$U_k - U_l = \frac{P}{K} + \alpha L \Delta T$$

– Control element status is by definition

$$U_k - U_l \le \Delta_0, \text{ status : on}$$
$$U_k - U_l > \Delta_0, \text{ status : off}$$

– Define break element to turn off when capacity, P_u, has been reached

$$\Delta_0 = \frac{P_u}{K} + \alpha L \Delta T$$

– Element capacity at room temperature is given as

$$P_{u.rm} = K\Delta_0$$

– Hence for a given P_u and ΔT relationship, the required thermal expansion to turn element off can be found by

$$\alpha = \frac{P_{u.rm} - P_u}{KL\Delta T}$$

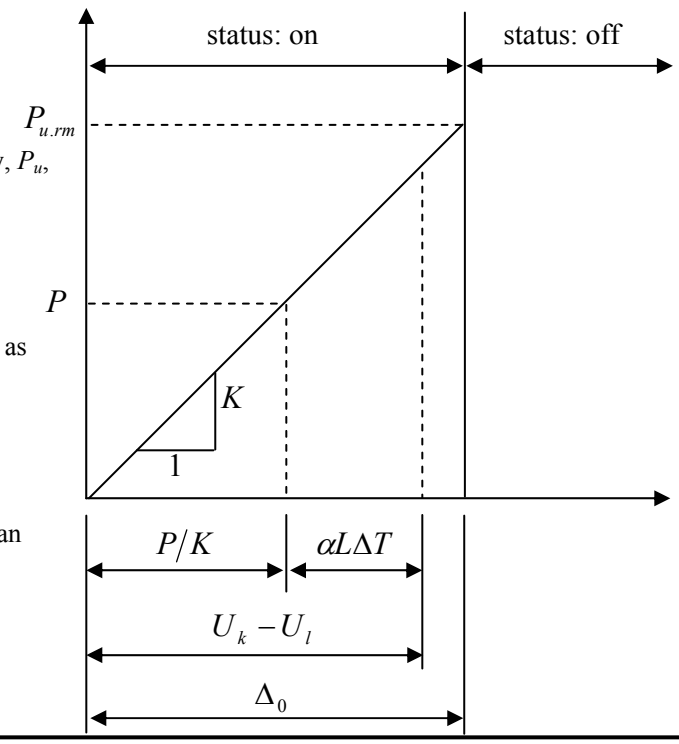

Figure K–30. Basic mathematical model of connection failure.

Multiple connection failure modes require use of different break elements that are connected together in a logical manner. For example, to model independent failure modes, that is, one failure mode that does not cause other failures, break elements are connected in parallel. If one break element turns off, the other break elements remain. For dependent failure modes, break elements are connected in series. If one break element turns off, then all elements turn off.

Simplified Model of the Interior and Exterior Seat

The failure modes of the interior seat include (1) the truss walking off the support, (2) exceeding the vertical temperature-dependent shear capacity of the truss seat, and (3) exceeding bolt temperature-dependent shear capacity when bolt bears against slotted hole. These failure modes are

captured by using four break elements and two beam elements as shown in Fig. K–31. Results of the simplified seat model capturing failure from the truss walking off support and failure from exceeding seat vertical shear capacity are shown in Fig. K–32 and Fig. K–33, respectively, which depict the relationship between the horizontal and vertical seat forces and the horizontal truss travel distance.

When truss reaction force on the seat is large in horizontal tension and small in vertical shear, the failure mode is bolt shearing off followed by truss walking off the support as shown in Fig. K–32. Bolt shear is controlling the seat horizontal resistance capacity. Bolt shear by itself however does not cause the truss to lose its vertical support, but it is the prerequisite of truss walking off the seat. The travel distance for a truss to walk off an interior seat is 4 in. When truss reaction force on the seat is large in vertical shear and small in horizontal tension, the failure mode is exceeding the seat vertical shear capacity as shown in Fig. K–33. This failure mode will cause the truss to lose both its vertical and horizontal support from the seat.

The simplified model of the exterior seat is the same as the simplified model of the interior seat, except for an additional beam element and a break element to model failure of the gusset plate shown in Fig. K–34.

Simplified Model of the Knuckle

Knuckle failure modes that must be captured by the simplified model are the horizontal shear and vertical tensile failure, which are both temperature-dependent. Finite element modeling assumptions for the knuckle are: (1) the knuckle has resistance in all translational DOF, (2) the knuckle does not have a vertical compression capacity limit, (3) capacities in the horizontal shear and vertical tension are dependent, and (4) vertical compression resistance is independent of the capacities in the other directions. Knuckle failure is captured by using 15 control elements and 5 beam elements as shown in Fig. K–35.

Simplified Model of the Stud on Strap Anchor and Stud on Spandrel

Simplified models of stud on strap anchor and stud on spandrel were developed using the same technique as described for the knuckle model.

K.7.5 Truss Model

Objectives

The objectives of the truss model study are to:

- Capture the potential failure modes and failure sequence of the truss under combined gravity load and thermal load;
- Develop an understanding of the relative importance of different structural features and failure modes; and
- Develop a simplified model that replicates the expected failure and the limit loads of the truss to be used for analysis of the full floor subsystem model.

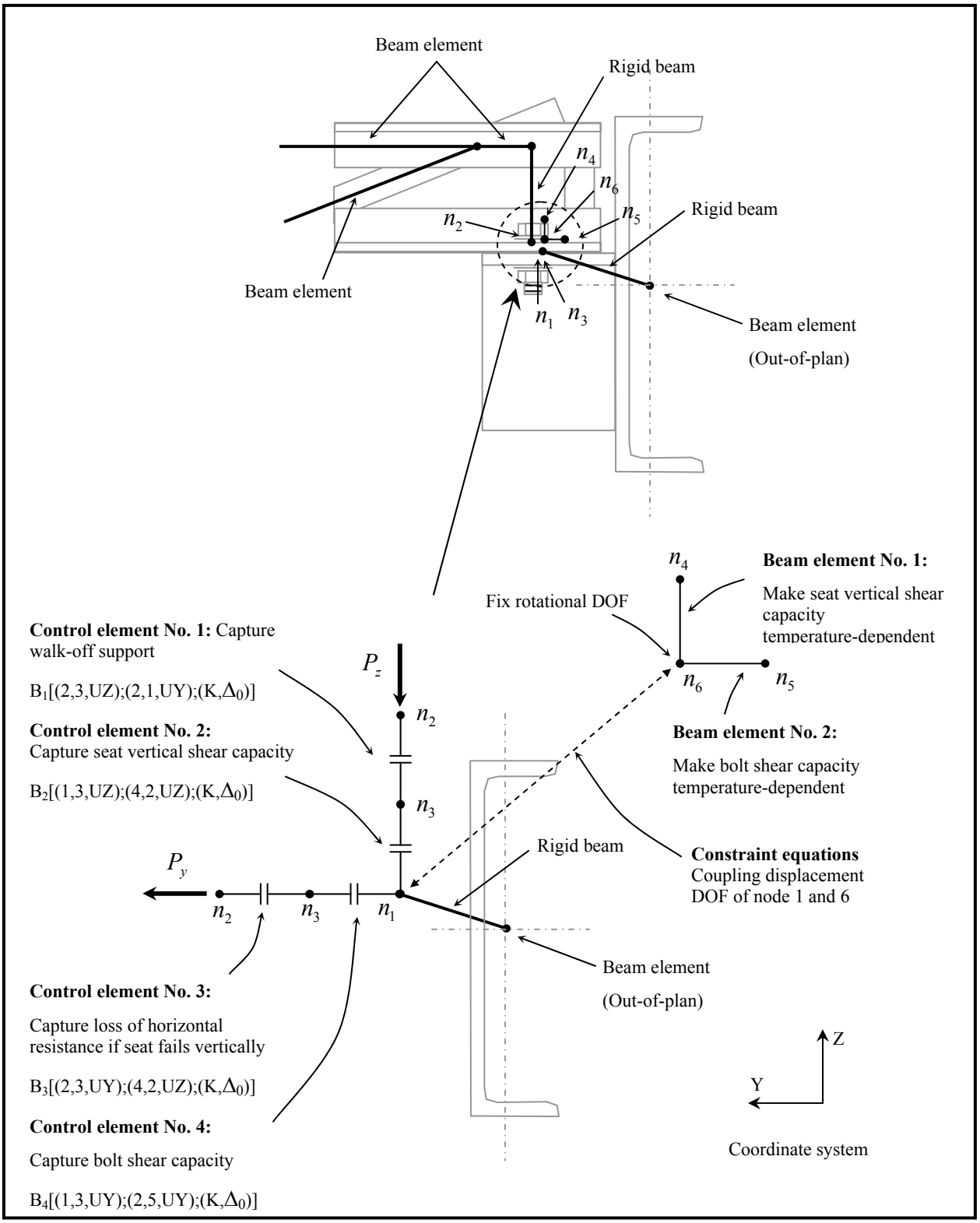

Figure K–31. Simplified model of interior seat.

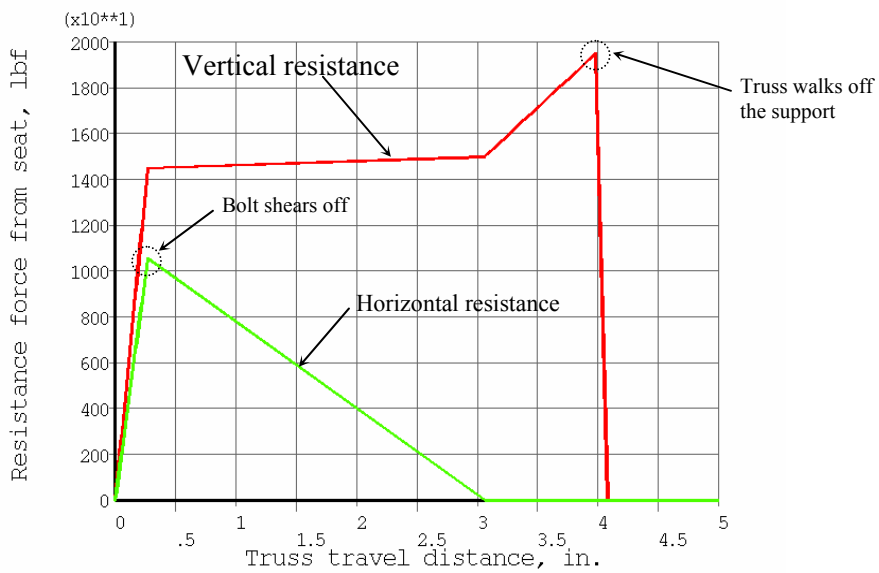

Figure K–32. Results of simplified seat model capturing failure from truss walking off interior seat.

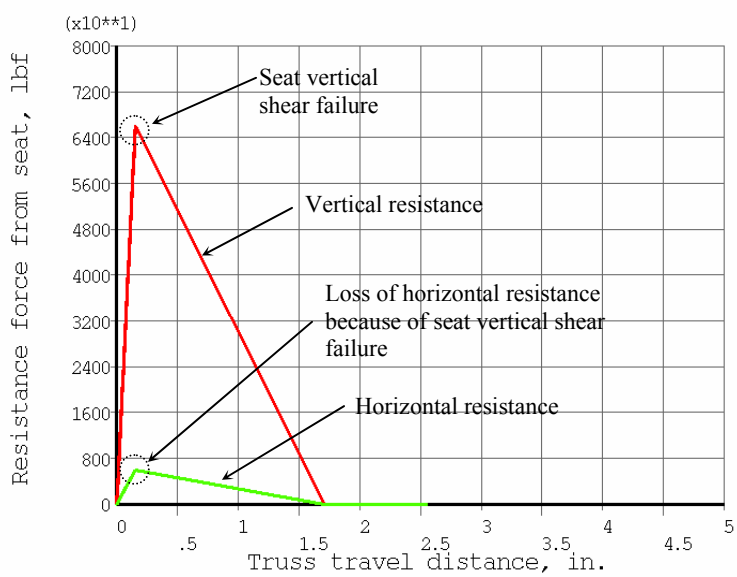

Figure K–33. Results of simplified seat model capturing failure from exceeding the interior seat vertical shear capacity.

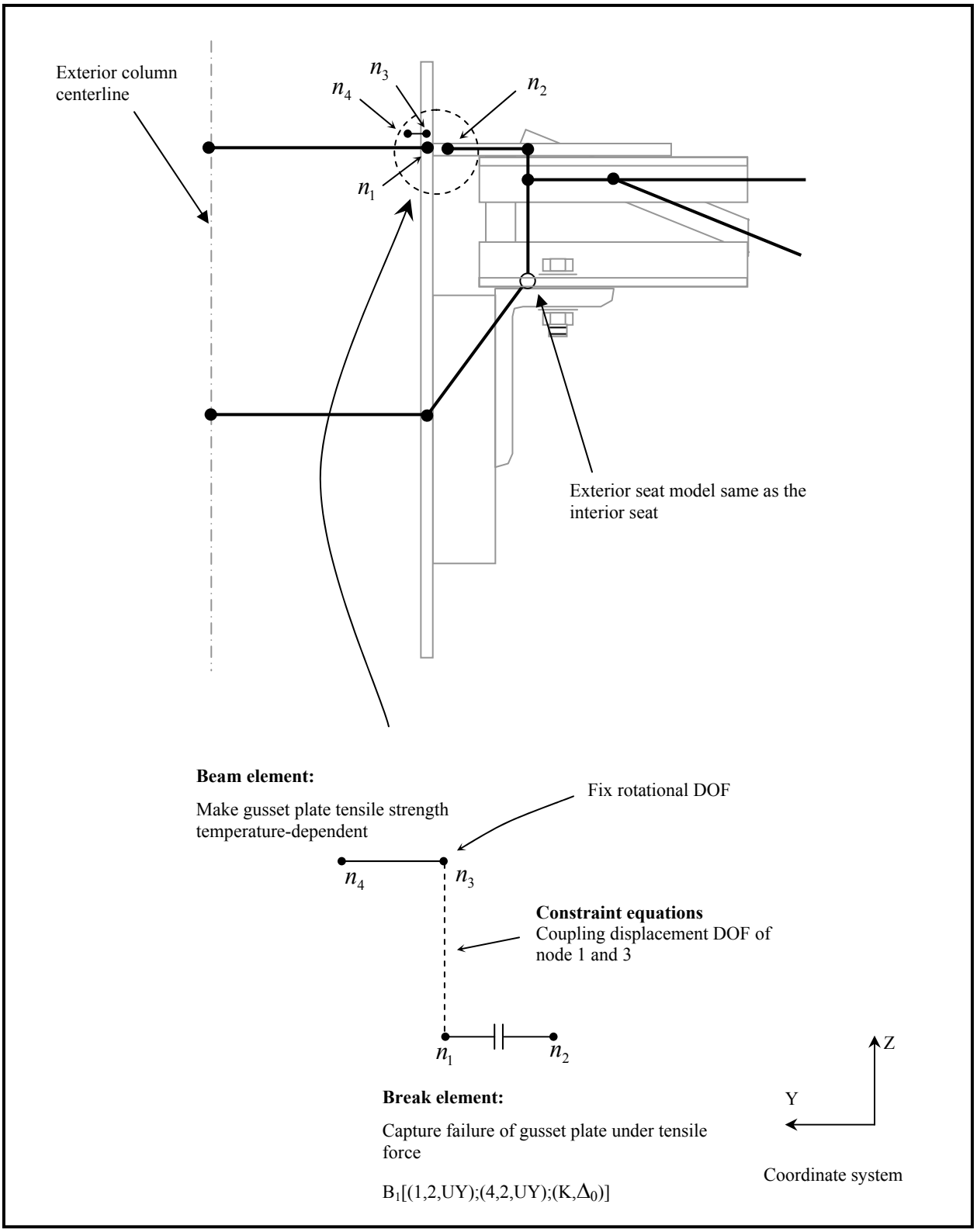

Figure K–34. Simplified model of exterior seat.

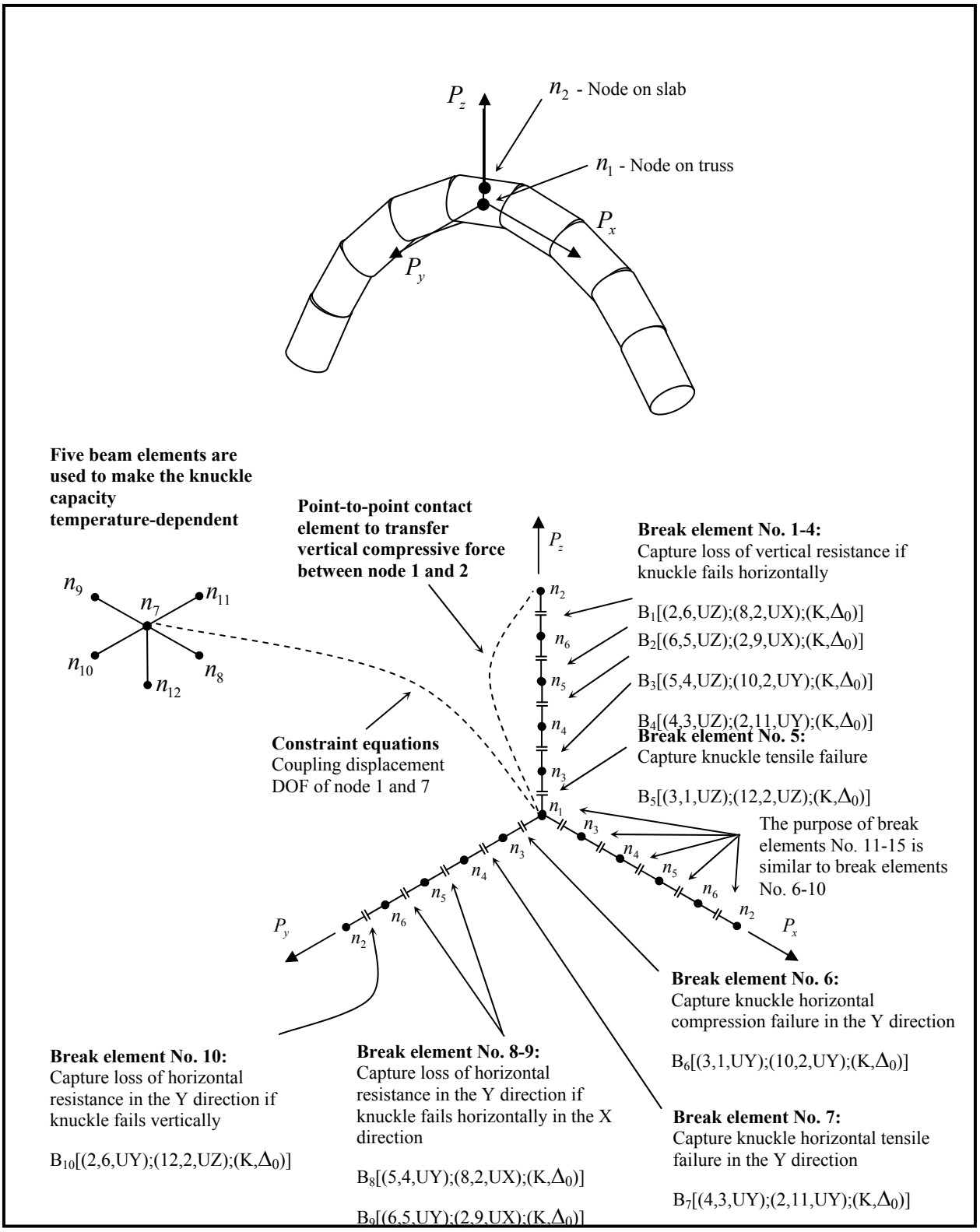

Figure K–35. Simplified model of knuckle.

Failure Modes

The model can capture the following failure modes:

Softening and Sagging of Truss—The top and bottom chords and diagonals of the truss are exposed to the hot gas layer below the floor slab. As described in Section K.5, the steel in the truss exhibits stiffness degradation, yield strength reduction, plastic softening, and creep at high temperatures. A truss with softened chords sags. The heat may also reduce the stiffness and strength of the concrete slab, especially its bottom layer where temperature is the highest, and around the knuckle where concrete temperature rises by conduction through the steel.

In addition to direct thermal effects, sagging and weakening of the truss can be caused by the following failure modes:

- Buckling or failure of web diagonal members, which reduces the truss action and causes the truss to act as a catenary;
- Buckling or failure of the top and bottom chord members;
- Knuckle failure and loss of composite action of the concrete slab and the steel truss; or
- Weld failure between the diagonal and the chord.

Loss of Support of Truss—The truss can fail by loss of support due to seat failure. Loss of support at either the exterior or interior seat can be caused by the extreme sagging and catenary action of the truss due to plastic deformation and buckling of truss members.

As discussed under Boundary Conditions later in this section, the bottom chord of the truss is restrained in the lateral direction at the bridging truss locations. Although the out-of-plane deformation of the bottom chord due to thermal expansion of bridging trusses will result in a reduction in the vertical load capacity of a primary truss, the truss model studied here cannot capture this phenomenon. The interaction between the bridging trusses and the primary trusses is intended to be captured in the full floor model.

Model Description

Figure K–36 shows the truss model. A typical long-span truss designated C32T1 (SHCR 1973:WTC Drawing Book 7, Sheet AB1–2) is modeled to study its response to failure when subjected to dead and live loads and thermal loads. The model includes the following:

- One truss of the pair of trusses at column line 143 of floor 96 in WTC 1;
- Two exterior columns (columns 143 and 144) with half the area and bending properties, and a length of 24 ft (12 ft above and below the floor level);
- The portion of the spandrel between the two exterior columns;

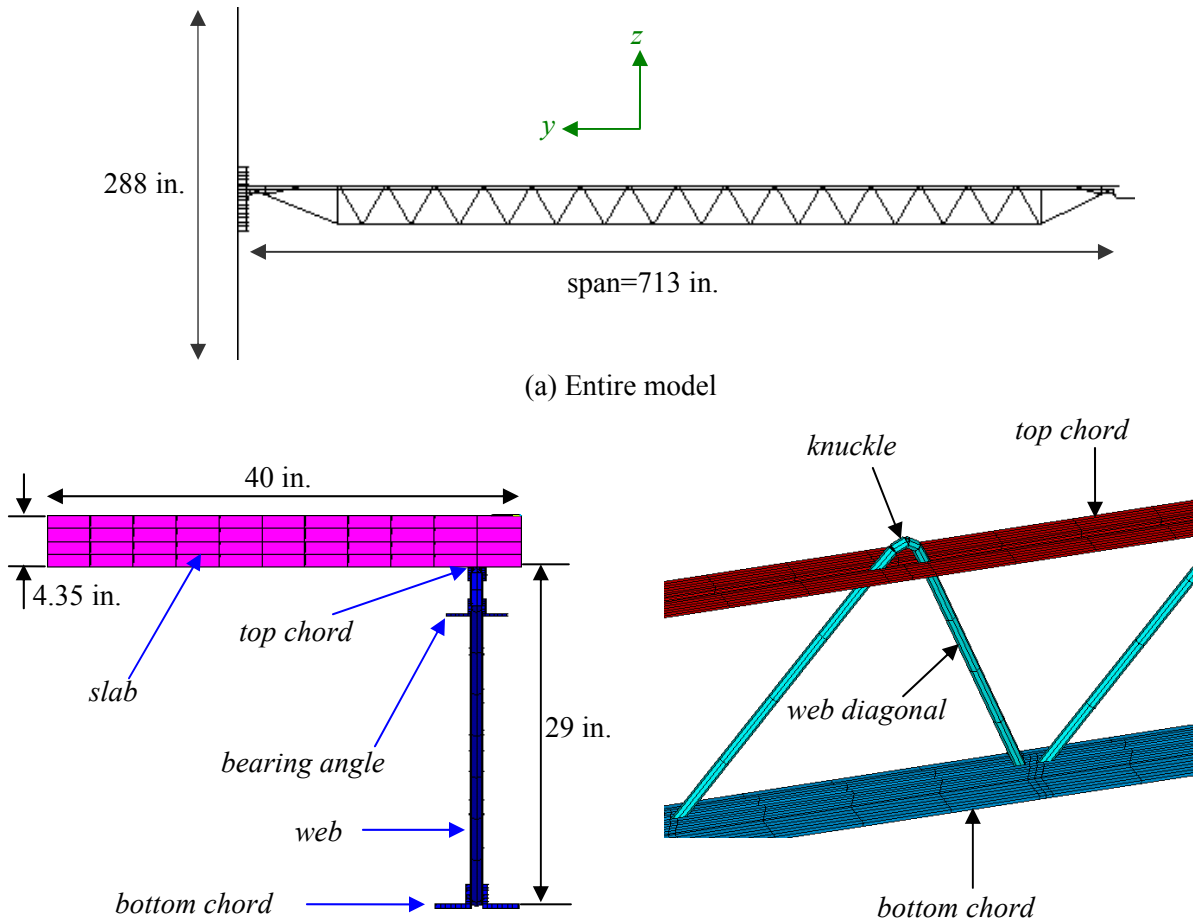

(b) Cross section

(c) Top and bottom chords and web diagonals

Figure K–36. Truss model.

- The portion of the slab (40 in. wide) between the two exterior columns;
- One strap anchor that is attached to the truss top chord, concrete slab and the adjacent exterior column (column 144); and
- Exterior and interior seats, and the gusset plate at the exterior end.

A typical slab section consists of 4 in. thick lightweight concrete on 22 gauge metal deck with flutes 6.8 in. on centers. Two layers of welded wire fabric were provided in the slab. The reinforcement ratios are 0.21 and 0.735 in the directions along and transverse to the truss, respectively. A flute is 2 in. wide at the top, 1.25 in. wide at the bottom, and 1.47 in. high. An equivalent thickness of 4.35 in. is used as the slab thickness in the truss model. By using the equivalent thickness, the bending stiffness in the direction transverse to the truss is about 15 percent higher than the actual stiffness. However, since the bending in the transverse direction in this truss model is insignificant, the slab is modeled as an isotropic plate. The metal deck and the welded wire fabric are not included in the truss model.

The top and bottom chords and the diagonals of the truss are modeled by 3–D quadratic finite strain beam (BEAM189) elements with temperature-dependent elastic, plastic, and creep material properties. The top

chord consists of double angles of 1 1/2 × 2 × 0.25 (long legs horizontal), while the bottom chord consists of double angles of 3 × 2 × 0.37 (long legs horizontal). Web members are round bars of either 1.09 in. or 1.14 in. diameter. A typical diagonal member has a 1.09 in. diameter. Top and bottom chords are divided into four elements between panel points, and a diagonal is also divided into four elements between top and bottom chords. The concrete slab is modeled with 4-node finite strain shell (SHELL181) elements. The nodes of the concrete slab are located at the neutral plane of the concrete slab with an offset relative to the nodes of the top chords. The cast iron model (Hjelm model) can be used with the SHELL181 elements that allow different "yield" in tension and compression. A low "yield stress in tension" is used to simulate cracking.

At knuckle locations, the top chord elements and the elements representing the concrete slab are connected by control elements (COMBIN37) with capacities determined from the detailed knuckle analysis. By including point-to-point contact (CONTA178) elements, compression can always be transferred even after knuckles fail. Studs on the strap between the top chord and column 144 are also modeled by COMBIN37 elements that connect the strap to the slab and have temperature-dependent capacities. The slab and the strap are tied by the COMBIN37 elements horizontally while their vertical displacements are coupled. The exterior and core seats are modeled by COMBIN37 elements that have temperature-dependent capacities determined from the seat analysis. A stud on the spandrel is also modeled by a COMBIN37 element, which ties the spandrel with the slab and has temperature-dependent capacities. Because only one 5/8 in. stud was provided over 80 in. between the slab and the spandrel, a half stud capacity is considered for the stud in the model. In addition, the first stud on the strap is located near this stud on the spandrel. Therefore, COMBIN37 elements between the slab and the spandrel have a capacity of a combination of these studs, including a group effect. Damping unit connecting the truss bottom chord to the spandrel plate is assumed to have little effect on the behavior of the floor truss under sustained loading; therefore, it was not included in the model.

Three–D elastic beam (BEAM44) elements model the exterior columns. SHELL63 elastic shell elements model the spandrel.

Boundary Conditions

Boundary conditions on the truss model are shown in Fig. K–37.

The entire top chord of the truss is supported in the x direction. The bottom chord is supported in the x direction at four bridging truss locations. Two edges of the concrete slab are restrained against rotations about the y and z axes, but can move in the x direction.

The interior truss seat is fixed in all directions. The exterior seat is fixed to the spandrel. The truss is pinned at both exterior and interior truss seats.

The exterior end of the slab is tied to the spandrel by only COMBIN37 elements representing studs. The interior end of the slab is fixed in the z direction and in rotation about the z direction. In the y direction at the interior end of slab, break elements that have temperature-dependent tensile capacities are implemented as show in Fig. K–38. Therefore, the interior slab end is fixed in the y direction until the tensile force exceeds the capacity that is calculated based on the amount of steel reinforcement (#3@10″ top and #4@12″ bottom).

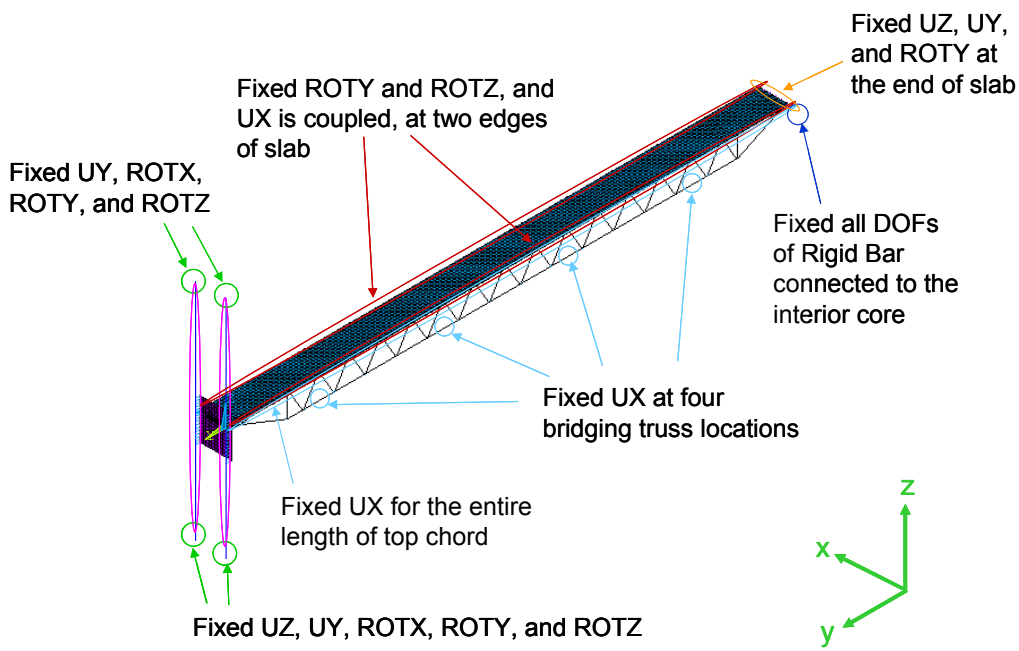

Figure K–37. Boundary conditions.

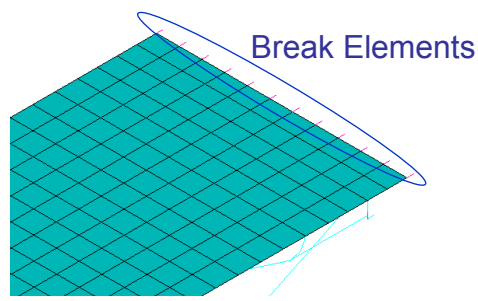

Figure K–38. Break elements at the interior end of slab.

In the analysis with increasing gravity load, a model different from the current model is used, where boundary conditions of the slab are slightly different from the current model described above. In this model, the exterior end of the slab is tied to the spandrel, and the core end of the slab is fixed in the *y* and *z* directions and in rotations about the *x* and *z* directions. Also, COMBIN37 elements for seats are not included in this model.

Loading

The loading on the truss model consists of gravity dead and live loads and temperature time-histories for all steel members, including the truss seats. The gravity loads include weight of the structure, 8 psf superimposed dead load (including nonstructural dead loads due to architectural items and fixed service equipment), and 13.75 psf of live load equal to 25 percent of design live load of 55 psf. The thermal load is a linear temperature gradient through the slab from 300 °C at the top surface of the concrete slab to

700 °C at the bottom surface of the slab. The temperature is ramped from 20 °C to 700 °C in steel members; from 20 °C to 700 °C at the bottom surface of the slab and from 20 °C to 300 °C at the top surface of the slab at 1,800 s; thereafter, the temperatures do not change for another 1,800 s. Temperature is not applied to the columns.

In order to determine the effect of debris load on the truss behavior, a parametric study will be performed.

Material Properties

Table K–12 shows material assignments for different structural components in the truss model.

Table K–12. Material assignments in truss model.

Structural Component	Specified Yield Strength	Material ID
Top chord	50 ksi	21
Bottom chord	50 ksi	21
1.09 in. diameter web	36 ksi	20
1.14 in. diameter web	50 ksi	21
Strap	36 ksi	1
Column 143	65 ksi	15
Column 144	65 ksi	15
Spandrel	42 ksi	11
Lightweight concrete slab	3,000 psi (f'c)	83

Columns 143 and 144 and the spandrel, use only elastic properties. In the current model, the concrete slab also remains elastic.

Resistance Welds

Table K–13 shows the resistance weld strength between a chord (double angles) and a diagonal based on the test data found at Laclede Steel. Weld strength shown in Table K–13 is the sum of the capacities of two resistance welds. Figure K–39 compares resistance weld strength between top or bottom chord and a diagonal with yield strength of a diagonal at elevated temperatures. As can be seen in Fig. K–39 (a), a typical diagonal (1.09 in. diameter) will yield before the resistance weld fails. For 1.14 in. diameter diagonal, the resistance weld strength cannot yield the bar at temperatures below 550 °C, as can be seen in Fig. K–39 (b). However, shop drawings show additional arc welds between the chord and 1.14 in. diameter bar at most locations.

Table K–13. Resistance weld strength.

Chord	Diagonal Size (in.)	Average Strength (kip)
Top chord	1.09	36.9
Top chord	1.14	37.7
Bottom chord	1.09	41.0
Bottom chord	1.14	40.5

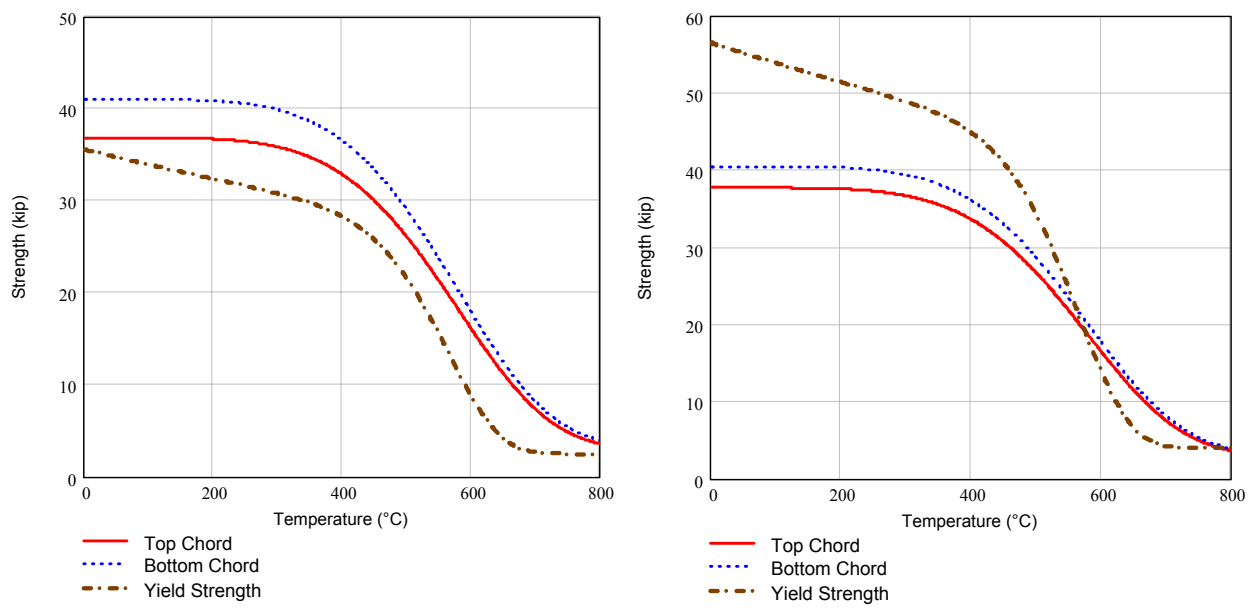

(a) 1.09 in. diameter bar (b) 1.14 in. diameter bar

Figure K–39. Comparison of resistance weld strength and yield strength of web member at elevated temperatures.

Current Status

The truss model can capture the following:

- Temperature-dependent elastic material properties for both steel and concrete;
- Temperature-dependent steel plasticity;
- Buckling of truss members;
- Failure of knuckle—loss of composite action;
- Failure of studs on the strap;
- Failure of stud between the spandrel and the concrete slab; and
- Failure of the exterior and interior truss seats.

The following features are being added to the truss model:

- Crushing and cracking of concrete;
- Creep strain in steel at elevated temperatures; and
- Failure of welds (Calculations show section yielding can occur prior to weld failure in nearly all cases.).

Model Verification

The maximum vertical displacement is checked against the single truss model extracted from the ANSYS full floor model that was converted from the SAP full floor model. The difference in the vertical displacement is only 3.5 percent.

FEA Results

Gravity Loading—The maximum calculated vertical deflection is 1.1 in. downward. The maximum calculated horizontal column deflection is 0.022 in. inward. The maximum forces in top chord, bottom chord, and diagonal are 13,357 lb, 39,514 lb, and 7,647 lb, respectively.

Gravity Plus Thermal Loading—The analysis is carried out dynamically with 5 percent Rayleigh damping. To shorten the run time, the total time period is set to 1.0 s for the temperature ramp. The analysis proceeded to a temperature of T=663 °C. Figure K–40 shows horizontal and vertical displacement results. A positive horizontal displacement indicates that the exterior columns are pushed out, and a negative vertical displacement indicates that the truss is deflected downward. At 340 °C, the horizontal displacement at the exterior column starts to decrease. At 560 °C, the exterior columns are pulled in, and the truss becomes catenary from that point on.

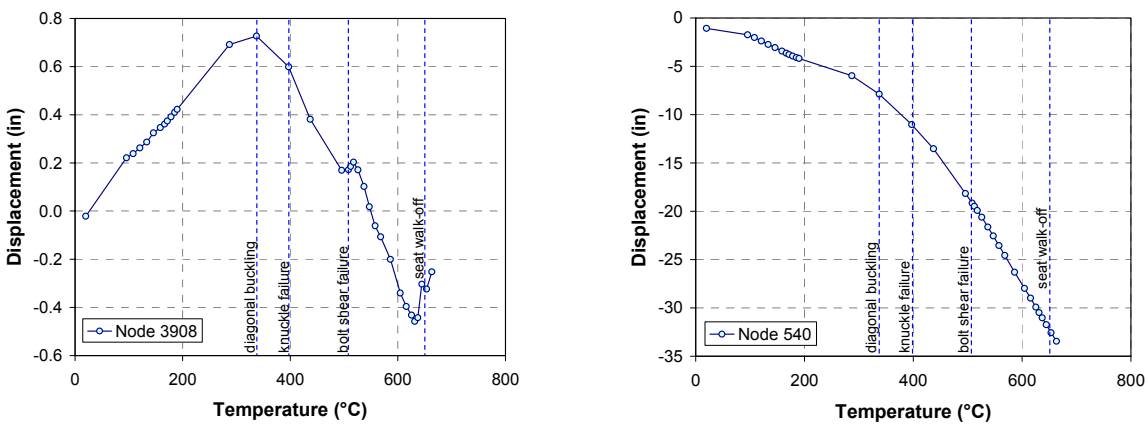

(a) Horizontal displacement at column 143 (b) Vertical displacement at midspan

Figure K–40. Displacement versus temperature.

Figure K–41 shows axial forces in the truss members. In the figure, Py is the axial force at yield and equals the product of the net area of the member and the yield strength which varies with temperature. Pc is the compressive strength per AISC formula (AISC 2003) for the top chord with fixed ends in Fig. K–41 (a) and for 1.09 in. diameter diagonal bar with pinned ends in Fig. K–41 (c).

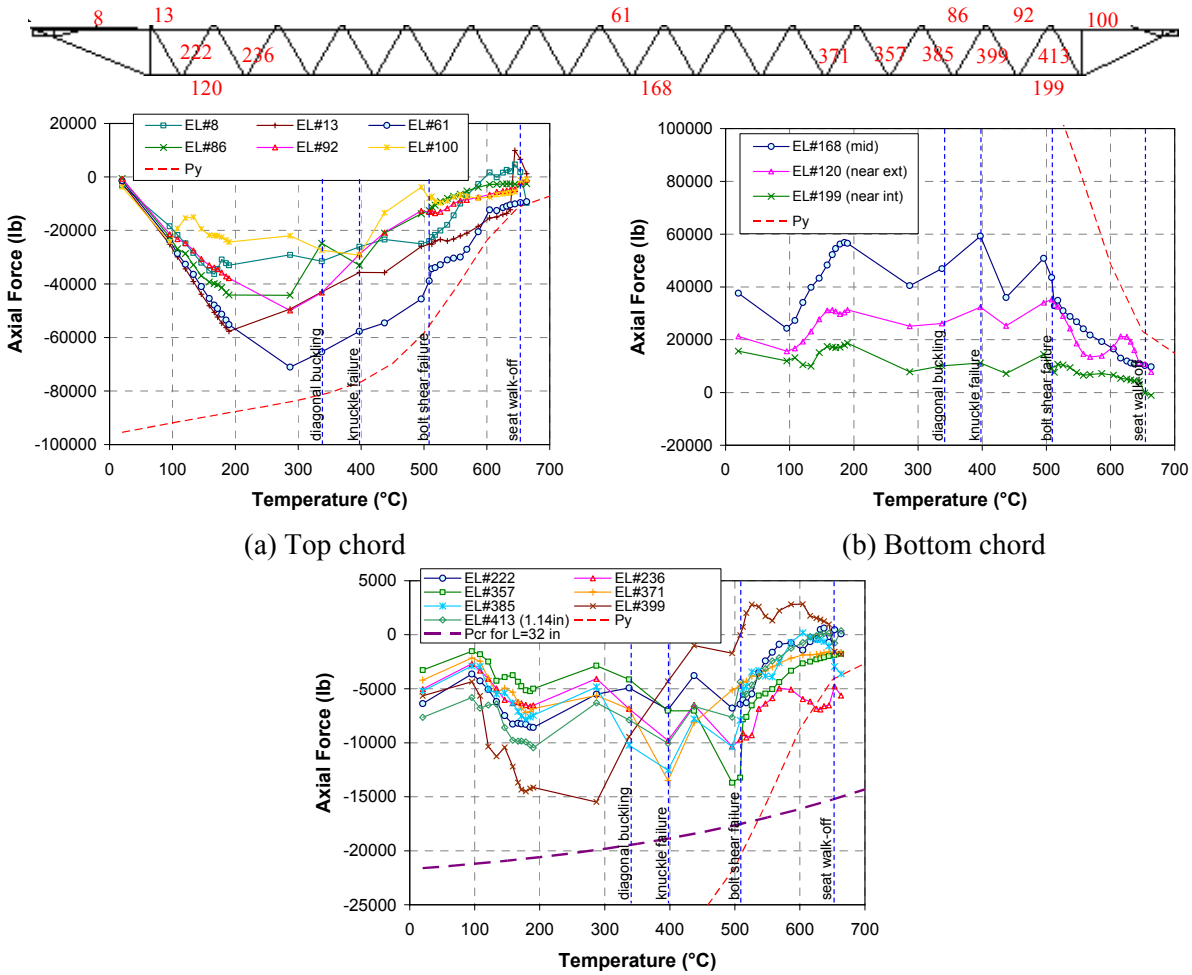

(a) Top chord (b) Bottom chord

(c) Compression diagonal

Figure K–41. Axial force in truss members versus temperature.

Figure K–42 (a) shows the top chords yielding beyond 300 °C. This is due to a significant difference of coefficients of thermal expansion (CTE) between concrete and steel. At 500 °C, the CTE of steel is twice that of lightweight concrete. Bottom chords are still in the elastic range at the end of analysis. Some diagonals are bent significantly in the plane of the truss by high axial force and end moments (see Fig. K–42 for the deformed shape at the interior end). This diagonal buckling starts at approximately 340 °C.

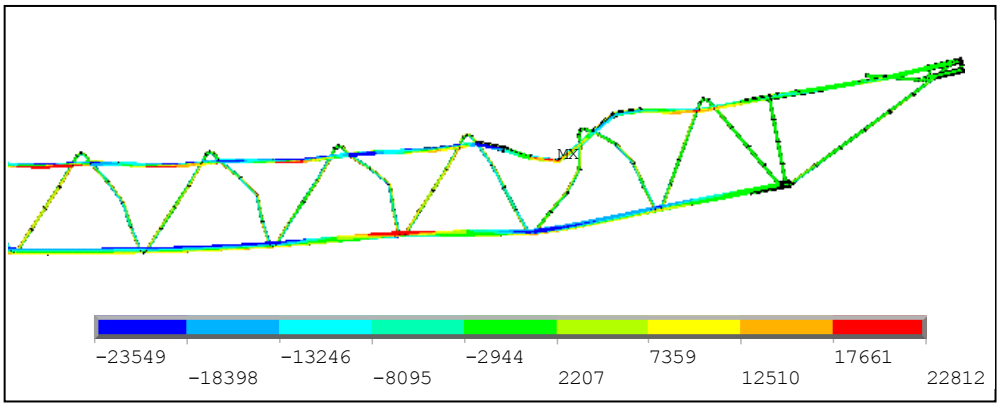

Figure K–42. Axial stress contour in the truss members at 663 °C (displacement magnification factor = 1.0).

Figure K–43 shows knuckle forces in the y direction (longitudinal truss direction) and the z direction (vertical direction). The capacity of a knuckle in the y direction is assumed to be 30,000 lb, and in the z direction 15,000 lb in tension. Knuckles 14 and 15 fail due to horizontal shear around 400 °C. Knuckle 1 also fails due to the horizontal shear around 650 °C.

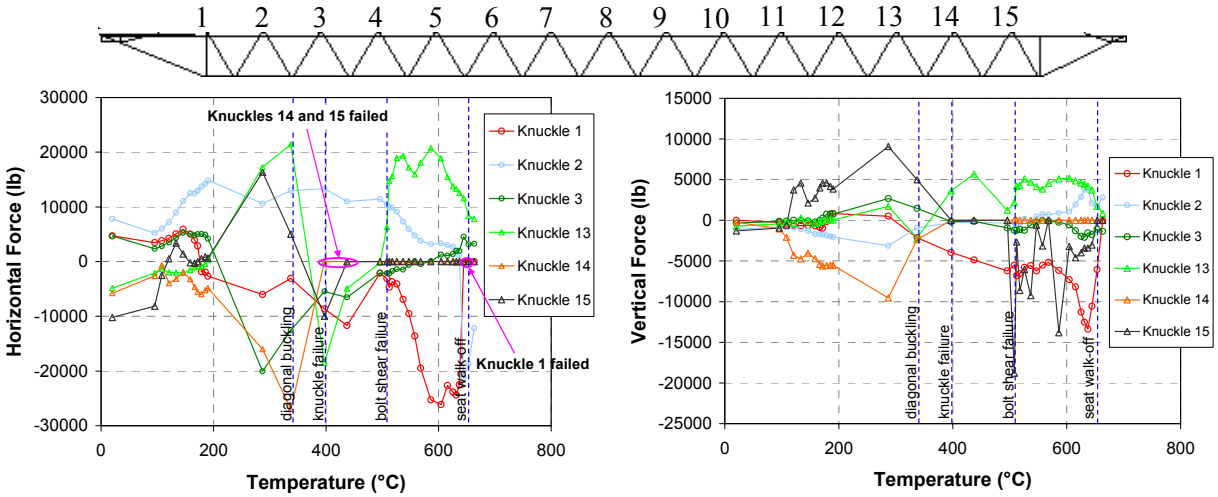

(a) Horizontal Force (b) Vertical Force

Figure K–43. Force in the knuckles versus temperature.

Figure K–44 (a) and (b) show horizontal and vertical reaction forces at seats, respectively. At 510 °C, the interior seat bolt shears off. At 650 °C, the truss walks off the interior seat. At 660 °C, the gusset plate at the exterior end fails in tension.

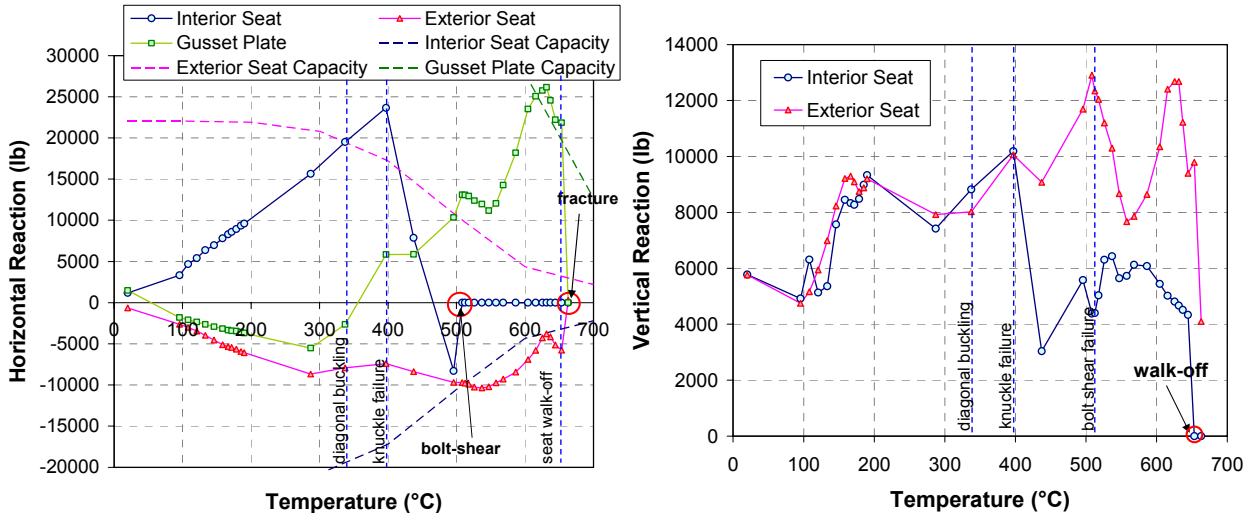

(a) Horizontal reaction force (b) Vertical reaction force

Figure K–44. Reaction forces at seats.

Additional Debris Load

The capacity of the truss model against additional debris load is determined by increasing the gravity loading at room temperature. The analysis is performed with the previous model, where boundary conditions of the slab are as described in the section "Bounding Conditions." Let us define load factor as the ratio of the gravity load plus debris weight to the gravity load, where gravity load includes self weight, superimposed dead load, and 25 percent of the reduced live load. The analysis was terminated at a load factor of 3.4. Figure K–45 (a) shows midspan vertical displacement versus load factor. At 2.4 times the gravity loading, 11 knuckles from the core end fail in the truss direction. At 2.8 times the gravity loading, the fourth knuckle from the exterior end fails. Figure K–45 (b) shows the sum of horizontal reaction forces measured at the exterior columns. Note that seat capacities are not modeled in this analysis.

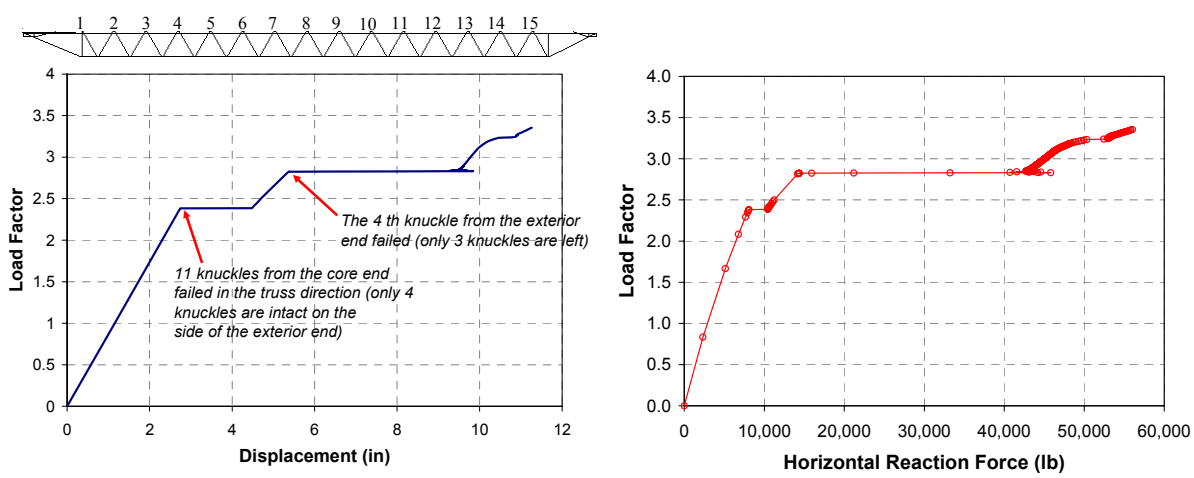

(a) Load factor versus midspan vertical displacement (b) Load factor versus horizontal reaction force

Figure K–45. Finite element analysis results from increasing gravity.

Summary and Discussion

The truss behavior under the gravity plus thermal loading, where the temperature is ramped up to 663 ^{o}C can be summarized as follows:

- Top chords yield above 300 ^{o}C due to the difference in CTEs of steel and lightweight concrete.
- Compression diagonals start to buckle in the plane of the truss due to a high axial force and end moments at 340 ^{o}C.
- At 400 ^{o}C, knuckles start to fail.
- The interior seat bolt shears off at 510 ^{o}C.
- The truss walks off the interior seat at 650 ^{o}C, followed by fracture of the gusset plate at the exterior end at 663 ^{o}C.

The results for the additional debris weight show that the knuckles start failing when the load factor is 2.4. Most knuckles fail before load factor reaches 3.0. After the knuckle failure, the truss loses composite action between the truss and the concrete slab, and the vertical displacement increases significantly. As a result, horizontal reaction force increases.

Models of the truss including knuckles with temperature-dependent capacities, diagonal weld failure, and concrete cracking and crushing are under study.

Simplified Model

To be used in the full floor subsystem model, the truss model will be simplified based on the results from the truss model analysis. Characteristics of the simplified truss model are listed in the following:

- The geometry of the truss will be preserved.
- Pin-ended Link elements will be used for truss members.
- User-defined elements will be used to model failure modes of knuckles, seats, and diagonal members. They will be implemented at the ends of link elements.
- Slab softening or cracking will be incorporated into the model.

K.8 EXTERIOR WALL SUBSYSTEM

The exterior wall subsystem represents the impact zone and includes nine prefabricated wall panels, three panels high by three panels wide.

The exterior wall subsystem model includes nine columns, extending vertically from the column splice located below floor 91 to the column splice above floor 99, and nine spandrels, extending horizontally

from the spandrel splice located at mid-span between columns 149 and 150 to the spandrel splice at mid-span between columns 158 and 159, of the WTC 1 exterior wall.

Figure K–46 shows the subsystem pictorially. Tables K–14 through K–16 give the properties of the column component plates, the spandrels, and the column and spandrel splices. Figure K–47 shows pictorially the spandrel plate thickness, nominal yield strengths, and spandrel splice types. Figure K–48 shows the column plates notation used.

The odd numbered columns support floor trusses. Pairs of strap anchors extend diagonally from the top chord of truss pairs to the even numbered columns. The trusses and the straps partially brace the columns both in-plane and out-of-plane of the exterior wall.

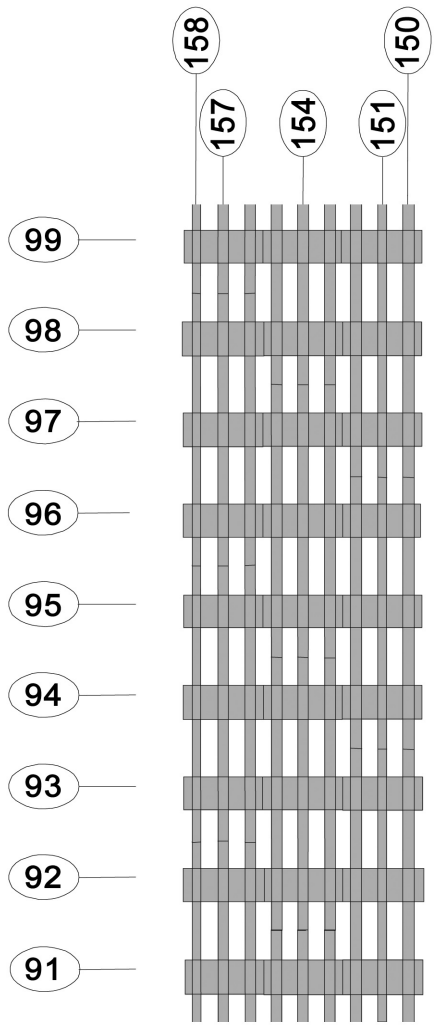

Figure K–46. Exterior wall subsystem structure.

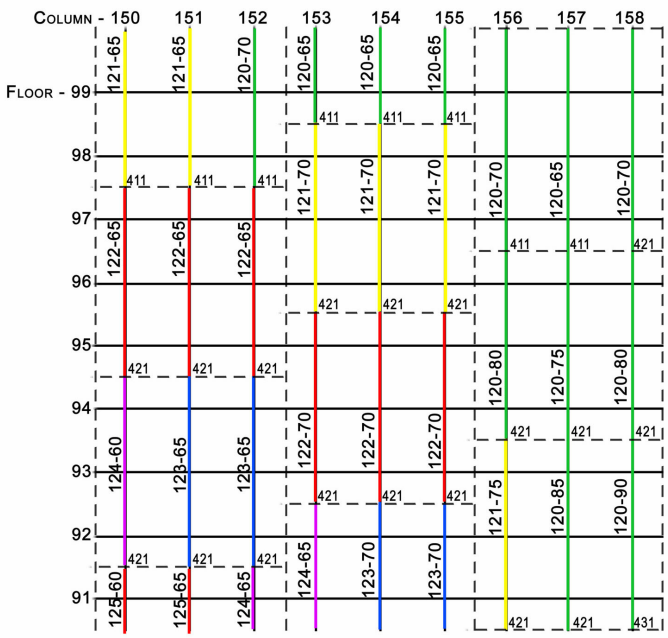

XXX-XX - Indicates type and nominal yield strength of column
xxx - Indicates type of column splice

a) Columns and Column Splices

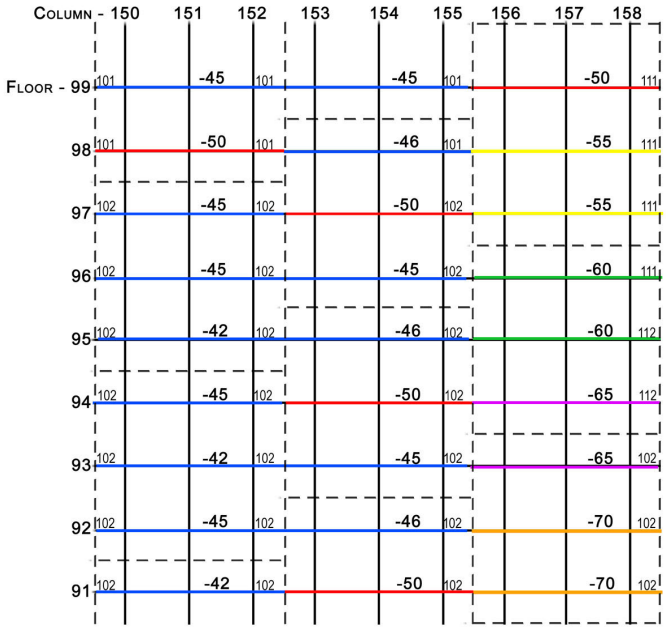

XXX-XX - Indicates nominal yield strength of spandrel
xxx - Indicates type of spandrel splice
Spandrel Thickness 3/8 in.

b) Spandrels and Spandrel Splices

Figure K–47. Column and floor number materials and splice types.

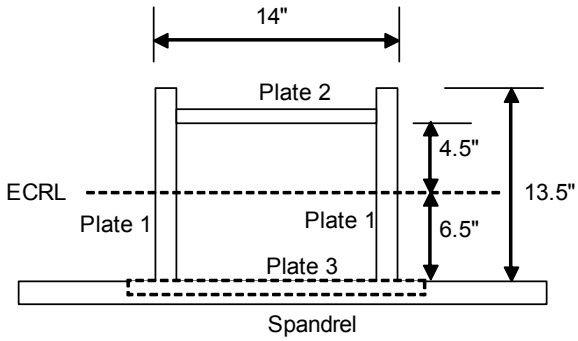

Figure K–48. Spandrels and spandrel splices.

Table K–14. Column sectional properties.

Column Type	Plate 1 l × t	Plate 2 l × t	Plate 3 l × t	Col. Type ID
120	13.5 × 0.25	13.5 × 0.25	15.75 × 0.25	0
121	13.5 × 0.3125	13.375 × 0.25	15.75 × 0.25	1
122	13.5 × 0.375	13.25 × 0.25	15.75 × 0.25	2
123	13.5 × 0.4375	13.125 × 0.25	15.75 × 0.25	3
124	13.5 × 0.5	13 × 0.25	15.75 × 0.25	4
125	13.5 × 0.5625	12.875 × 0.25	15.75 × 0.25	5

Note: All spandrels in wall model are 52 in. deep × 3/8 in. thick.

Table K–15. Spandrel splice details.

Spandrel Splice Type	Number of Bolts/Row	Total Number of Rows	Bolt Spacing	Gage	Overall Splice Plate Dimensions	Bolt to Centerline of Splice	Gap B/W Spandrels	Spandrel Splice ID
101	6	2	5@9		49 × 6.75 ×.25	1.875	0.75	101
102	8	2	3,6,3@ 9,6,3		49 × 6.75 ×.25	1.875	0.75	102
111	6	4	5@9	3	49 × 12.75 ×.25	1.875	0.75	111
112	8	4	3,6,3@ 9,6,3	3	49 × 12.75 ×.25	1.875	0.75	112

a. All spandrel splices use 7/8 in. A325 bolts; spandrel plate yield strength is 36 ksi.
b. Holes in spandrel are 1/4 in. larger than bolts; holes in plates are bolt + 1/16 in. or option to match spandrel holes.

Table K–16. Column splice details.

Column Splice Type	Butt Plate Thickness	Number of Bolts	Bolt Diameter	Gage	Bolt Spacing	Column Splice ID
411	1.375	4	0.875	3.5	6	411
421	1.625	4	0.875	3.5	6	421
431	1.875	4	1	3.5	6	431

a. Butt plates have specified yield strength of 50 ksi.
b. Bolts are A325.

K.8.1 Description of Exterior Wall Subsystem Model

Figure K–49 shows the model in elevation. BEAM189 elements model the columns. SHELL181 plate elements model the spandrels. Figure K–50 shows the number of elements used to model columns and spandrels. MPC184 rigid elements connect the center of gravity of a column to the mid-plane of a spandrel at each shell element. Figure K–51 shows this use of the MPC184. MPC184 rigid elements also model the spandrel connections. A simplified model, consisting of two BEAM189 elements for each of the four bolts, four pairs of CONTA178 contact elements at the faying (contact) surfaces, and MPC184 rigid elements connecting the tops of the bolts to the CONTA178 contact elements, model the column splice. COMBIN37 elements model the fracture of the column splice bolts.

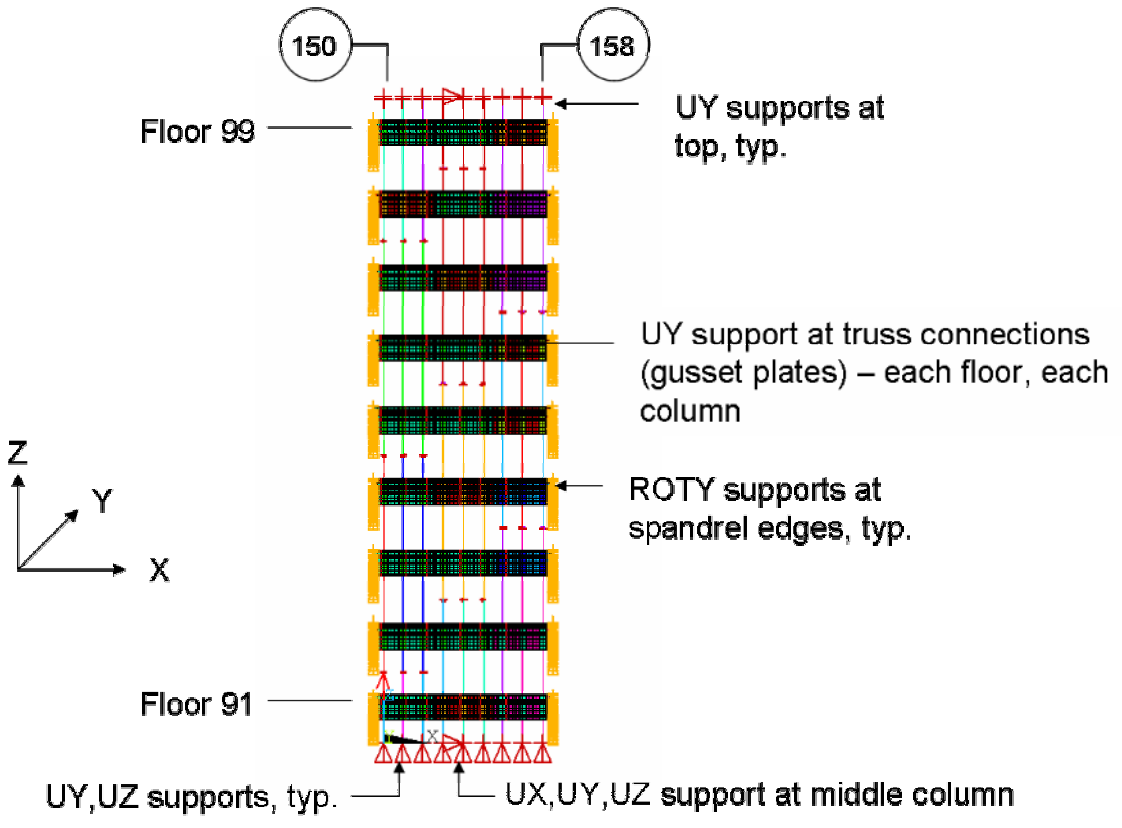

Figure K–49. Exterior wall subsystem model, viewed from inside of WTC 1.

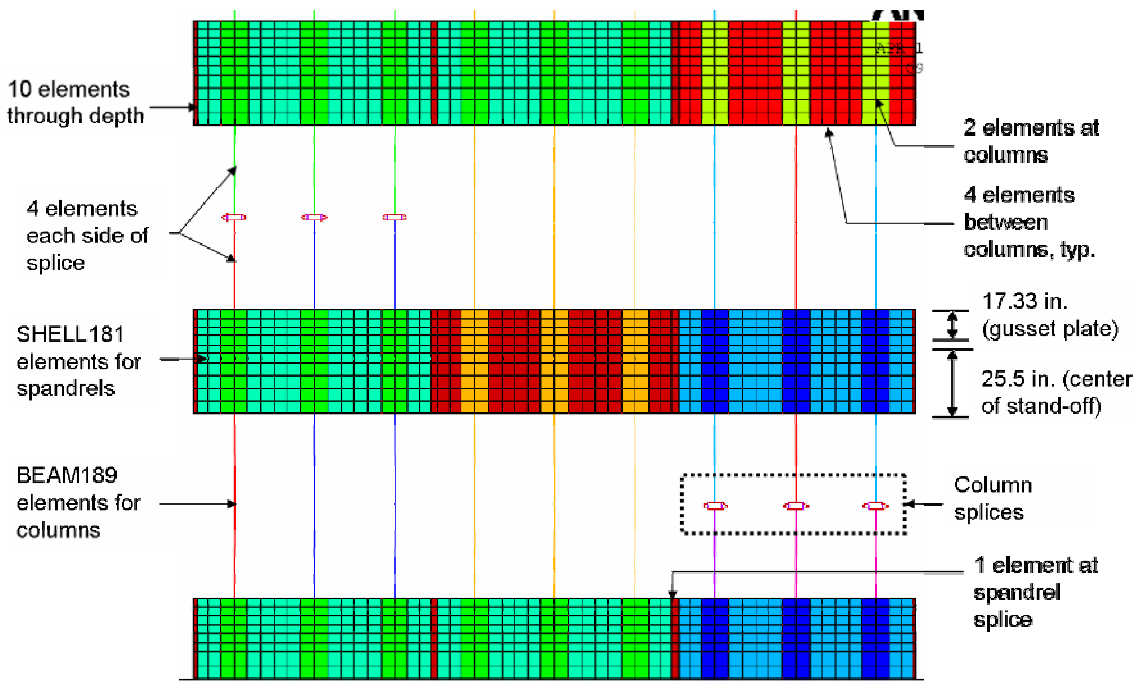

Figure K–50. Portion of exterior wall subsystem model showing number of elements used.

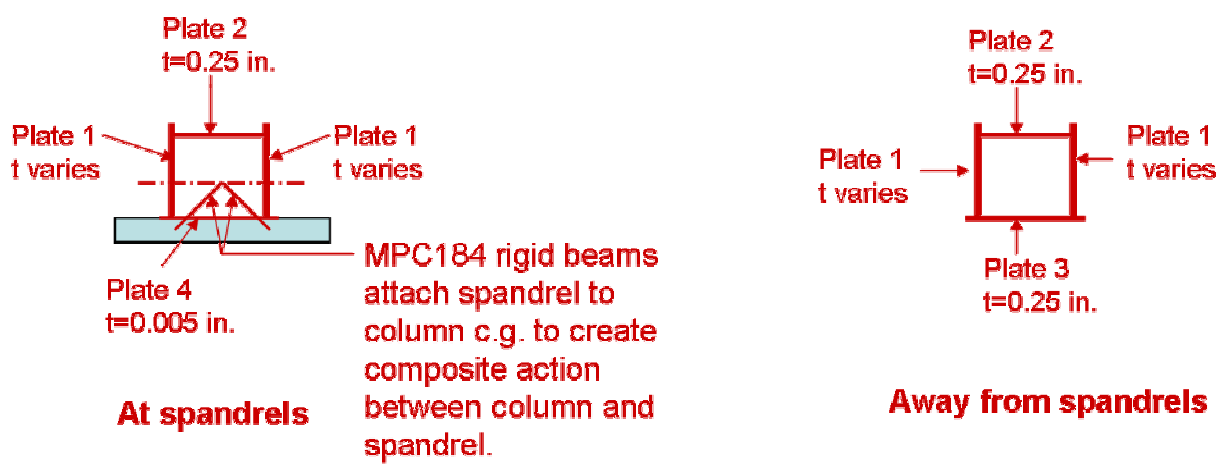

Figure K–51. Schematic representation of columns used in the exterior wall subsystem model.

The capabilities of the BEAM189 and SHELL181 elements include large deflections, plastic deformation, and creep at elevated temperatures. Materials are assigned as described in Section K.5.

The loads on the model include the following:

- Self weight;
- Dead load of floor trusses;

- 25 percent of floor live load;
- Column splice bolt preload; and
- Temperatures of fire scenarios.

A concentrated vertical load and an out-of-the-wall-plane moment due to the dead and live load of the structure above floor 99 load the top of each column. A concentrated vertical load and an out-of-the-wall-plane couple due to the dead and live load of the floor truss load each odd numbered column at the truss seats. Mean temperature at the center of gravity of the column and a linear gradient in each of two directions through the section of the column strain the BEAM189 elements at each node. Temperatures at the nodes strain the SHELL181 elements. Loads and/or deflections at the truss seats model the outward motion or the caternary action of the floor truss due to fire scenarios. The 7/8 in. diameter column splice bolts are preloaded with 36.05 kip (AISC 1964).

Simple supports out of the plane of the wall restrain the tops and the bottoms of all columns in the model. In addition, supports horizontally in the plane of the wall restrain the top and the bottom of central column 154. Simple supports in the vertical direction restrain the bottoms of all columns in the model. Symmetry conditions are imposed on the spandrels at the extremities of the model, except that the spandrels are free to expand in the plane of the wall. In the plane and out of the plane of the wall restraints brace the column at floor truss seats and diagonal straps.

The model captures the following failure modes:

- Column collapse due to large lateral deformations;
- Column buckling due to loss of bracing at floor truss seats and diagonal straps;
- Failure of column splice bolts; and
- Failure of spandrel splice bolts.

The model does not capture the local buckling of the column plates and the formation of plastic hinges due to the interaction of local plate buckling and high stresses in the column from axial load and bending moments. Section K.8.4 below includes the justification for excluding this structural behavior from the wall subsystem model.

K.8.2 Validation of the Exterior Wall Subsystem Model

The behavior of models of the following components of the exterior wall subsystem validate the exterior wall subsystem model:

- Model of a one-story-high exterior column.
- Model of a nine-story-high exterior column.

- Detailed and simplified models of the column splice.
- SAP2000 and ANSYS models of a prefabricated wall panel.

K.8.3 Model of One-Story High Exterior Column

Figure K–52 shows the model of a one-story-high exterior column. The model includes a one-story-high portion of column 151 extending from floor 95 to floor 96 and portions of spandrels at floor 95 and floor 96. The model also represents column 151 from floor 96 to floor 97 since the dimensions, plate thicknesses and material properties are identical to those of column 151 from floor 95 to floor 96. SHELL181 plate elements model the plates of the column and the spandrels. CERIG rigid elements connect the center of gravity of the column to its component plates and the spandrel at both the top and bottom of the model. The column is simply supported in three directions at the bottom and simply supported in the horizontal direction at the top. Increments of axial displacement applied at the top load the model.

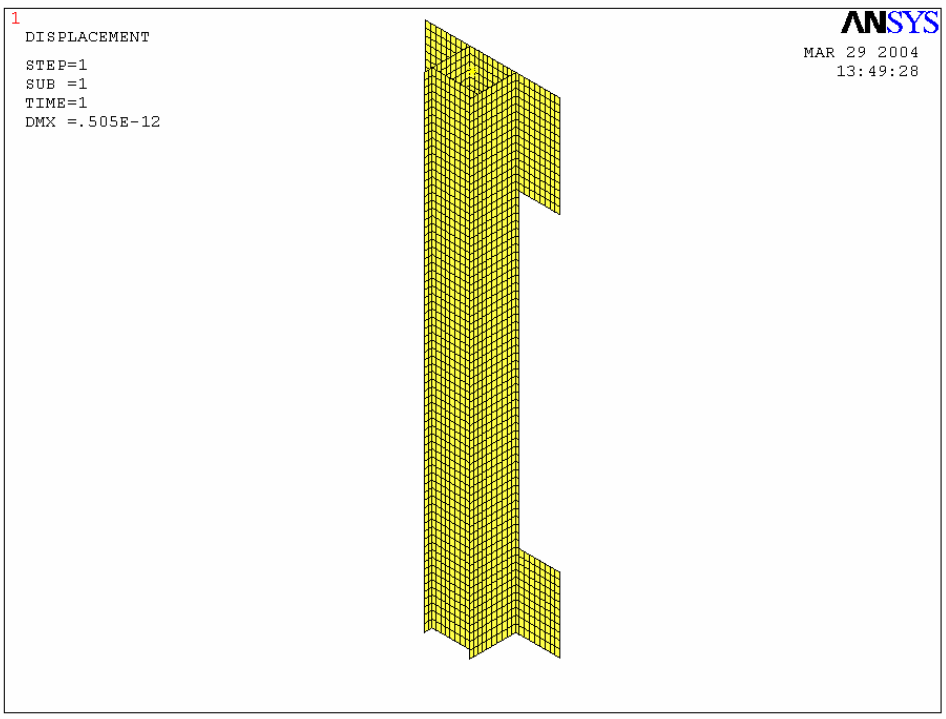

Figure K–52. One-story exterior column model.

Figure K–53 shows the variation of axial load with enforced axial displacement and resulting lateral deflection at room temperature and 700 °C. This figure also shows the hand calculated column load levels at room temperature and 700 °C for:

- Local buckling of Plate 2 and Plate 3;
- Uniform yielding of the column; and
- Axial load due to dead and live load at floor 96 in the exterior wall subsystem model.

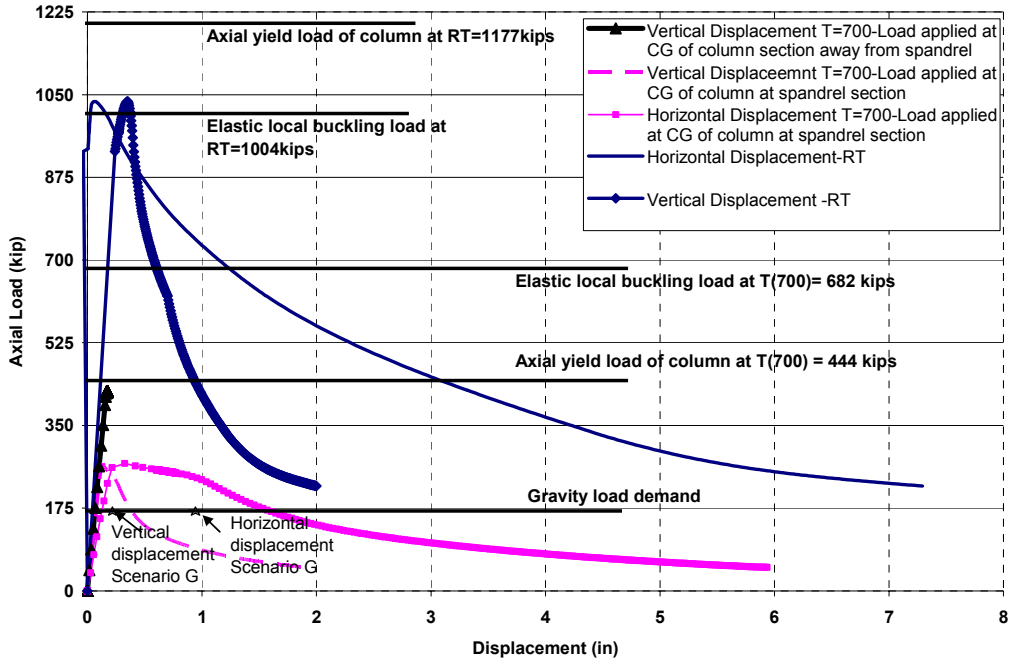

Figure K–53. Load-deflection of column at room temperature and 700 °C.

Figure K–54 shows the local bucking deformation of Plate 2 and Plate 3 at the maximum load level. Figure K–55 shows a plastic hinge at mid-height of the column for an axial displacement of 2 in. Figure K–56 shows the presence of local buckles in Plate 2 and Plate 3 at the maximum load.

Figure K–53 shows that at room temperature Plate 2 and Plate 3 buckle locally at a load that is less than the maximum column load, but that at 700 °C the column yields before it buckles locally. This figure also shows that the expected column demand load of 175 kip is substantially lower than the local buckling load at room temperature and the column yield load at 700 °C. For these results, the axial displacement was applied along the center of gravity of the column cross section away from the spandrel. If axial displacement is applied at center of gravity of the column cross section at the spandrel, there will be additional bending moment in the column section away from the spandrel. The presence of moments reduces the axial load capacity of the column. The resulting load-deflection diagram is also shown in Fig. K–53.

K.8.4 Model of Nine-Story High Exterior Model

Figure K–57 shows the nine-story-high exterior column model. The model includes column 151 extending from near mid-height between floor 91 and floor 92 to mid-height between floor 100 and floor 101, spandrels at floors 92 through 100, and column splices located at the mid-height between floors 94 and 95 and floors 97 and 98. SHELL181 plate elements model the plates of the column, the spandrels, the butt plates at the column splice, and the stiffeners. BEAM189 elements model the column splice bolts. CONTA174 and TARGE170 elements model the faying surfaces of the column splice. MPC184 rigid elements connect the tops of the bolts to the butt plates. At the bottom the column is restrained from displacement and rotation in all three directions. At the top the column is restrained from translating in the horizontal directions and from twisting.

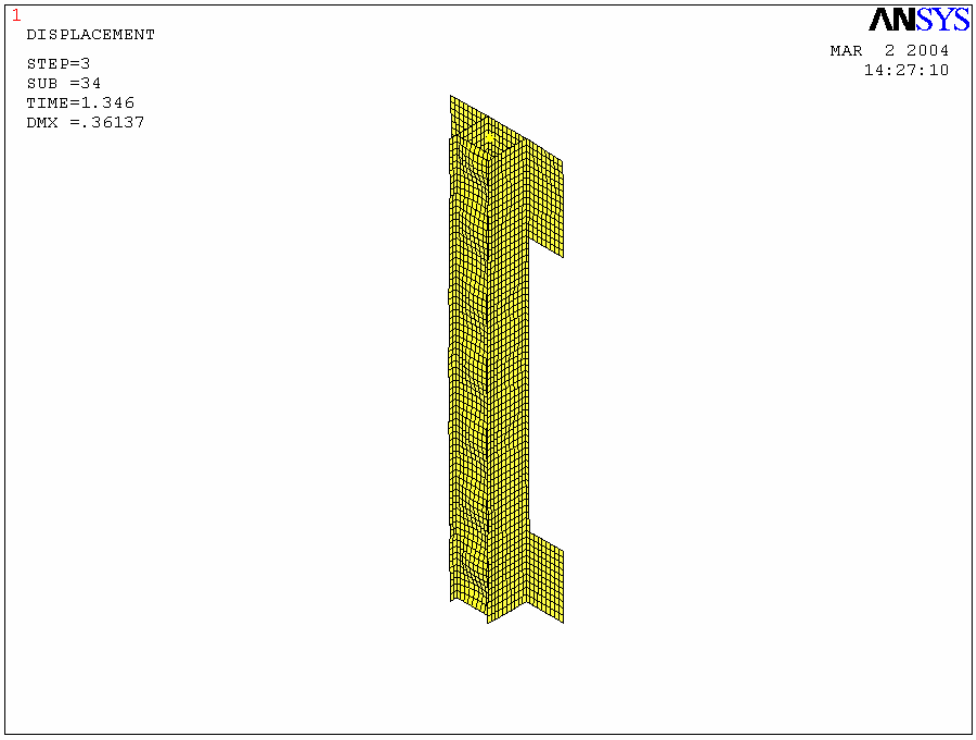

Figure K–54. Local buckling of column at room temperature.

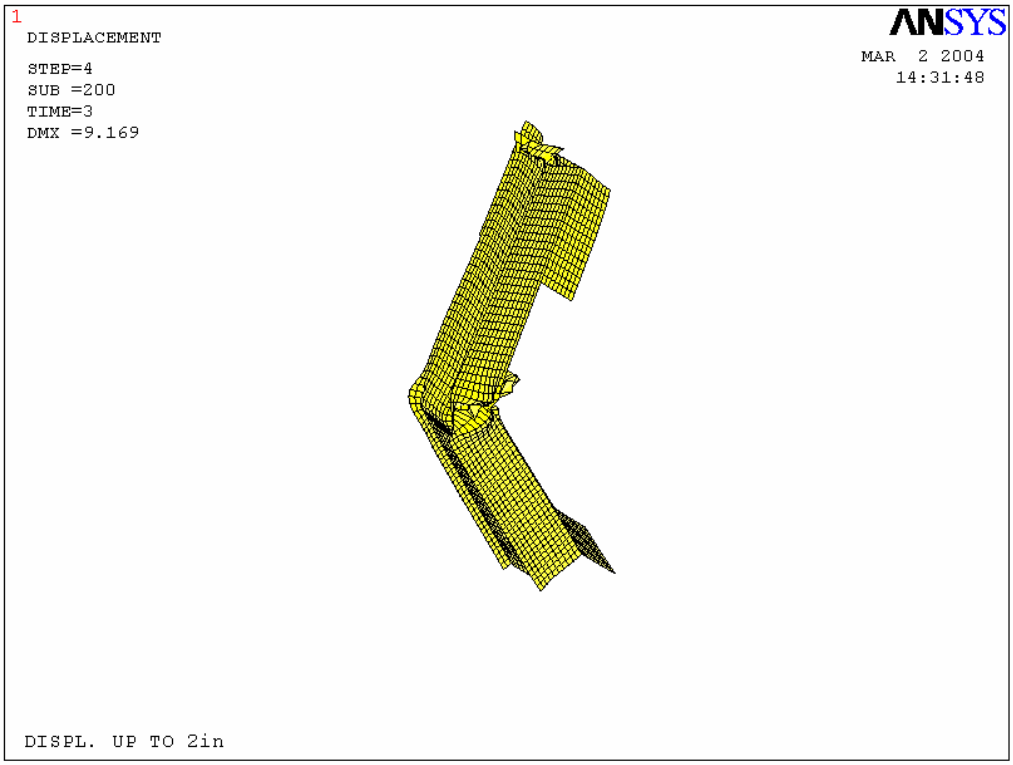

Figure K–55. Plastic hinge in column at room temperature.

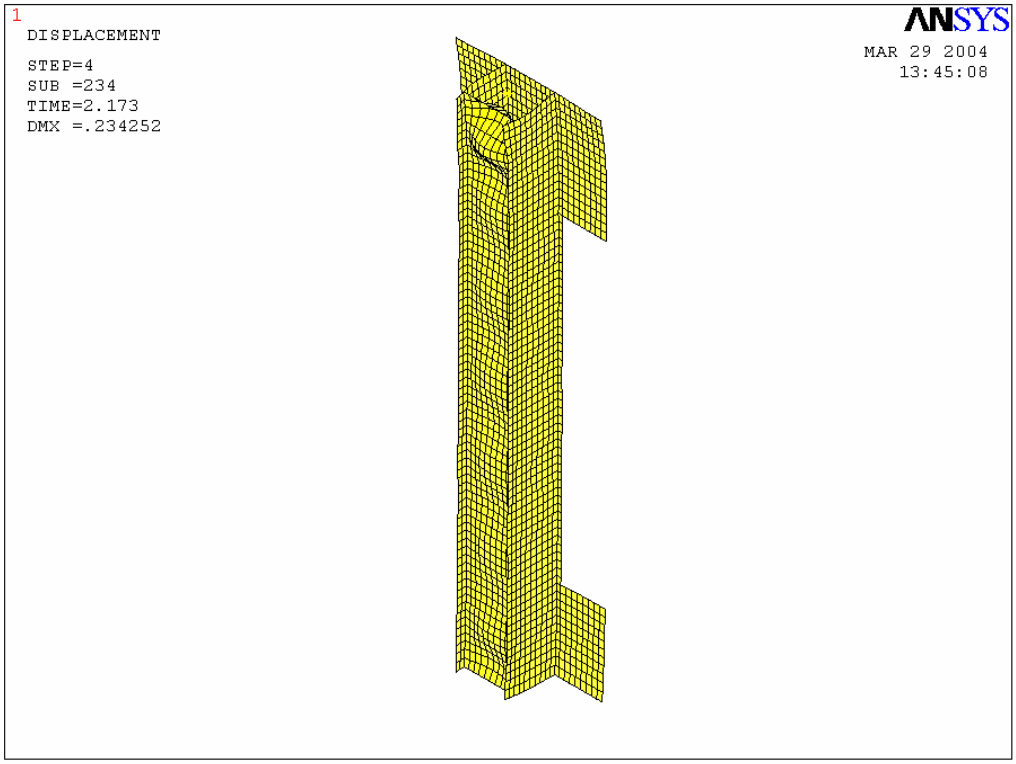

Figure K–56. Deformed shape of column at maximum axial load at 700 °C.

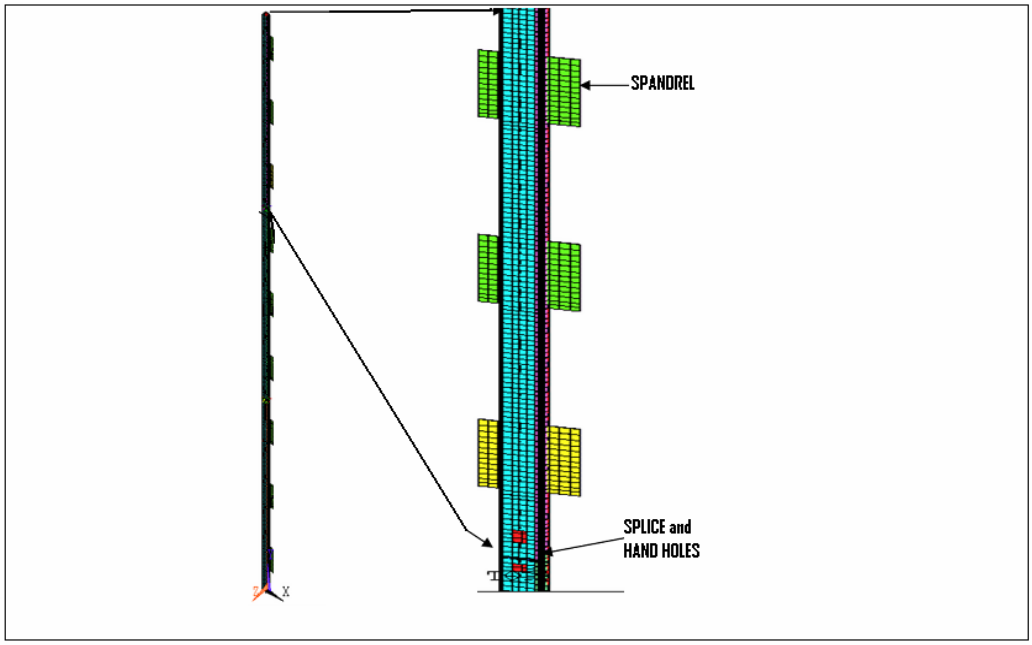

Figure K–57. Nine-story column model.

The capabilities of the BEAM189 and SHELL181 elements include large deflections and plastic deformation. For these elements, gives the material property identification numbers, which in turn are described in Chapter 4 above.

The loads on the model include the following:

- Self weight;
- Dead load of floor trusses;
- 25 percent of floor live load;
- Column splice bolt preload; and
- Temperature of Fire Scenario G.

In Fire Scenario G, the fire starts on floors 95, 96, and 97 and spreads to floors 93 through 98. Gas temperature reaches 1,100 °C. Convection cools the outside face of the column. Radiation heats the other three faces. The inside face of the column is not fireproofed. Temperatures are provided at 200 s intervals up to 5,000 s. Figure K–58 shows the variation of the maximum temperature anywhere in the column with time and the yield stress at the point of maximum temperature. The temperature reaches a maximum of 706 °C at 5,000 s.

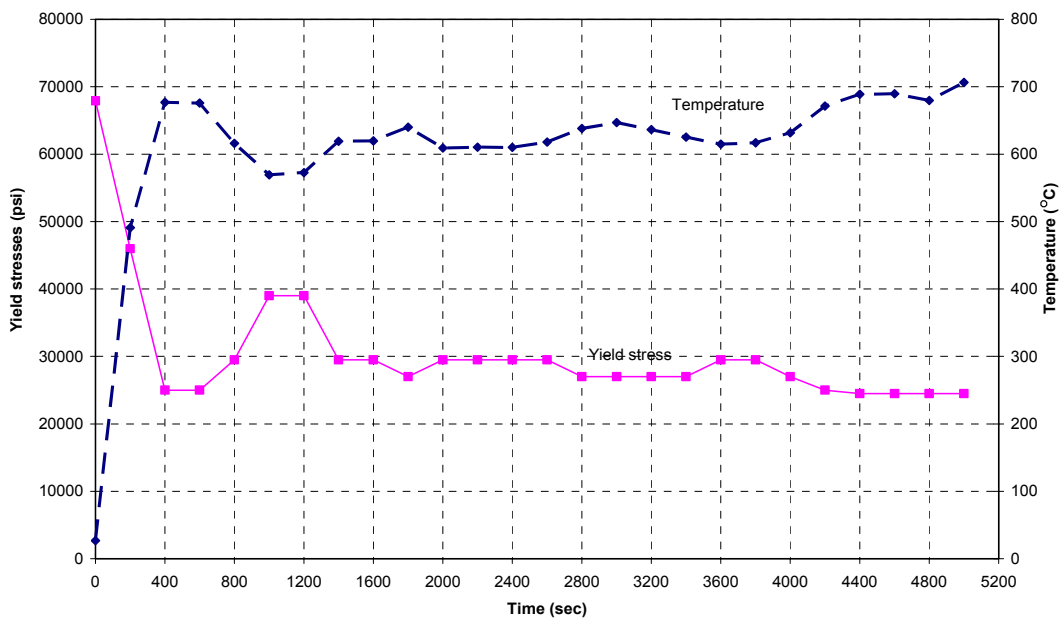

Figure K–58. Variation of maximum temperature and corresponding yield stress with time, fire scenario G.

To account for the dead and live load of the structure above floor 100 and of the floors that connect to the column, concentrated vertical loads and bending moments about a horizontal axis in the plane of the wall are applied to the top of the column and at all truss seats. Furthermore, the 7/8 in. diameter column splice bolts are preloaded to 36.05 kip (AISC 1964).

Figure K–59 shows the variation of maximum tensile and maximum compressive stresses with time and the corresponding yield stress. Figure K–60 shows the deformed shape of the column at 400 s when the compression stress in the column is a maximum. Figure K–60 also shows the deformed shape of the column at 3,200 s when the tensile stress in the column is a maximum. Figure K–60 also shows the deformed shape of the column at 5,000 s when the temperature in the column is a maximum.

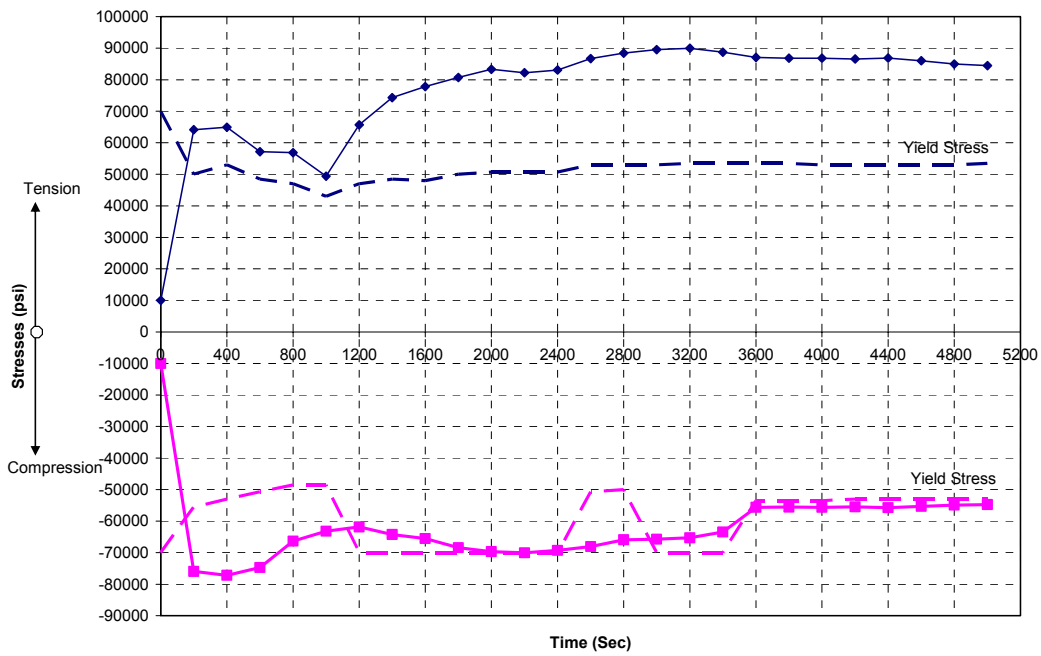

Figure K–59. Maximum compressive and tensile axial stress and corresponding yield stress with time, fire scenario G.

Figure K–59 shows that the tensile and compressive stresses exceed the yield stress for most times during the duration of the fire.

Figure K–60 shows that for Fire Scenario G, an extreme scenario that assumes no fireproofing on the inside face of the column, plastic hinges do not form in the column. This justifies the exclusion of local buckling of the column plates from the wall subsystem model.

K.8.5 Models of the Column Splice

The plate model of the column splice, shown in Fig. K–61 includes a 92 in. tall section of the nine-story column model centered on the column splice located below floor 98.

Figure K–62 shows a simplified model of the column splice. The simplified model consists of two BEAM 189 elements for each of the four bolts, four pairs of CONTA178 contact elements at the faying surfaces, and MPC184 rigid elements connecting the ends of the bolts to the CONTA178 contact elements. A BEAM189 element extends from each side of the splice to match the length of the plate model. Figure K–63 shows the details that model the faying surfaces of the splice.

Figure K–60. Deformed shape of column at 400 s, 3,200 s, and 5,000 s (floors 95–97).

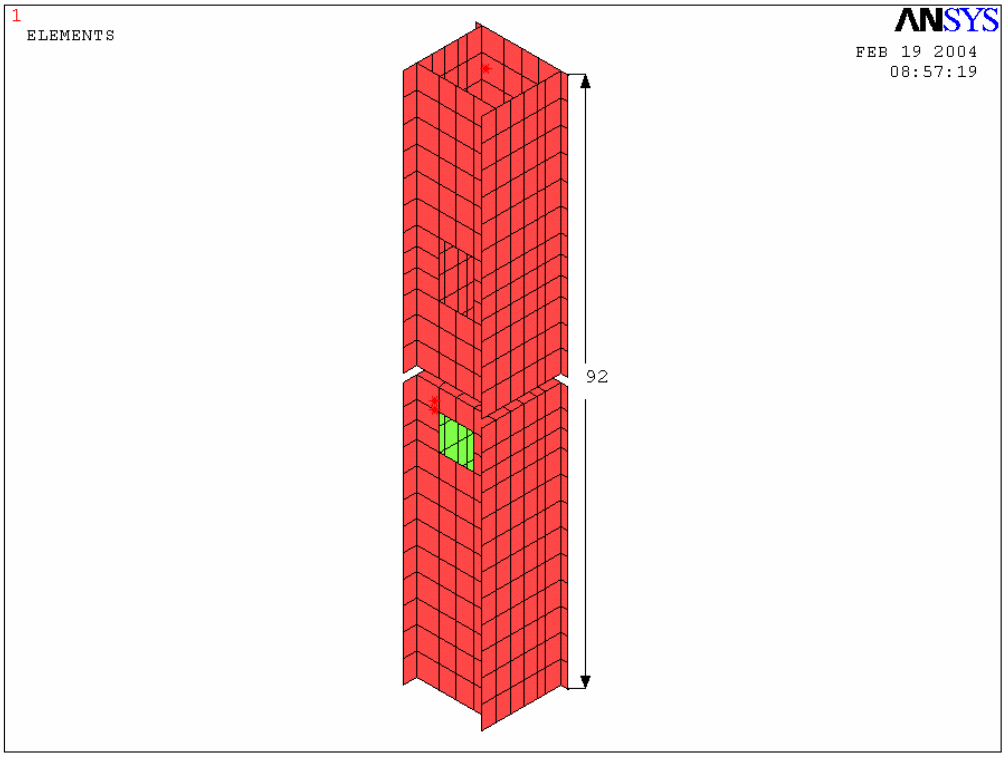

Figure K–61. Plate model of column splice, floors 97-98.

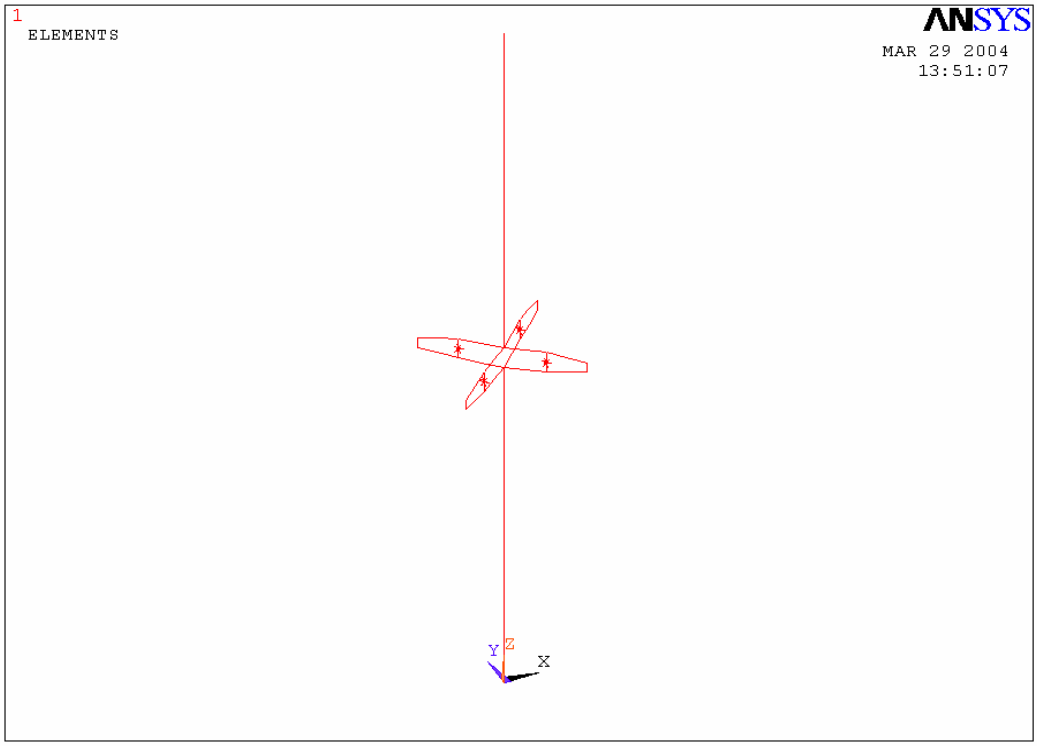

Figure K–62. Simplified model of column splice.

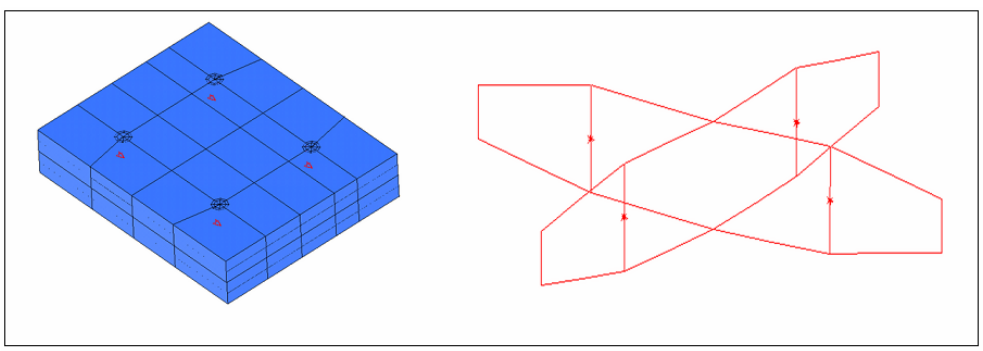

Figure K–63. Column splice details, plate model and simplified model.

Both models are subjected to the following loads:

- Axial tension;
- Shear transverse to the plane of the wall;
- Moment out of plane of the wall;
- Moment in plane of the wall; and
- Torsion.

Figure K–64 shows the variation of axial displacement with axial force load. Figure K–65 shows the variation of transverse displacement with transverse shear fore. These figures show excellent agreement of the simplified model with the plate model.

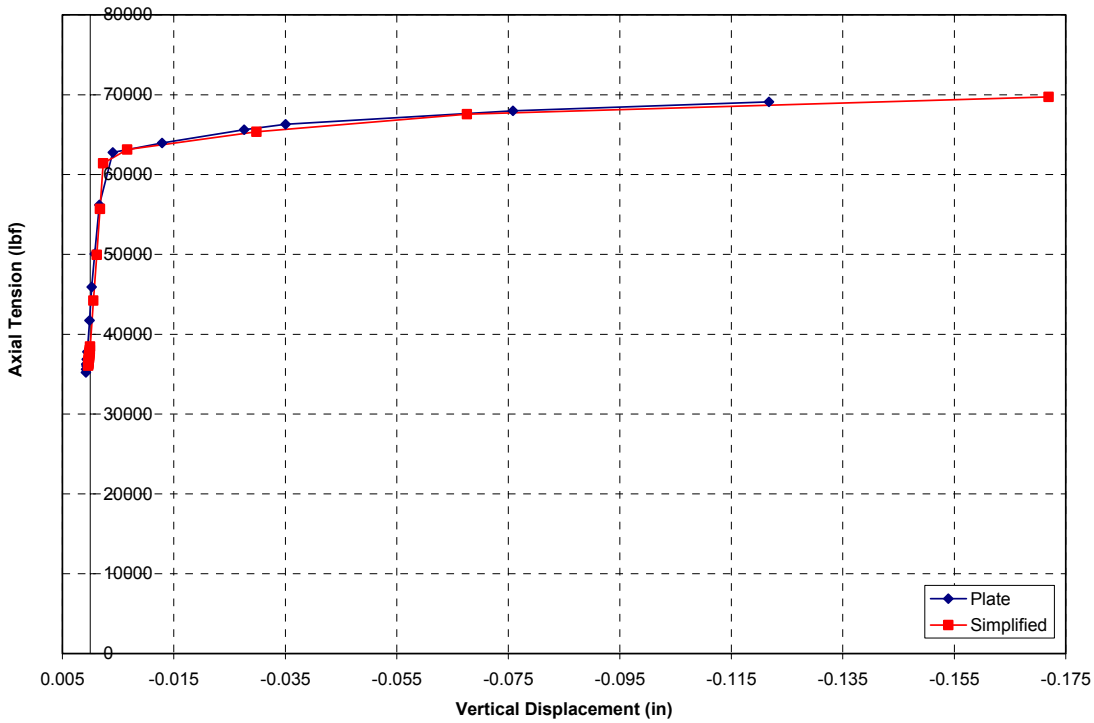

Figure K–64. Variation of axial displacement with axial load.

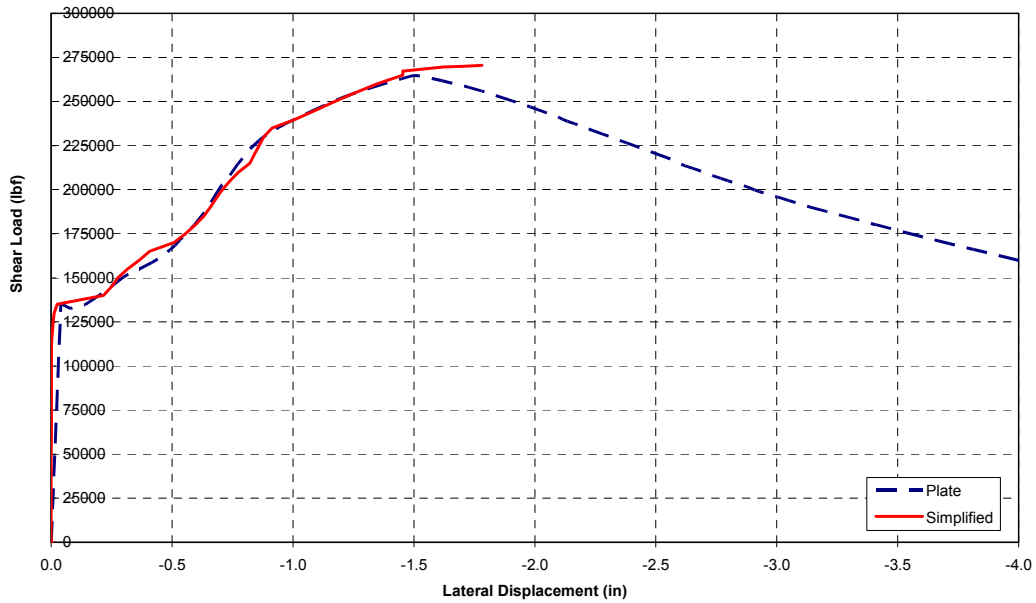

Figure K–65. Variation of lateral displacement with shear load.

Figure K–66 shows the rotation variation with out-of-plane of the wall moment. Figure K–67 shows the rotation variation with in-plane-of-the-wall moment. Figure K–68 shows the twist variation with torque. Figures K–66, K–67, and Fig. K–68 show large differences between the results of the simplified and plate models of the column splice. These differences are due to the fixed locations of pivot points in the simplified model, provided by pairs of CONTA178 point-to-point contact elements, about which the faying surfaces rotate. The CONTA174 and TARGE170 surface contact elements for the faying surfaces in the plate model permit the location of the pivot point to adjust to the demand of the applied moment. Adjusting the location of the point-to-point contact elements can minimize these differences, but they cannot be eliminated. In the exterior wall subsystem model, the locations of the single point contact elements in the column splices will be adjusted and the sensitivity of the response of the model results to these locations computed.

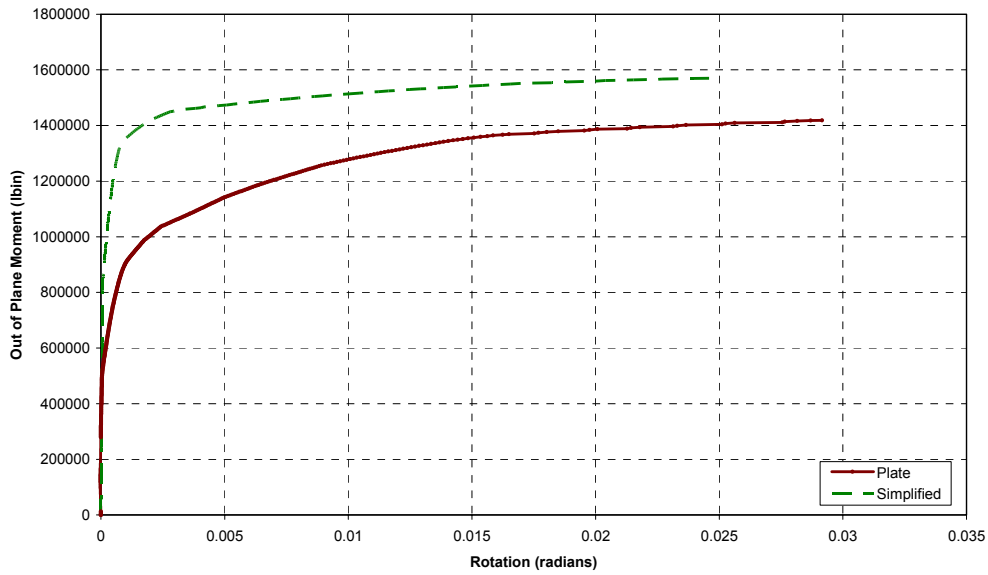

Figure K–66. Variation of rotation with moment, out of wall plane.

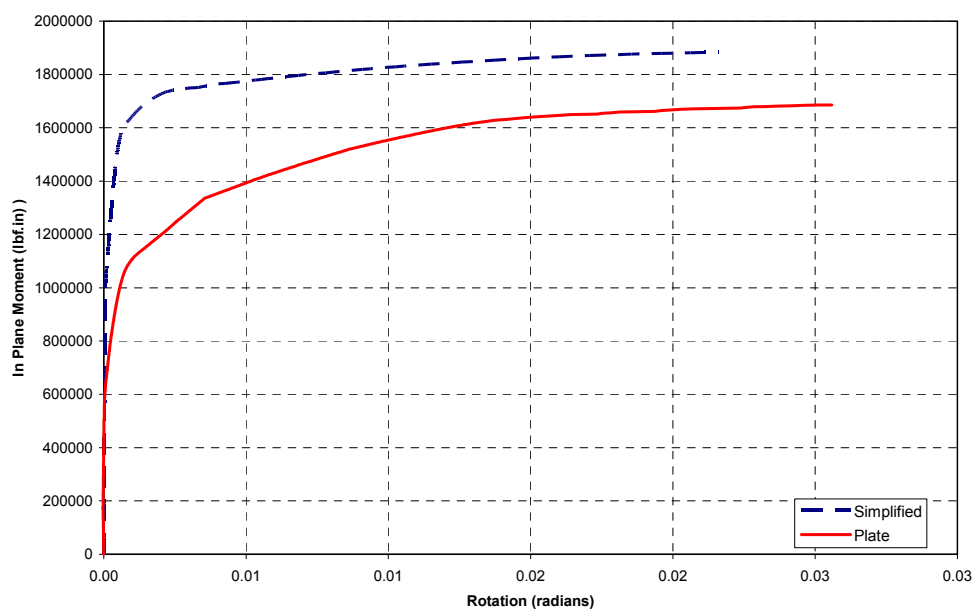

Figure K–67. Variation of rotation with moment, in plane of wall.

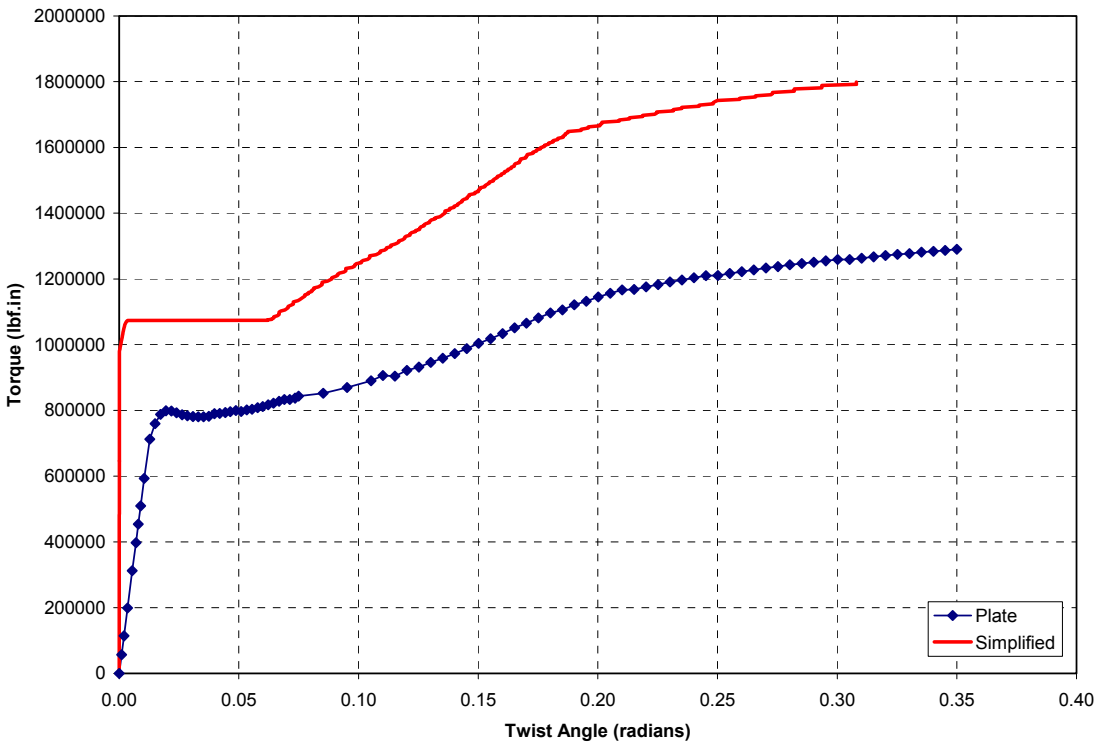

Figure K–68. Variation of twist angle with torque.

K.8.6 Prefabricated Panel Model

Description of Model

Figure K–69 shows the SAP2000 model of a typical prefabricated panel at floors 79 to 82. The model is modified as follows:

- Eliminated self-weight from loading conditions.
- Provided stiff members at the tops of the columns and replaced the four concentrated loads with a single concentrated load.
- Added out-of-plane of the wall supports (UY) at top of columns for out-of-plane loading.

Figure K–70 shows the ANSYS model for matching the behavior of the SAP2000 exterior wall subsystem model. In the ANSYS version of the panel model BEAM189 elements model the columns and MPC184 rigid elements attach the spandrels to the columns.

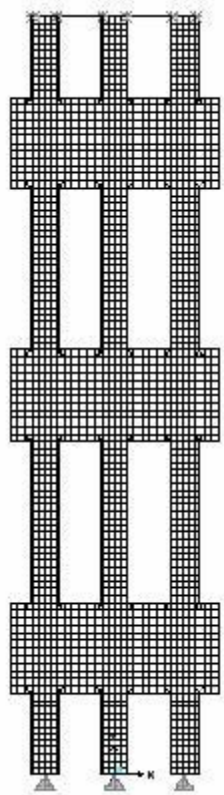

Figure K–69. SAP2000 model of prefabricated panel.

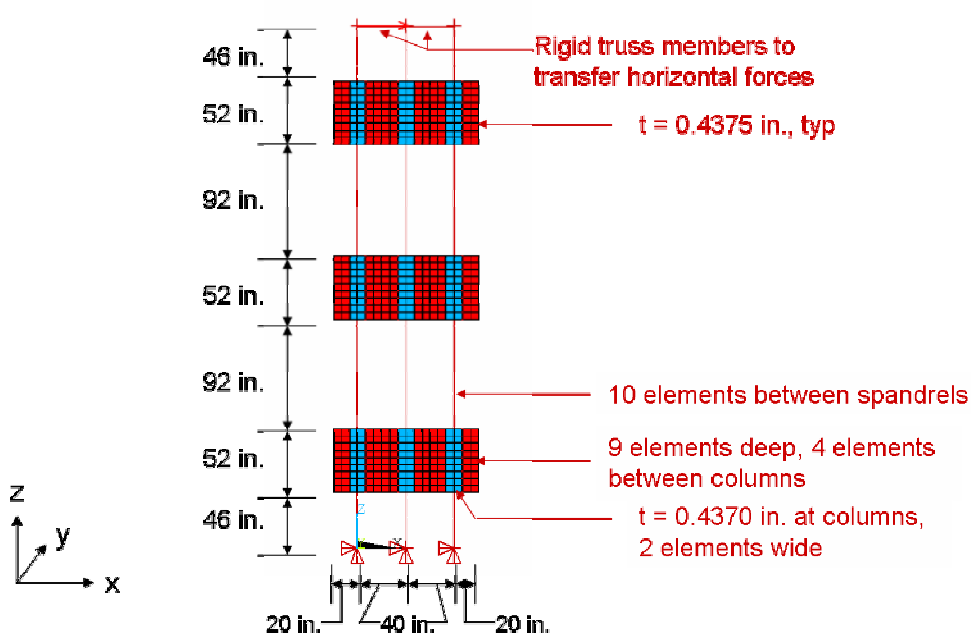

Figure K–70. ANSYS model of prefabricated panel showing geometry and number of elements used.

Both models are subjected to the following loadings at room temperature:

- A concentrated vertical load (FZ) at the top of one of the outside columns.
- A concentrated horizontal load in the plane of the wall (FX) at the top of one of the outside columns. The stiff members described above distribute this shear load evenly to the tops of all three columns.
- A concentrated transverse load (FY) on the middle column at floor 81.

The above loadings do not include self-weight. Figure K–71 shows the various loadings applied to the ANSYS model.

Simple supports in the plane and out of the plane of the wall (UX,UY) restrain the tops of the columns. Simple supports in all three directions restrain the bottoms of the columns. The spandrels at the extremities of the model are free. See Figure K–71.

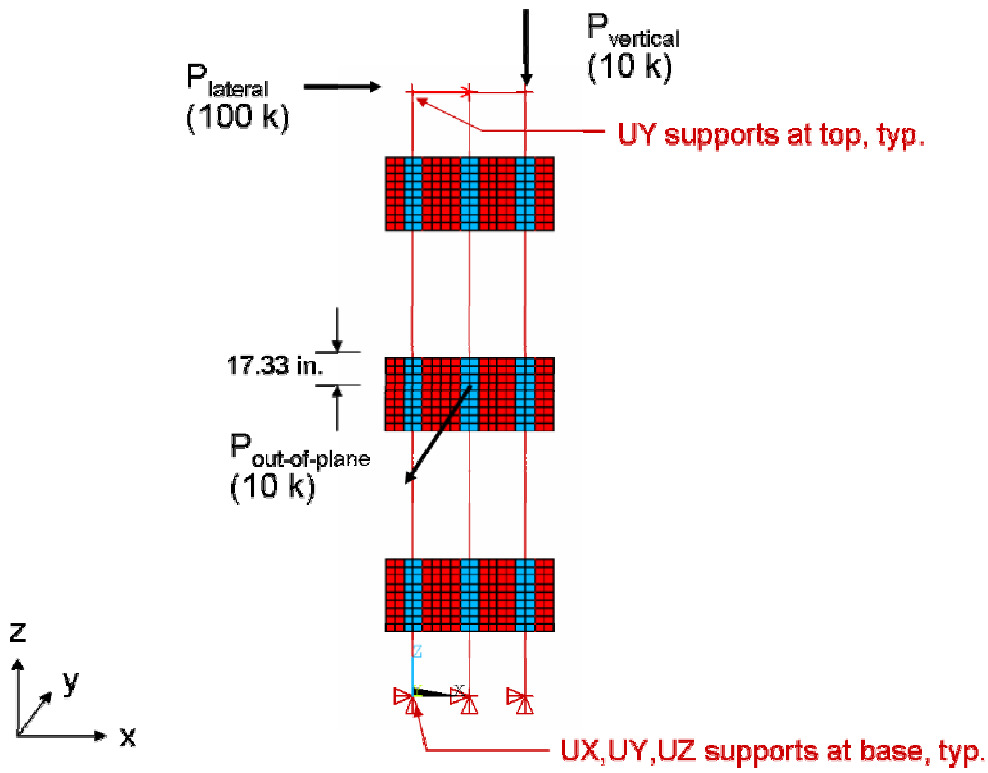

Figure K–71. ANSYS model of prefabricated panel showing loading and boundary conditions.

Validation Results

Figures K–72 through K–74 show deflected shapes and indicate the displacement at the points of applied load for the SAP and ANSYS models. Table K–17 summarizes the differences in reactions and displacements between the SAP and ANSYS models.

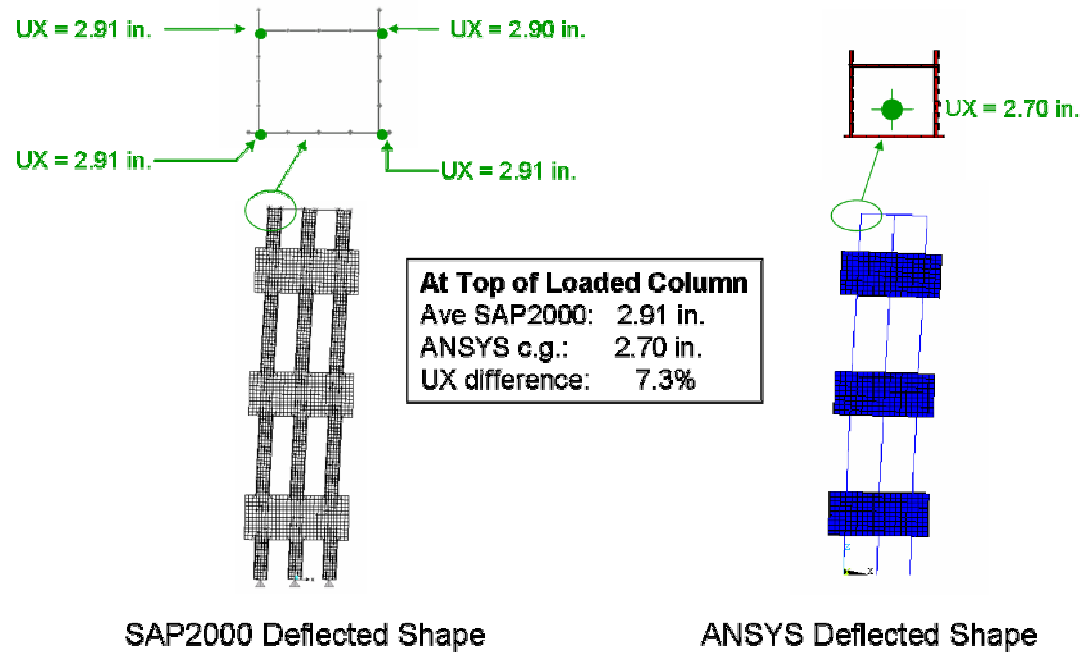

Figure K–72. Deflection of prefabricated panels under 100 kip lateral load.

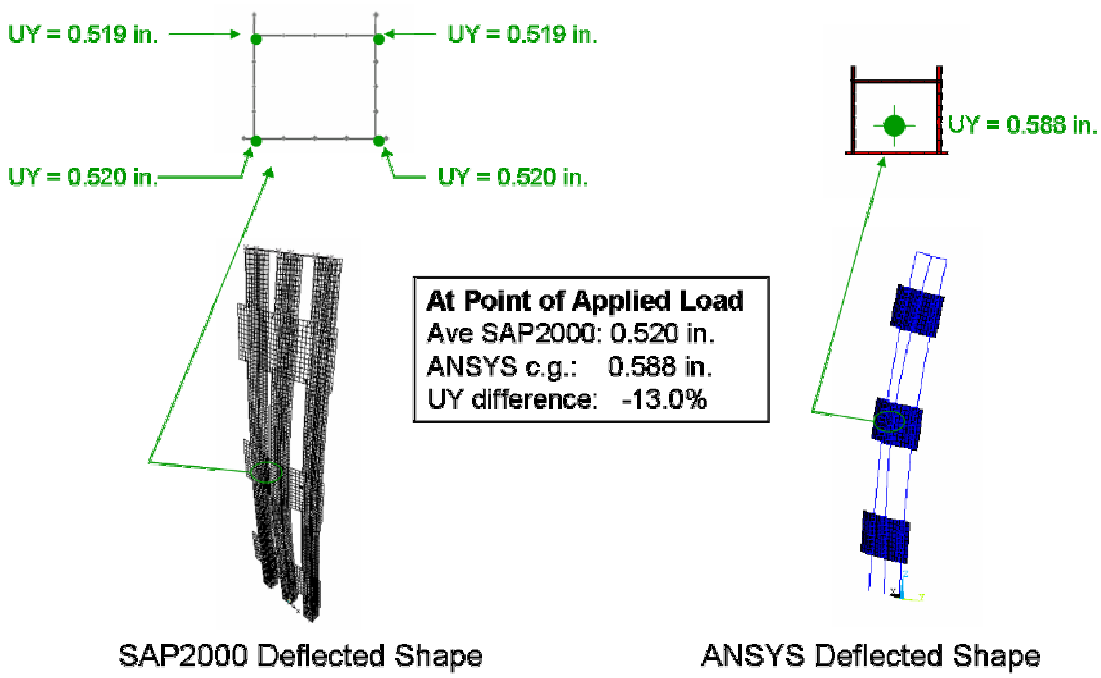

Figure K–73. Deflection of prefabricated panels under 100 kip transverse load.

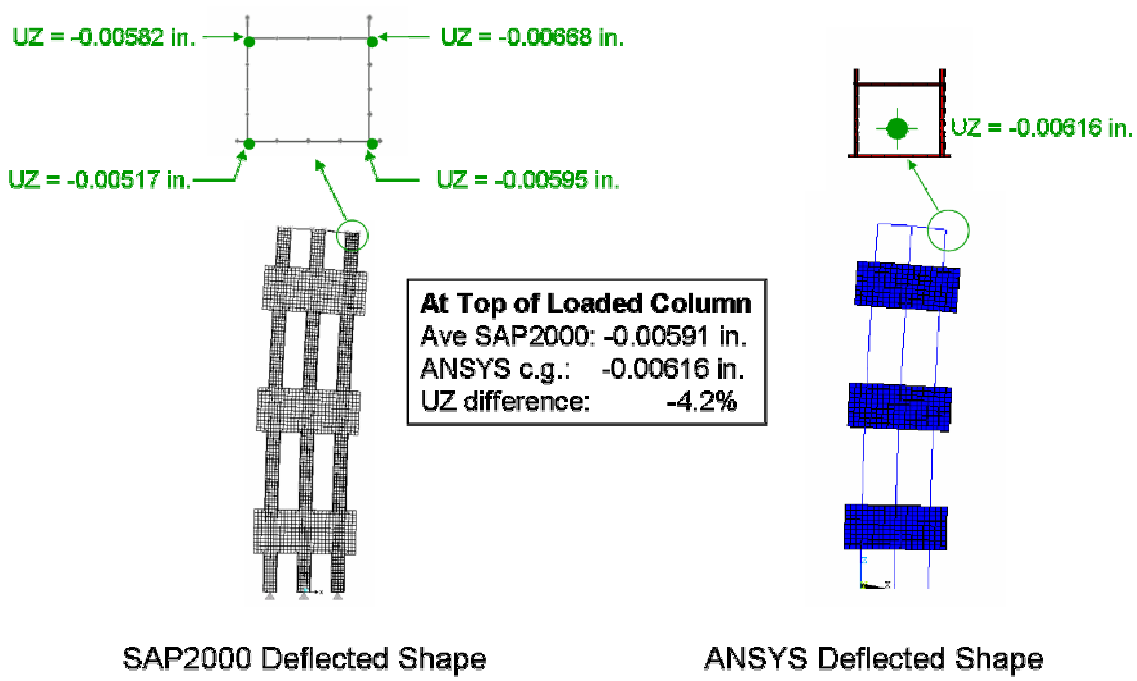

Figure K–74. Deflection of prefabricated panels under 10 kip vertical load.

Table K–17. Validation results.

Loading Condition	SAP2000/ANSYS Displacements[a] Difference Range	
Lateral FX	RX: -2 % to +1 %	UX: 7 %
Transverse FY	RY: -6 % to +7 %	UY: -13 %
Vertical FZ	RZ: -1 % to +2 %	UZ: -4 %

a. Displacements considered at tops of columns for FX and FZ, and at points of load application for FY.

K.8.7 Ongoing Work on the Exterior Wall Subsystem Model

The ongoing work includes the following:

- Stability of a two-story-high exterior column unbraced at the middle floor.
- Stability of a three-story-high exterior column braced at the top and bottom floor levels only.
- Stability of nine-story-high exterior column (floor 92 to 100) unbraced at floors 96 and 97 and subjected to fire scenarios.
- Response of exterior wall model to fire scenarios

K.9 FLOOR TRUSS DYNAMIC RESPONSE DUE TO IMPACT OF DROPPING FLOOR

K.9.1 Impact of Dropping Floor

The failure of dropping floor may occur due to thermal response and/or additional debris weight on the truss, and/or as a result of the aircraft impact. A floor truss or a group of floor trusses could lose support at both the exterior and interior supporting ends and drop onto the floor below. This failure mode, which is shown in Fig. K–75, will be referred to as "full truss drop." Alternatively, a floor truss or a group of floor trusses could lose support on one side and drop down to impact the floor below. This failure mode, which is also shown in Fig. K–75, will be referred to as "partial truss drop."

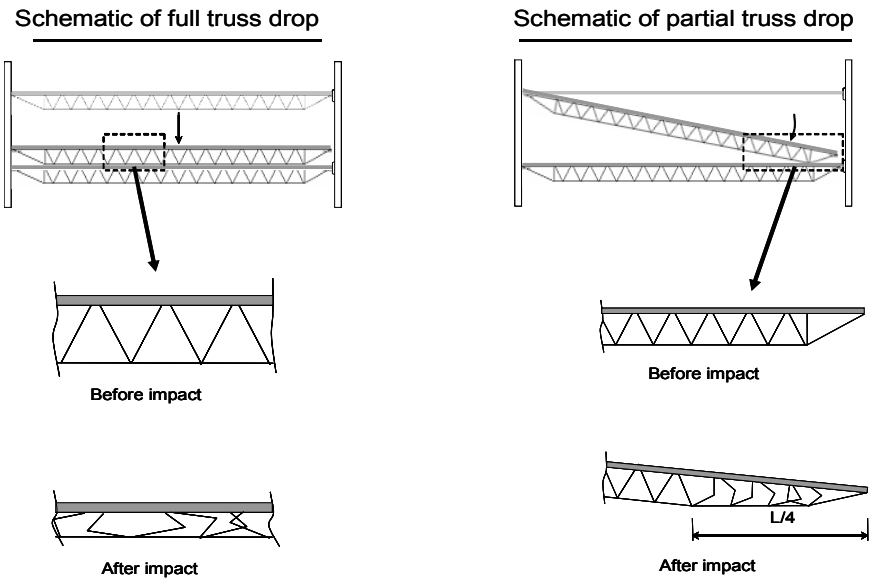

Figure K–75. Schematic of full truss or partial truss drop and diagonal crushing at impact.

K.9.2 Purpose and Scope

The purpose of this study is to determine the dynamic response of the target truss from the impact of full and partial truss drop, to determine whether the target truss seats can resist such an impact load and to determine whether the target truss will lose its composite action, become a catenary, and thus fail to restrain the exterior column to which it is connected against instability.

K.9.3 Method of Analysis

The simulation of a floor drop is idealized with a truss drop. This has the inherent assumption that all seats for the floor fail simultaneously to cause a full or partial drop. The dynamic response of the target truss from the impact of a dropping truss is calculated using conservation of energy principle. The potential energy of the truss just before drop, which is a function of drop height, converts to the kinetic energy of the truss just before impact. As the dropping truss starts to impact the target truss, the diagonal members of the dropping truss are assumed to deform plastically to absorb some of the kinetic energy.

The energy absorption due to crushing of the furniture and partitions are neglected in this study. The energy absorption due to diagonal member crushing reduces the kinetic energy available at impact to deform the target truss. All the diagonal members are assumed to deform plastically for the full truss drop case, while only one quarter of the diagonal member are assumed to deform plastically for partial truss drop, representing one quarter of the length of the truss that may come in contact at impact with floor below. The kinetic energy loss at the time of impact of the dropping truss and the target truss is calculated based on conservation of momentum. The two trusses are assumed to travel together after the impact, at one-half of the velocity of the dropping floor before impact.

The dynamic load due to the impact of the dropping truss onto the target truss will result in the target truss to deform plastically beyond the static load due to the weight of the two trusses. The maximum dynamic deformation of the trusses is calculated by conservation of energy principle assuming that the resistance of the truss is a bilinear function of displacement. This assumption is based on fitting the FEA calculated acceleration-deflection relationship of target truss as shown in Fig. K–76.

K.9.4 Results

The ratios of demand-to-seat capacity for the gravity loads of the dropped and impacted trusses moving together for temperatures of 20 ^{o}C, 400 ^{o}C, 600 ^{o}C, and 700 ^{o}C; and the gravity plus dynamic impact loads for temperatures of 20 ^{o}C and 400 ^{o}C, are calculated. The demand-to-capacity ratio of less than one shows that the truss seat has sufficient capacity to resist the load, and the demand-to-capacity ratio of larger than one, implies that the seat could fail. The range of the demand-to-capacity ratios are due to the different assumptions for the amount of energy loss due to crushing of the diagonal members of the dropped truss.

The demand-to-capacity ratio of the long-span truss for gravity loads is shown in Table K–18 and for gravity plus impact load is shown in Table K–19. The result for gravity load alone shows that both the exterior and interior truss seats have sufficient capacity to support the weight of two floors for all temperatures considered. The result for gravity plus impact load shows that at temperatures below 400 ^{o}C neither the exterior nor interior truss seat is expected to fail. Peak deflection response due to gravity and the dynamic impact of the dropping truss is given in Table K–20. The results show that at room temperature, and more so at 400 ^{o}C, the impacted truss will deflect to an extent that it loses composite action, and become a catenary. At 400 ^{o}C the truss walks off the interior seat. Obviously, a catenary truss is not able to restrain the exterior column against transverse movement and cannot restrain it from instability. Although a truss response to increasing acceleration at 700 ^{o}C has not yet been developed, the strength reduction of the truss seats clearly indicates that the failure of truss seats will occur. The results for long-span truss, for partial truss drop, and for the short-span truss are in progress.

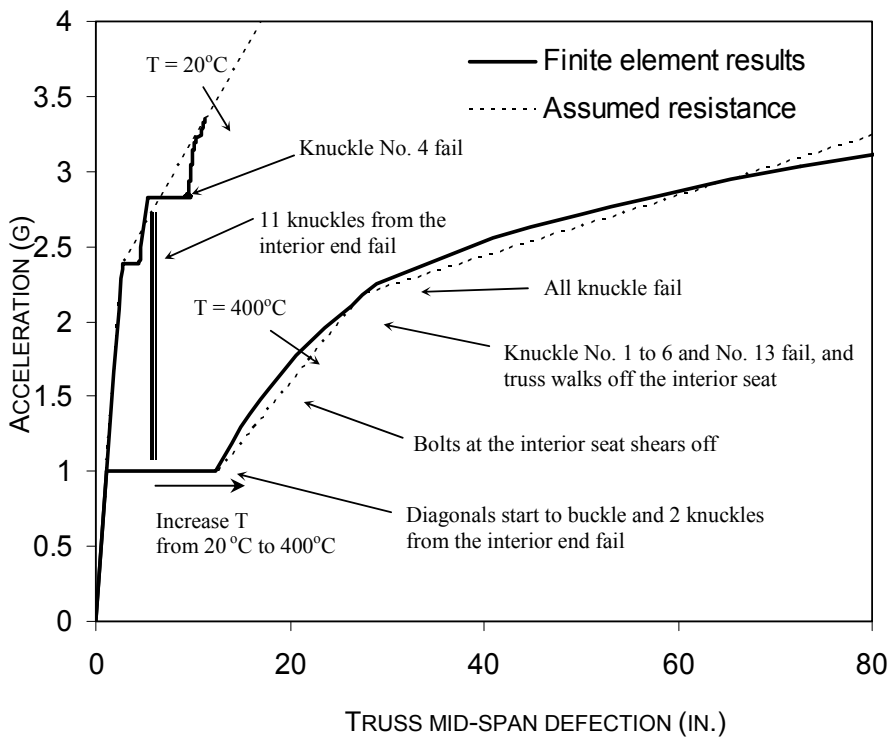

Figure K–76. Target truss resistance against increasing acceleration.

Table K–18. Demand-to-Capacity ratio of long-span truss for static gravity load.

Temp. (°C)	Demand (kip)	Capacity (kip)			Demand/Capacity	
		Int. Seat	Ext. Seat		Int. Seat	Ext. Seat
20	26.4	187.3	140.0		0.14	0.19
400	26.4	166.9	125.7		0.16	0.21
600	26.4	81.6	77.8		0.32	0.34
700	26.4	37.2	35.5	0.71	0.74	

Table K–19. Demand-to-Capacity ratio of long-span truss for dynamic impact load from full truss drop.

Temp. (°C)	Demand (kip)			Capacity (kip)		Demand / Capacity					
				Int. Seat	Ext. Seat	Int. Seat			Ext. Seat		
20	38.6	-	65.3	187.3	140.0	0.21	-	0.35	0.28	-	0.47
400	39.1	-	45.2	166.9	125.7	0.23	-	0.27	0.31	-	0.36

Table K–20. Peak deflection response due to static gravity and dynamic impact.

Temp. (°C)	Static Deflection (in.)	Dynamic Deflection (in.)		
20	2.3	7.6	-	25.4
400	24.2	66.4	-	89.6

K.9.5 Conclusions

At room temperature, the impact of a dropping truss will not cause failure of truss seats, but will cause the impacted truss to deform into a catenary. At 400 ^{o}C, the impacted truss will walk off the interior seat. In either case, the impacted floor will not restrain the exterior column against transverse movement and instability. The impact of a dropping truss at 700 ^{o}C will cause failure of truss seats.

K.10 REFERENCES

ACI (American Concrete Institute) Committee 209. 1992. "Prediction of Creep, Shrinkage, and Temperature Effects in Concrete Structures", ACI 209R–92.

AISC (American Institute for Steel Construction). 2001. Manual of Steel Construction: Load and Resistance Factor Design, 3rd ed.

AISC (American Institute for Steel Construction). 2003. Manual of Steel Construction, Load and Resistance Factor Design.

ANSYS, Inc. 2004. Theory Reference, ANSYS, Inc.

ASTM (ASTM International). 2001. "Standard Test Methods for Fire Tests of Building Construction and Materials," ASTM Standard Test Method E119.

Bartlett, F.M. and MacGregor, J.G. 1996. "Statistical Analysis of the Compressive Strength of Concrete in Structures," ACI Materials Journal, March–April, pp. 158–168.

Fields, B.A. and Fields, R.J. January 1991. The Prediction of Elevated Temperature Deformation of Structural Steel Under Anisothermal Conditions, NIST.

Fields, R. March 22, 2004. Recommended Multiaxial Fracture Criterion, NIST.

LERA (Leslie E. Robertson Associates). 2001. The World Trade Center Design Criteria. Worthington, Skilling, Helle, and Jackson, original document dated 8/20/65.

LERA (Leslie E. Robertson Associates). August 2003. Development of Structural Databases and Baseline Models for the World Trade Center (WTC) Towers–Progress Report #4: Structural Analysis Computer Models.

Phan, Long T. December 1996. Fire Performance of High-Strength Concrete: A Report of the State-of-the-Art, NIST.

Phan, Long T. December 2003. Properties of Concrete at Elevated Temperature, NIST.

Seanz, L.P. 1964. "Discussion of Equation of the Stress-Strain Curve of Concrete by Desayi and Krishman," Journal of the American Concrete Institute, Col. 61, No. 9, pp. 1229–1235.

SHCR (Skilling, Helle, Christiansen, Robertson). 1973a. World Trade Center Drawing Book 8, Concrete Reinforcing, Chapters 1-4.

SHCR (Skilling, Helle, Christiansen, Robertson). 1973b. World Trade Center Drawing Book 7, Floor Panels and Truss Details, Chapters 1-5.

Stevick, G.R. March 1994. "Failure of Welds at Elevated Temperatures," Welded Research Council Bulletin 390, Welding Research Council, pp. 1–39.

This page intentionally left blank.